ICFA Beam Dynamics Newsletter, No. 24

Editors in chief
K. Hirata, J. M. Jowett
Editors
S. Chattopadhyay, W. Chou, S. Ivanov, H. Mais, J. Wei, and C. Zhang

April 2001

Contents

1: Forewords

1.1 From the chairman of the ICFA Beam Dynamics Panel

John M. Jowett John.Jowett@cern.ch The Chairman

1.1.1 Changes, Role and Activities of the Panel

As he announced in the previous issue, Kohji Hirata has resigned from this post. He was Chairman of the ICFA Beam Dynamics Panel from 1994 to the end of 2000 and it is appropriate to review what was achieved during his tenure.

Few would disagree that the profile of the Panel has been boosted considerably and that much has been done to further the Panel's mission:

> To encourage and promote international collaboration on beam dynamics studies for present and future accelerators.

No fewer than 15 Advanced ICFA Beam Dynamics Workshops were held. As their collective title implies, our workshops explore topics in beam dynamics at the deepest level and bring together leading researchers and advanced students. They are not associated with any particular existing or future project but may be of very practical relevance to several. Since beam dynamics is not widely studied in universities, they might often not be held at all were it not for the framework provided by the Beam Dynamics Panel and the approval given by ICFA. On occasion, our workshops have spawned new and fertile sub-disciplines. A recent example is the subject of Quantum Beam Physics that has emerged from two workshops and forges new links between the fundamentals of our field and those of others like astrophysics, condensed matter or particle physics.

Information on all our past and future workshops is available via our home page (see below). Published proceedings are an essential feature of all our workshops.

The Beam Dynamics Newsletter has been rejuvenated and expanded in scope and is widely read among our community[1]. It is hard to know exactly how many people read it since our primary means of distribution is now the Web (we don't count the "hits" of our pages) but my impression is that most people in our field are now well aware of and read at least some of it. In addition we still print (thanks to the support of various labs) some 1300 paper copies that are distributed around the world.

Panel members have founded various topical working groups. At present there are three:

- High Intensity, High Brightness Hadron Beams, chaired by Weiren Chou.
- Future Light Sources, chaired by Kwang-Je Kim.
- High Luminosity e^+e^- Collider, chaired by Yoshihiro Funakoshi. This working group was formed late last year to encourage world-wide efforts to achieve a luminosity at least 10 times larger than the present limit. It will consider existing and future machines for ϕ, τ-c, B, Z, Higgs, t, ... physics.

[1] A much mis-used word, but it genuinely applies here.

What of our mother body, ICFA itself? One of my first duties as Chairman was to attend its recent meeting at DESY. It was brought home to me there that, at the level of the laboratory directors and ICFA members, the world of high-energy particle accelerators is quite small and interdependent. In science, as in commerce or politics, this is an excellent state of affairs. The Beam Dynamics Panel plays a similar role within the international community of accelerator physicists, facilitating the creation and propagation of the knowledge needed to realise the particle accelerators of the future. Now, more than ever in the history of high energy physics, these depend on innovation and our ability to collaborate world-wide.

For many of these gains, we should be grateful to Kohji who handled the Chairmanship with wisdom, assiduity and—often very important—diplomacy. I would like to thank him on behalf of the Panel. He will stay on as a Panel Member and Chief Editor of the newsletter to ensure continuity and provide advice on policy based on his experience.

There have been other changes in the Panel membership. David Whittum of SLAC has left; he deserves our thanks for maintaining the Web pages of the Americas region and acting as an editor of the newsletter. He has been replaced by Swapan Chattopadhyay of LBNL who, by the time this is published, will have moved to a new post as Associate Director at Jefferson Lab. I would like to welcome Swapan to the Panel and know that he will be an active and creative member. Among other things he will take over the Web pages for the Americas.

Other members will come and go in the gradual but necessary processes of rejuvenation and distribution of Panel positions equitably among regions, laboratories and individuals. One might wonder whether a little affirmative action is not required here: in terms of, say, sex, the balance of Panel members is even worse than in the wider population of physicists.

It is important too, that the Panel should not be perceived as an exclusive club but as an open service to the community. It is not possible to have a member in every accelerator lab but that does not matter because Panel membership is not a matter of representing the institution that employs you (it is some kind of supplement to your ”day job”). Geography has become irrelevant to human communication in recent years and the old idea of regional representation is all but obsolete too. Everyone should feel free to influence the Panel via the most appropriate member, based perhaps on common interests rather than proximity. By and large, this is what happens. Many people outside the Panel participate in our working groups and in the programme and organising committees for our workshops.

Although panel members are expected to contribute regularly to the newsletter, this is by no means their preserve alone. I would like to exhort *everyone* in our field to submit articles. These can range from the conventional activity reports and announcements or accounts of beam dynamics events to letters or articles drawing attention to current problems or expounding opinions. Announcements of recently awarded theses provide valuable exposure for new entrants to the field. We do *not* publish technical accounts of theoretical or experimental work that belong in the usual conferences or journals.

Finally, I think we should also be wary of closing in on ourselves. Specialism in accelerator physics or its associated technologies has many virtues that lead, among other things, to well-engineered projects. On the other hand, as Maury Tigner has argued recently (Physics Today, Vol. 54, No. 1, January 2001), it is not always conducive to the innovation that is our life-blood. So the pages of this newsletter remain open (but still under editorial control!) to everyone who has something interesting to say about particle accelerators. And I hope that the Beam Dynamics Panel will do everything it can to foster collaboration and embrace new ideas regardless of the largely spurious compartments into which physicists are thrust.

1.1.2 Next Panel Meeting

The next meeting of the Panel will be held at the Particle Accelerator Conference in Chicago, 18-12 June 2001. Like all other information pertaining to the Panel and its activities, the agenda will be available from our home page

http://wwwslap.cern.ch/icfa

in advance of the meeting. Anyone who would like to propose a topic for the agenda is welcome to do so. Any proposals for workshops should be made well ahead of the proposed dates to allow for the ICFA approval process. There are already 4 or 5 ICFA Advanced Beam Dynamics Workshops scheduled for the remainder of this year and the early part of next (see later).

1.2 From the Editor

Helmut Mais mais@mail.desy.de DESY

Dear colleague

As an editor of this issue of the ICFA Beam Dynamics Newsletter let me quote what our former chairman, K. Hirata, has written in the previous edition:

> The beam dynamics is the physics of the beam with a lot of application to accelerators. It is a study of the accelerator beam as a special state of the matter, where the practical and immediate usefulness is of secondary value ... it is impossible to divide the beam dynamics into useful and useless parts.

A good understanding of beam physics is essential for the optimal performance of existing accelerators and for an optimal design of future projects. Concepts, methods and tools are needed and used from many branches of physics, ranging from classical mechanics to statistical dynamics and quantum field theory. This makes beam physics a fascinating interdisciplinary field with widespread theoretical and experimental activities. I hope that a little bit of this variety of beam dynamics is reflected in this issue.

In this edition the activity reports of the high energy laboratories DESY and CERN describe upgrade programs for existing machines and future developments. The beam dynamics activities for synchrotron light sources and FEL's are described by M. Böge, A. Streun, E. Karantzoulis and G. Dattoli et al. Furthermore, and this is a great pleasure for me, we have activity reports from university groups in Bologna, Rostock, and Albuquerque covering a wide range of problems from space charge, nonlinear collective phenomena, spin dynamics to computational aspects of beam dynamics in accelerators. One category of articles supported by the Beam Dynamics Newsletter is *Review of Beam Dynamics Problems*. M. Conte and his colleagues present a review of the Stern-Gerlach force, an interesting but also controversially discussed topic.

At the end of these remarks I want to draw your attention to the Snowmass Workshop on the Future of Particle Physics with many working groups on beam dynamics issues. More information can be found on the workshop webpages

http://www.snowmass2001.org

2: Letters to the Editors

2.1 Errata for the Accelerator Handbook

A. W. Chao SLAC
achao@slac.stanford.edu

Dear Colleague,

As you probably know, there was a significant community effort devoted to the creation of a Handbook of Accelerator Physics and Engineering, published in 1999 by World Scientific. Maury Tigner and I were the editors, but the Handbook is the result of very hard work by many of the best minds in our field. Since its publication, the Handbook has received many good comments from the users.

However, we do have errors in the Handbook as printed. We also have sometimes additional pertinent material to be added to the content. For this purpose, I would like to bring your attention to the fact that, as mentioned in the Preface of the Handbook, there is an "Errata and Additions" document that runs on the Handbook webpage

http://www.wspc.com.sg/books/physics/3818.html

This Errata and Additions is being updated every few months or so. The latest update has been version Nov. 2, 2000. We encourage you to use these pages. We also ask for your help to please send us any errata or necessary additions you find by sending e-mails to the address given above so that we can include them on the next update. Your help will be much appreciated. Thanks for your attention and help in advance.

2.2 First Run of the Tevatron Electron Lens

V. Shiltsev shiltsev@fnal.gov FNAL

Since 1997 a team of Fermilab scientists and engineers carries out experimental R&D on compensation of beam-beam effects in the Tevatron proton-antiproton collider with use of low energy, high current electron beams (see Phys. Rev. STAB vol.2, 071001 (1999)). Our efforts focused on design and fabrication of a Tevatron Electron Lens (TEL) and resulted in creation of a 3.5 m long system of solenoid magnets in which we have propagating 3 mm diameter beam of 10 kV electrons with upto 3.5 A of current. When the beam collides with 1TeV antiprotons it can shift pbar's betatron frequency by some dQ=-0.01. A system of two TELs with time dependent currents can be used for equalizing betatron frequencies of different bunches in a multibunch operation of the Tevatron collider during Run II (so called, linear beam-beam compensation). Another TEL with Gaussian transverse current profile is thought to be useful for the elimination of the nonlinear tune spread in the antiproton bunch due to collisions with a strong proton beam.

The first TEL has been fabricated, tested and installed in the Tevatron in March 2001. It should demonstrate validity of the technique, that is provide the needed tune shift while not deteriorating the collider performance (vacuum, orbit, lifetime, etc.).

On March 23, 2001 in the very first beam shift we were able to demonstrate a betatron tune shift of 150 GeV proton beam which is proportinal to the electron current, namely dQ=+0.005*Je, or about 0.012 maximum for Je=2.3 A. In the following months we plan to continue the studies with 980 GeV beams, perform the system tuning, lifetime and emittance measurements, etc, to make the TEL a really operational device.

3: Activity Reports

3.1 Beam Dynamics Activities at DESY

3.1.1 The Luminosity Upgrade of HERA

Georg H. Hoffstaetter for the DESY
HERA Luminosity Upgrade Group
Georg.Hoffstaetter@desy.de

After the design luminosity has been exceeded [1, 2] in the electron–proton collider HERA, the interaction regions are being rebuilt to obtain smaller β^* at the two interaction points (IPs) [3, 4, 5]. This should increase the luminosity by about a factor of 4 yielding $\mathcal{L} = 0.74 \times 10^{32}$ cm^{-2}s^{-1}. To achieve this, it can not be avoided that the beam–beam tune shift of the e–beam is increased and that the vertical β^*_{py} of the protons becomes comparable to the proton bunch length. This implies new beam dynamical conditions. In accelerator studies, the beam–beam effects of the two HERA beams have been explored and the new low emittance optics has been implemented and tested with a polarized positron beam. These studies have been described in detail in [6, 7, 8] and will be summarized in this report. Part of these studies have also been reported in [9, 10, 11, 12, 2].

3.1.1.1 Introduction

With a length of 6336m, HERA is the largest accelerator at DESY in Hamburg. It provides collisions between a 920GeV proton beam and a 27.5GeV polarized electron beam and supplies four high energy physics experiments. H1 and ZEUS are the world's only high energy e/p collider experiments; HERMES and HERA–B have a fixed target. HERA–B scrapes the proton halo with wires, and HERMES has a polarized gas storage cell target in the polarized electron beam to analyze the polarized quark–gluon–structure of the nucleons. HERMES is currently the only experiment which takes advantage of the typically 60% polarization of the electron beam, since only around this experiment spin rotators bring the spins in a longitudinal direction.

Altogether there are 10 accelerators at DESY, 8 of which are required for providing HERA's high energy collisions. The other two are the 2nd generation light source DORIS and the TESLA Test Facility (TTF) with its integrated SASE FEL which produces the world's highest energy FEL x-ray beams with wavelengths between 180 nm and 80 nm. This facility will be upgraded to 6 nm wavelength by 2003 and is a test bed for the 33 km long TESLA linear collider.

Figure 3.1 shows how the integrated luminosity of HERA increased over the years in an exponential way to a total of around 180pb^{-1}. In the year 2000 HEAR exceeded its design goals with a luminosity of $\mathcal{L} = 0.2 \cdot 10^{32}$ cm^{-2}s^{-1} and an integrated luminosity of 67 pb^{-1}. But now a regime has been reached for which the curve is linear with time. To obtain a faster collection of integrated luminosity, a luminosity upgrade project is required. But this is not only a natural accelerator development, it is also strongly requested by the high energy physics community. HERA has been switched off in September 2000 to rebuild the interaction regions, and first beams are expected for the middle of July 2001.

For equal proton emittances $\epsilon_{px} = \epsilon_{py}$ and assuming that the proton beam size at the interaction point can always be matched by the electron beam ($\sigma_{ex} = \sigma_{px}$, $\sigma_{ey} = \sigma_{py}$), equation (3.1) shows that the luminosity can be increased by boosting the brightness N^p_{ppb}/ϵ_{px} of the p beam, by increasing the e current I_e, or by a decrease of the proton beta functions β^*_{px} and β^*_{py} at the collision

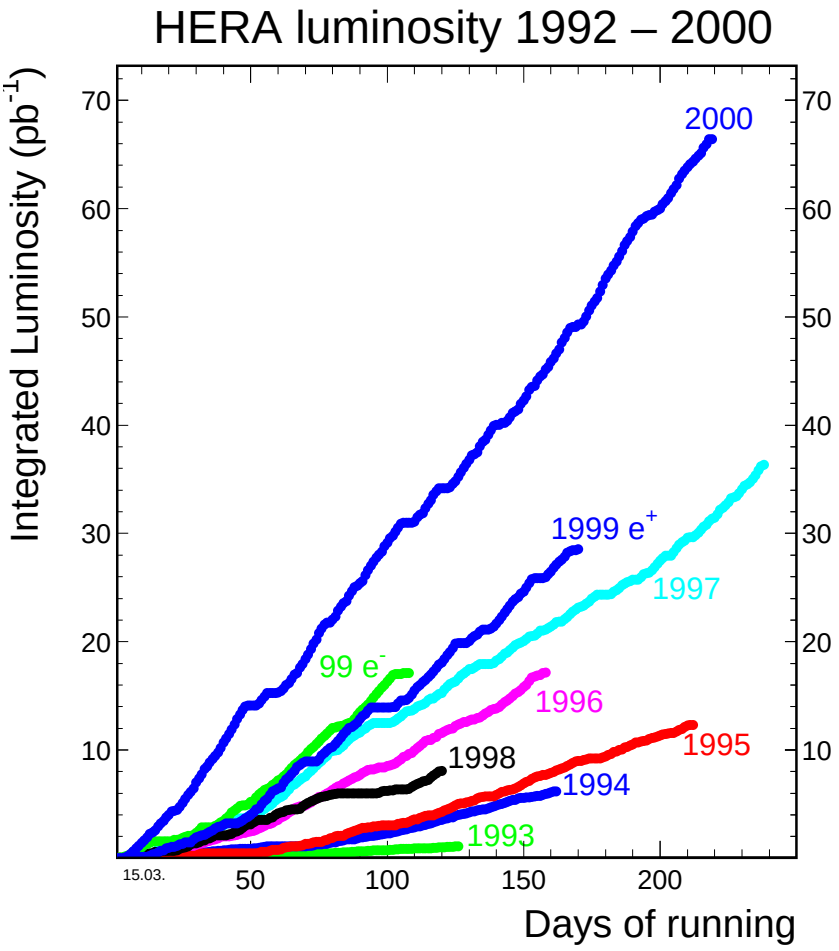

Figure 3.1: Integrated luminosity for each year of HERA running.

points,

$$\mathcal{L} = \frac{N^p_{ppb}}{\epsilon_{px}} \frac{I_e}{4\pi e} \frac{1}{\sqrt{\beta^*_{px}\beta^*_{py}}} \,. \tag{3.1}$$

These three measures have been found to be about equally expensive, but modifying the interaction region for obtaining smaller beta functions was found to be the safest method.

In order to focus the proton beam stronger in the experimental region, the electron beam has to be separated from the proton beam as early as possible [3, 4, 5, 9]. Whereas the first proton quadrupole is currently 26 m after the IP this distance will be only 10 m after the luminosity upgrade. Additionally the upgrade project includes 60 m long spin rotators at both sides of the H1 and ZEUS detectors. The complete upgrade involves 448 m of new vacuum pipes, 4 superconducting magnets for early separation of the e and p beams inside the detectors with a distance of only 2 m from the IP, and 54 normal conducting magnets. The superconducting magnets have been built by BNL and the normal conducting magnets have been built by the Efremov Institute in St. Petersburg.

Whereas the magnet arrangement around the detectors is currently symmetric, it will no longer be symmetric after the upgrade as shown in figure 3.2. Due to the bends inside the detectors the synchrotron radiation can no longer be collimated upstream of the experiment but has to be guided through the beam pipe. Starting at 11 m after the IP, the radiation fan has its own beam pipe

leading to a radiation absorber. Scattered electrons are collimated upstream of the detector by a bend section and gas scattering close to the detector is minimized by the installation of many NEG pumps.

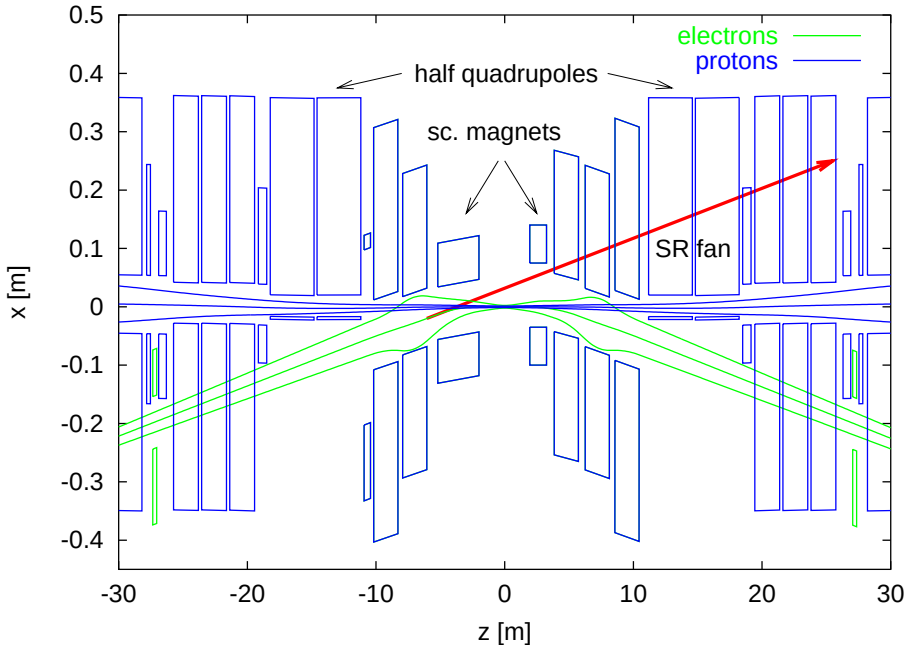

Figure 3.2: Layout of the interaction region after the luminosity upgrade.

Owing to the simultaneous presence of the proton beam, the electron beam, and the synchrotron radiation beam, some of the vacuum components are quite complicated. An example is shown in figure 3.3.

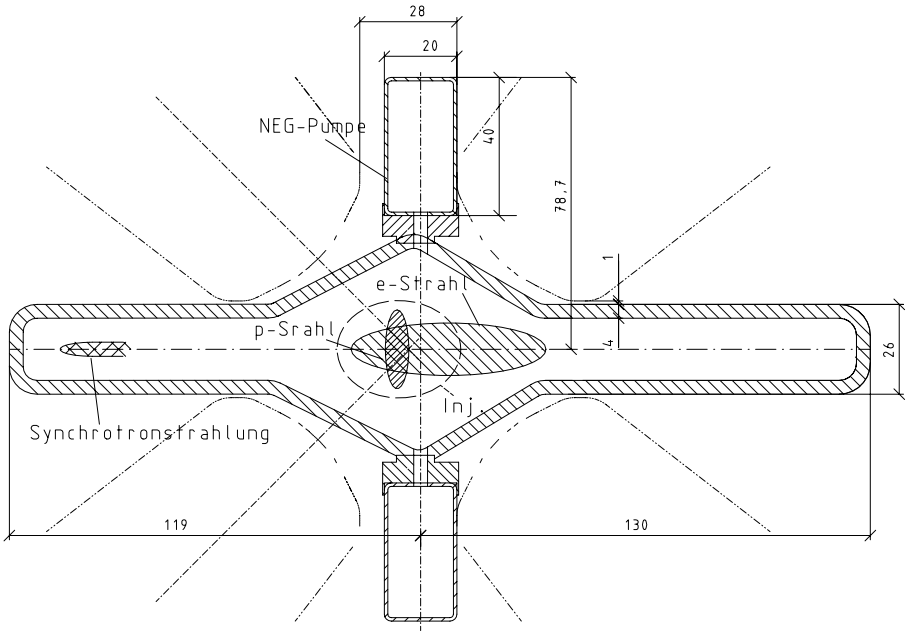

Figure 3.3: Custom designed vacuum chamber for the e beam, the p beam, and for the synchrotron radiation beam.

Also the detectors themselves will experience a major rebuild. Currently there are no magnets

Parameters	currently		after the Upgrade	
	e-ring	**p-ring**	**e-ring**	**p-ring**
E(GeV)	27.5	920	27.5	920
I(mA)	50	100	58	140
$N_{ppb}(10^{10})$	3.5	7.3	4.0	10.3
n_{tot}	189	180	189	180
n_{col}	174	174	174	174
β_x^*(m)	0.90	7.0	0.63	2.45
β_y^*(m)	0.60	0.5	0.26	0.18
ϵ_x(nm)	41	$\frac{5000}{\beta\gamma}$	20	$\frac{5000}{\beta\gamma}$
ϵ_y/ϵ_x	10%	1	17%	1
$\sigma_x/\sigma_y(\mu$m)	192/50	189/50	112/30	112/30
σ_z(mm)	11.2	191	10.3	191
$2\Delta\nu_x$	0.024	0.0026	0.068	0.0031
$2\Delta\nu_y$	0.060	0.0007	0.103	0.0009
Polarization	60%	0%	45%	0%
$\mathcal{L}$	$0.172{\cdot}10^{32}$		$0.744{\cdot}10^{32}$	
$\mathcal{L}_s$	$6.70{\cdot}10^{29}$		$17.9{\cdot}10^{29}$	

Table 3.1: Parameters of HERA before and after the luminosity upgrade.

inside the detector except of its huge solenoid for particle identification and the corresponding compensation solenoid. After the luminosity upgrade there will be two combined function magnets inside each detector. They are superconducting, to allow for a small diameter which can be fitted inside the detectors. The compensation solenoid will be eliminated and coupling will be compensated by skew quadrupole windings in these superconducting magnets and by 4 additional dedicated skew quadrupoles, 2 on each side of the interaction region. Together with the asymmetry of the interaction region, this will make spin matching more difficult and providing longitudinal electron polarization in the experiment will become quite challenging.

Important parameters of the luminosity upgrade project are shown in table 3.1. One of the critical points will be the exceptionally large vertical electron beam–beam tune shift $2\Delta\nu_{ey}$ due to the 2 collider experiments. The luminosity $\mathcal{L}$ is given in units of $\mathrm{cm}^{-2}\mathrm{s}^{-1}$ and the specific luminosity in units of $\mathrm{cm}^{-2}\mathrm{s}^{-1}\mathrm{mA}^{-2}$. The polarization has not been accurately simulated yet and 45% is only a rough estimate.

To reduce the electron spot size and to simplify the early separation of the beams, the electron emittance will be reduced from currently 41 to 20 nm by using $72°$ phase advance per FODO cell rather than the current $60°$, furthermore the frequency of the 500 MHz rf system will be shifted by about 250 Hz. The smaller beam sizes at the IPs and these emittance reduction schemes lead to changes in the beam dynamics which could lead to problems after the luminosity upgrade. Therefore potential problems have been identified and analyzed in accelerator physics studies. The following questions were analyzed:

- Will the reduced electron spot size cause too strong beam–beam forces on the protons?
- Will the reduced proton spot size cause too strong beam–beam forces on the electrons?
- Will the $72°$ focusing cause a too small dynamic aperture of HERA–e?
- Will the $72°$ focusing cause a reduction in polarization?

- Will the 72° focusing increase the luminosity as expected?
- Does the current rf frequency allow for the required frequency shift?
- Will the rf frequency shift cause a reduction in polarization?
- Will the rf frequency shift increase the luminosity as expected?

3.1.1.2 Investigation of Upgrade Concepts

Beam–Beam Force on the Proton Beam: The stronger beam–beam tune shift parameters shown in table 3.1 go along with stronger nonlinearities of the particle dynamics and could lead to a reduced dynamic aperture for the proton beam and therefore to reduced proton lifetimes.

To study these effects, a very irregular fill pattern of the electron ring was used [10, 13]. In this fill pattern some electron bunches were filled with only about 100 μA and others with up to 450 μA. These different electron intensities lead to different beam–beam forces for different proton bunches and therefore to different beam–beam tune shift parameters. For luminosity upgrade conditions, the total electron currents in HERA which would produce these beam–beam parameters would vary between 16 mA and 73 mA. But the design electron current is only 58 mA.

An investigation of the bunch by bunch specific luminosity showed that the specific luminosity was not smaller for the bunch pairs with large electron bunch current and also the luminosity lifetime did not diminish with a stronger beam–beam force for the protons.

It has however been observed that the proton lifetime diminished from about 200 h to 50 h for the bunches which collided with high current electron bunches. Furthermore the proton tail population was measured with the HERA–B target wire and could be shown to increase due to collisions with high current electron bunches.

The proton dynamics will therefore be significantly influenced by the stronger beam–beam forces after the luminosity upgrade but the achievable luminosity will not be limited by this effect.

Beam–Beam Force on the Electron Beam: The increased electron beam–beam tune shift parameters could lead to a blowup of the electron emittances and therefore to a reduction of the luminosity and of the electron lifetime.

The accelerator studies which have been performed to investigate the influence of an increased beam–beam force on HERA's electrons have been described in detail in [6]. The beam–beam force on the electrons can currently not be increased to the force expected for the luminosity upgrade since the proton currents are currently limited to about 110 mA and the proton beam can not be focused to a smaller spot at the IP before the upgrade magnets are installed specifically for that purpose. But a significant dependence of the specific luminosity on the proton current for today's HERA might hint at a beam–beam force induced increase of the e^+ emittance after the luminosity upgrade. To test whether such a dependence exists for today's HERA parameters, the specific luminosity at H1 for each bunch pair was plotted against the proton bunch current in figure 3.4. The bunch by bunch specific luminosity is displayed for each luminosity run of the first four months of the year 2000, where for each run the data were taken shortly after the start of the run. To establish that a beam–beam force induced blowup of the electron beam diminishes the luminosity, a noticeable drop of the luminosity at high proton currents would have to be visible, which is not the case.

With two collision points the beam–beam tune shift is larger than with one IP and a reduction of the specific luminosity due to a second IP in HERA could indicate a beam–beam induced blowup of an electron emittance. But it was observed that the luminosity with two IPs was slightly higher than with only one IP, which has been shown to be compatible with the creation of a beta beat

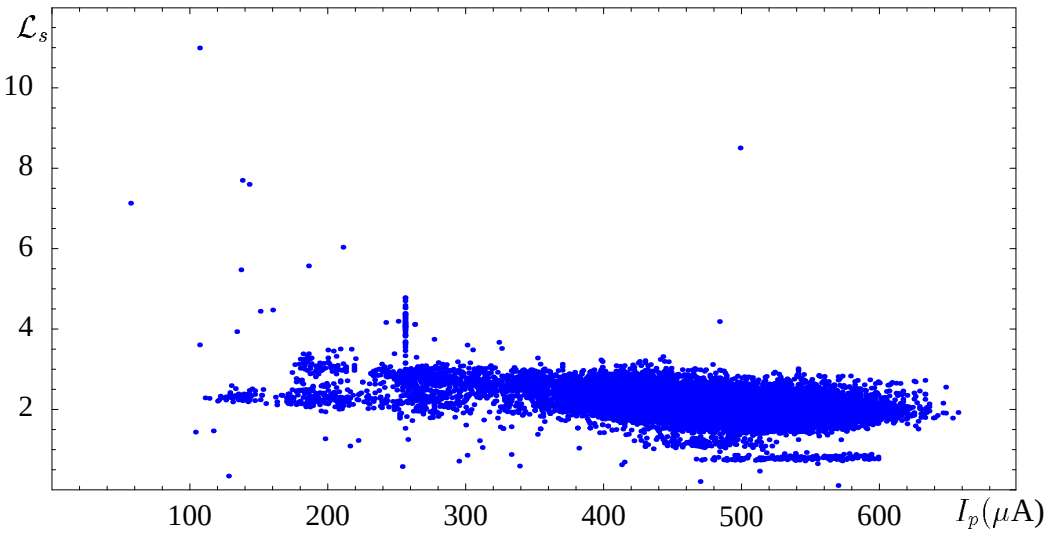

Figure 3.4: The specific luminosity $\mathcal{L}_s$ (arbitrary units) for each colliding bunch against the proton bunch current I_p (μA) as obtained by H1.

in one experiment which changes the luminosity in the other experiment. But no indication of an increased electron emittance has been found.

For a given proton current and spot size, the electron beam–beam tune shift can be increased by increasing the electron's beta functions at the IP above the luminosity values of $\beta^*_{ex} = 0.9$ m and $\beta^*_{ey} = 0.6$ m. To investigate if an increased electron beam–beam tune shift leads to an emittance blowup, e/p collisions were established for the electron injection optics with the current $60°$ focusing scheme in the arcs. This injection optics has beta functions of $\beta^*_{ex} = 2.2$ m and $\beta^*_{ey} = 0.9$ m which lead to beam–beam tune shift parameters of $\xi_{ex} = 0.026$ and $\xi_{ey} = 0.047$. For these parameters, which are similar to those expected for the luminosity upgrade conditions, no unexpected reduction in luminosity has been observed.

Since no beam–beam limitation has been observed under these simulated luminosity upgrade conditions, β^*_{ey} has been increased dramatically in 5 stages up to $\beta^*_{ey} = 4$ m. For these beta functions, the proton beam sizes were no longer matched to the electron beam sizes. To diminish this mismatch, the optics with increased beta functions had $72°$ focusing in the arcs and nominal emittances of $\epsilon_{ex} = 32$ nm. The luminosity was optimized by varying a vertical decoupling bump through sextupoles, which lead to an emittance coupling of less than 10%.

With a proton current of 90mA, a specific luminosity of $\mathcal{L}_s = 8.8 \cdot 10^{29}$ cm^{-2}mA^{-2}s^{-1} was reached for a spin matched $72°$ optics with $\beta^*_{ex} = 1$ m and $\beta^*_{ey} = 0.7$ m. The proton emittance was not measured but $\epsilon_{px} = 15\pi$ mm mrad, $\epsilon_{py} = 12.5\pi$ mm mrad would lead to this luminosity. Then five different optics with $\beta^*_{ex} = 2.5$ m, $\beta^*_{ey} \in \{1, 1.5, 2, 3, 4\}$ m were installed with separated beams at the interaction points and then luminosity was established and optimized for each of these optics. The value of $\beta^*_{ex} = 2.5$ m was chosen for each of these optics since the corresponding horizontal beam–beam tune shift of $2\Delta\nu_{ex} = 0.082$ is slightly higher than expected for the design proton current of 140mA after the luminosity upgrade. Figure 3.5 shows the luminosity which was achieved at ZEUS for the different β^*_{ey}. The fitted curve does not take into account the optics with $\beta^*_{ey} = 0.7$ m since this optic has $\beta^*_{ex} = 1$ m rather than $\beta^*_{ex} = 2.5$ m as in the other cases. This figure shows that the luminosity would be significantly larger than what was measured when the beam–beam force would not have influenced the electron beam.

The emittances measured at H1 and ZEUS are shown in figure 3.6 and a fit to the average

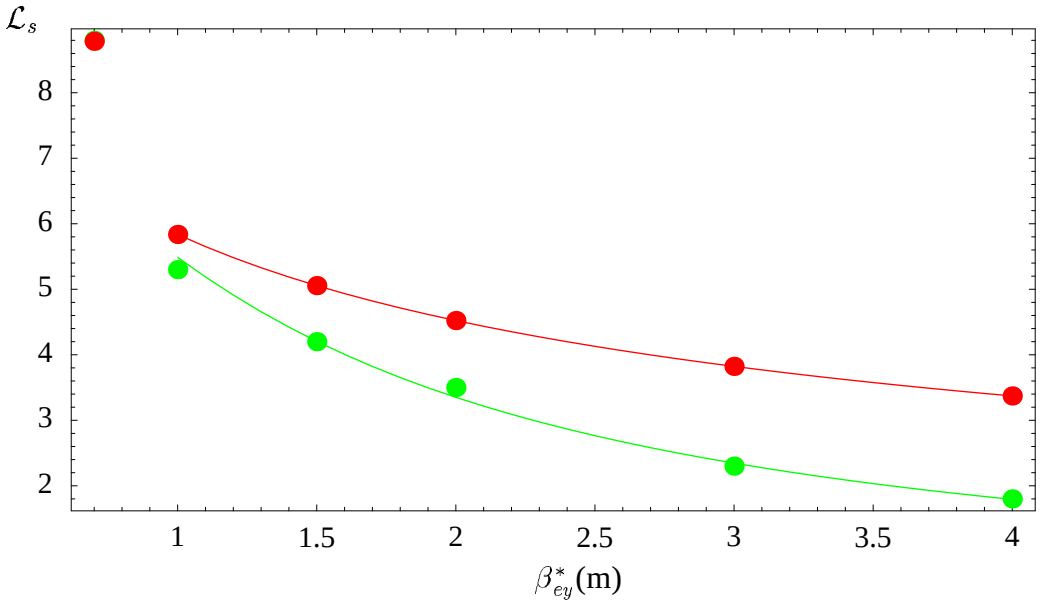

Figure 3.5: Bottom (green): The specific luminosity $\mathcal{L}_s$ in units of 10^{29} cm^{-2}mA^{-2}s^{-1} for six optics with different beta functions. Top (red): Computed specific luminosity when the beam–beam effect is not taken into account.

of the two measurements is also shown. It has been shown in [6] that the strong decrease of the luminosity in figure 3.5 is due to this blowup of the vertical emittance.

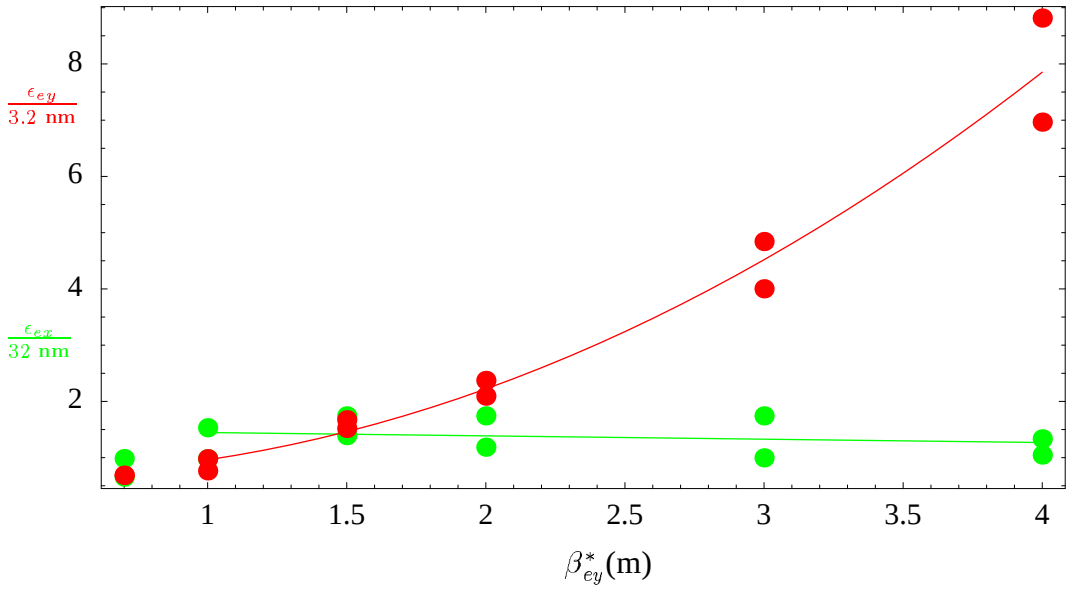

Figure 3.6: Top (red): The vertical emittance relative to the computed value of 3.2 nm. Bottom (green): The horizontal emittance relative to the computed value of 32 nm. While ϵ_{ex} does not seem to change much, the vertical emittance is blown up by up to a factor of 8.

While these studies show that the beam–beam tune shift parameter at HERA can lead to a very large blowup of the emittance, it is encouraging that such a blowup does not limit the luminosity for the vertical electron beam–beam tune shift parameter of the upgrade project which corresponds approximately to a vertical beta function of $\beta^*_{ey} = 1$ m in the figures 3.5 and 3.6. It is remarkable that HERA could be operated in stable luminosity condition with good lifetime for a

vertical emittance blowup of 8 and with a beam–beam tune shift parameter of 0.5, corresponding to $\beta^*_{ey} = 4$ m.

Dynamic Aperture: Changing from $60°$ to $72°$ focusing per FODO cell decreases the electron emittance, but it also increases the natural chromaticity. The chromaticity correction therefore requires stronger sextupoles which in turn reduces the dynamic aperture. Therefore a spin matched HERA–e luminosity optics with $72°$ was computed and the dynamic aperture for this optics was measured several times by kicking the beam to an amplitude where half the beam current is lost [8]. The dynamic aperture was found to be slightly above 12 σ which allowed an unproblematic operation of the electron ring.

Polarization: Figure 3.7 shows the first polarization optimization with the spin matched $72°$ optics [14]. First the vertical dispersion was minimized by an SVD procedure [15] and the vertical emittance was minimized by decoupling the linear optics with vertical bumps through sextupoles. Then energy scans and the harmonic spin matching bumps, which were computed for this $72°$ optics, were used very successfully to find a maximum polarization of 65% in only a few hours. Due to this extraordinary fast polarization optimization we trust that the stronger focusing after the luminosity upgrade will not cause a problem for the electron polarization.

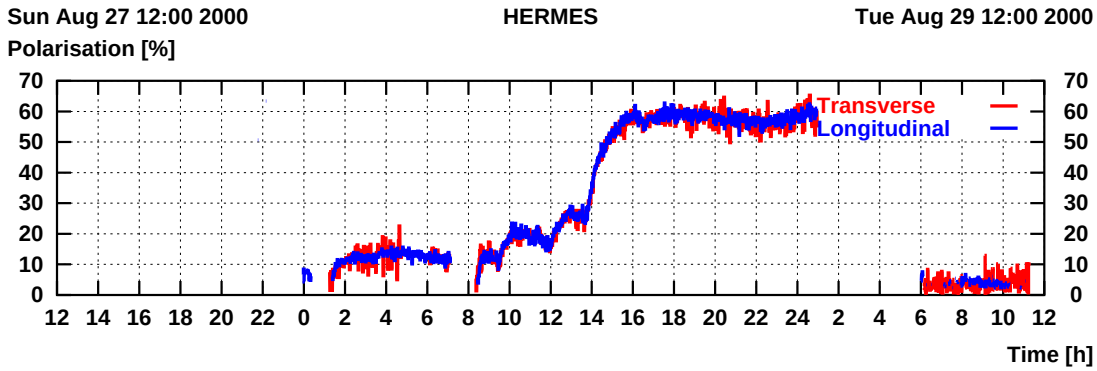

Figure 3.7: Polarization during optimization of the energy and the harmonic bumps of the $72°$ spin matched optics.

Luminosity: Finally we wanted to check whether the stronger focusing leads to the expected increase in luminosity. To check this, luminosity scans were performed as follows: The spin matched $72°$ optic was installed in the current ring and the e^+ and proton beams were brought into luminosity condition. Then the proton beam was shifted with respect to the e^+ beam and the luminosity was recorded as a function of the amplitude of the symmetric bump which shifted the proton beam. While a wire scanner was used to determine the proton beam size, this luminosity scan was used to determine the e^+ emittances. As a reference, a luminosity scan was also produced for the current optics of HERA-e with $60°$ phase advance per FODO cell.

The beam–beam force acting on the e^+ beam is changed during the luminosity scan. This leads to a varying kick on the e^+ beam and to a varying disturbance to the beta function. These two effects were taken into account when determining the emittances of the e^+ beam. The first of these effects turned out to be very important. The HERA proton beam was assumed to be unaffected by the beam–beam force during the luminosity scan.

While the specific luminosity in the $60°$ optics was around $7.4 \cdot 10^{29}$ $\mathrm{cm}^{-2}\mathrm{mA}^{-2}\mathrm{s}^{-1}$, the specific luminosity for the $72°$ optics was initially only about $5.4 \cdot 10^{29}$. A detailed analysis of the vertical

and horizontal luminosity scans was used to show that the electron motion had a strong coupling between the horizontal and the vertical plane. After this coupling was eliminated by vertical decoupling bumps through sextupoles and by an SVD based dispersion correction, the luminosity scan lead to $\epsilon_{ex} \approx 28$ nm and $\epsilon_{ey} \approx \epsilon_{ex} \cdot 3.3\%$, and a specific luminosity of up to $8.8 \cdot 10^{29}$ cm^{-2}s^{-1}mA^{-2} was obtained. The luminosity scan data are depicted in figure 3.8.

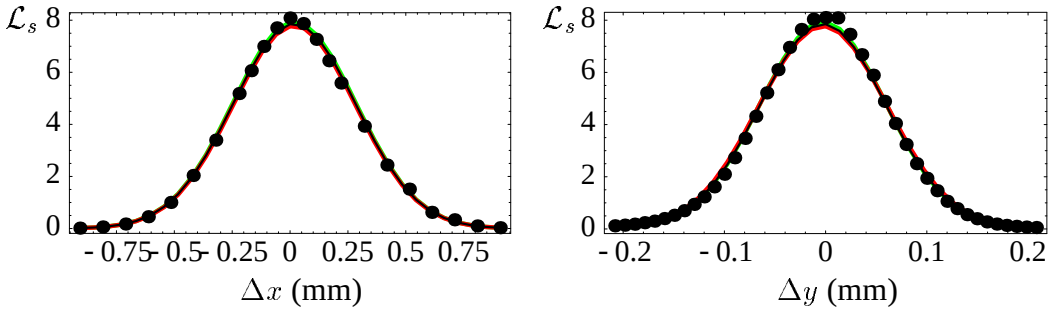

Figure 3.8: Luminosity scan at ZEUS. Left: The horizontal luminosity scan. Right: The vertical luminosity scan. The luminosity data (dots) and a bell curve fit (black) together with the expected luminosity (red and green) after correcting for the varying beam–beam kick and for the varying beam–beam lens.

RF frequency shift: An additional decrease of the emittance by shifting the frequency of the 500 MHz rf system by about 250 Hz is planed and therefore the deviation of the rf frequency from the center frequency was measured to find out whether there is sufficient margin for increasing the rf frequency. Table 3.2 shows the 6 different methods used to determine the current distance from the center frequency [8, 7]. The fact that HERA has so far been operated about 175 Hz below the center frequency shows that there is a comfortable margin for increasing the rf frequency for the luminosity upgrade.

Beam loss at damping poles	$\Delta f_{rf} = -163\text{Hz} \pm 20\text{Hz}$
Change in damping times	$\Delta f_{RF} = -250\text{Hz} \pm 150\text{Hz}$
Horizontal sextupole center of the ring	$\Delta f_{RF} = +130\text{Hz} \pm 25\text{Hz}$
Vertical sextupole center of the ring	$\Delta f_{RF} = -70\text{Hz} \pm 50\text{Hz}$
Change of the synchrotron light spot with Δf_{RF}	$\Delta f_{RF} = -175\text{Hz} \pm 70\text{Hz}$
Electron emittance from beam scraping	$\Delta f_{RF} = -160\text{Hz} \pm 60\text{Hz}$

Table 3.2: Different measurements for obtaining the center frequency of HERA.

Polarization: To check whether the electron polarization after the luminosity upgrade could suffer from the shifted rf frequency, the polarization was optimized in the 72° optics and then the rf frequency was increased by up to 500 Hz [14]. As shown in table 3.3 no significant decrease of the polarization has to be expected at frequency shifts of up to 400 Hz. This is an encouraging result since the envisioned frequency shifts are below 300 Hz. For each setting of the rf frequency, the magnetic field was suitably changed to keep the electron energy constant. If this had not been done, the frequency shift of 500 Hz would have produced an energy change of about -50 MeV, which would have greatly influenced the polarization.

Δf_{rf}(Hz)	$< x >$(mm)	P (%)
200	-0.28	59.7 $\pm$0.7
300	-0.43	61.1$\pm$0.6
350	-0.50	61.3$\pm$0.5
400	-0.57	59.6$\pm$0.5
500	-0.71	58.3$\pm$0.5

Table 3.3: Polarization for different frequency shifts. The rms closed orbit $< x >$ produced by changing the circulation time is also shown. For each setting of the rf frequency, the magnetic field was suitably changed to keep the electron energy constant.

Luminosity: After luminosity conditions had been established with the $72°$ optics, the frequency of the 500 MHz system was slowly increased by 250 Hz while the luminosity was recorded. The resulting relative increase in luminosity at H1 and ZEUS is shown in figure 3.9. The relative increase of the luminosity was stronger than initially expected but resembles the theoretical curve in figure 3.9 remarkably well after it was considered that the current rf frequency is about 175 Hz below the center frequency of HERA–e.

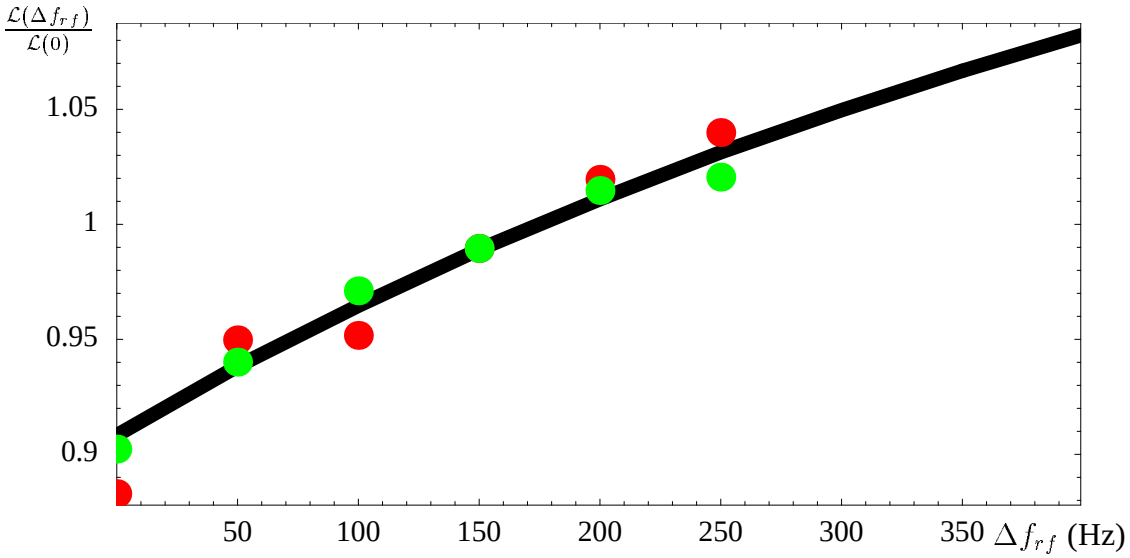

Figure 3.9: Relative increase of luminosity with increasing frequency in the 500 MHz electron rf system for ZEUS (red), H1 (green), and simulated (black).

3.1.1.3 Conclusions

We conclude that the performance goal of the HERA luminosity upgrade of $\mathcal{L} = 0.74{\cdot}10^{32}$ cm^{-2}s^{-1} is not unrealistic and we are confident that it will be achieved. In [2] it has been described that the available aperture margins and proton emittances which can be smaller than designed will be helpful to compensate a possible shortfall of beam intensity in the short term.

References

[1] G. H. Hoffstaetter, "Future Possibilities for HERA", *Proceedings EPAC 2000, Vienna* (2000)

[2] G. H. Hoffstaetter and F. Willeke, "Future HERA High Luminosity Performance", *Proceedings HEACC 01, Tsukuba* (2001)

[3] Editor: U. Schneekloth, "The HERA Luminosity Upgrade", Report DESY–HERA–98–05 (1998)

[4] M. Seidel, "The Upgraded Interaction Regions of HERA", Report DESY–HERA–00–01 (2000)

[5] M. Seidel, "Layout of the Upgraded HERA Interaction Regions", Proceedings of EPAC00, Vienna (2000)

[6] G. H. Hoffstaetter (ed.), "HERA Accelerator Studies 2000", *Report DESY–HERA–00–07* (November 2000)

[7] G. H. Hoffstaetter (ed.), "HERA Accelerator Studies 1999", *Report DESY–HERA–00–02* (May 2000)

[8] G. H. Hoffstaetter (ed.), "HERA Machine Studies December 1998", *Report DESY–HERA–99–03* (March 1999)

[9] G. H. Hoffstaetter, "Electron Dynamics after the HERA Luminosity Upgrade", *Proceedings EPAC 2000, Vienna* (2000)

[10] M. Bieler et al., "Recent and Past Experiences with Beam-Beam Effects at HERA", *Proc. Beam–Beam Effects, CERN* (1999) and in *Report DESY–HERA–99–04* (1999)

[11] G. H. Hoffstaetter, "New Beam Optics for HERA-e: Theoretical Investigations and Experimental Tests", in *Report DESY–HERA–99–04* (1999)

[12] G. H. Hoffstaetter and F. Willeke, "Electron Dynamics in the HERA Luminosity Upgrade Lattice of the Year 2000", *Proceedings PAC 99, New York* (1999)

[13] M. Bieler, E. Gianfelice, G. Hoffstaetter, T. Limberg, M. Minty, and F. Willeke, "Experiments about the Beam–Beam Effect at HERA", *in [7]* (2000)

[14] E. Gianfelice, "Measurement of Beam Polarization in a 72°/72° Spin Matched Optics", *in [6]* (2000)

[15] W. Decking, "Simultaneous Global Orbit and Dispersion Correction", *in [6]* (2000)

3.1.2 Lepton Beam Polarisation at HERA

E. Gianfelice mpyeli@mail.desy.de DESY

3.1.2.1 Polarised Electrons at HERA: Experience

Lepton beam polarisation has a relatively long tradition at DESY. Back in 1982, natural vertical beam polarisation (due to the Sokolov–Ternov effect) as high as 80% was measured at DORIS II at 5.02 GeV. For PETRA, working at larger energy, a special orbit correction scheme was developed by R. Schmidt and R. Rossmanith and successfully applied which, together with an adjustment of the machine energy (16.52 GeV), allowed to increase the natural polarisation from about 50%

to 75-80%. D. P. Barber, H. Mais and G. Ripken contributed later on to a generalisation of this correction method.

The experimental observations have been accompanied by valuable efforts of understanding the mechanism of beam polarisation (let me cite, in a roughly chronological order, A. Chao, who wrote the famous program SLIM during his stay at DESY, G. Ripken, H. Mais, D. P. Barber) in storage rings and developing the needed computational tools (A. Chao, L. Hand, J. Kewisch, D. P. Barber, T. Limberg, M. Böge).

An integral part of the original HERA design was the provision of *longitudinally* spin polarised $e^{\pm}$ beams for the collider experiments. The natural vertical beam polarisation is rotated into the longitudinal direction at the experiments by spin rotators. There were doubts in the scientific community about whether large beam polarisation could be observed in high energy storage rings (the design HERA-e energy was 30 GeV, the machine is actually running at 27.5 GeV) and whether it could be maintained in the presence of spin rotators. Moreover in a collider such as HERA the interaction with the counter–rotating beam was also expected to be a source of depolarisation.

Transverse beam polarisation (8%) was observed for the first time at HERA in November 1991 when the Compton polarimeter measuring the transverse polarization in the West section of the machine was brought in operation. After dedicated machine tuning in Summer 1992, transverse polarisation was increased to about 56%. Since that time high transverse polarisation (between 50 and 70%) became a routine aspect of the machine operation. This success played a decisive role in the approval of the HERMES experiment (which uses the lepton beam on a internal (un)polarised gas storage cell target) and of the installation of a first pair of spin rotators (designed by J. Buon and K. Steffen) during the 1993–1994 shut down to provide longitudinal polarisation of the lepton beam to that experiment.

The vertical bending magnets of the rotators were turned on for the first time on May 4, 1994 and polarisation attained 56%.

Since 1996 while the proton current and the specific luminosity have steadily increased, a clear correlation between $e^{\pm}$ polarisation and luminosity has been observed. By careful machine tuning it has nevertheless been possible to cope with the beam–beam interaction and to deliver longitudinal beam polarisation between about 50% and 60% to HERMES.

Since 1996 a second polarimeter, measuring the longitudinal beam polarisation at the HERMES location, has been made available by that collaboration, allowing to measure the single bunch polarisation. This gave the opportunity of making very interesting observations related to the beam-beam interaction.

3.1.2.2 Polarised Electrons at HERA: Future

Since September 2000, HERA has been undergoing important changes of the interaction region layout in order to increase the collider luminosity. Moreover the aim of the project is not only to preserve the lepton beam polarisation for HERMES, but also to deliver longitudinal polarisation to the collider experiments for which two more pairs of rotators are being installed. It is not easy to cope with all these tasks.

The beam polarisation aspects of the luminosity upgrade project have been studied by D. P. Barber, M. Berglund and myself.

In the new design the size of the $e^{\pm}$ and p beams at the Interaction Point (IP) has been reduced and the machine magnets have been moved closer to the IP. Owing to lack of space, the anti-solenoids, which were located beside the experiment solenoids, had to be removed. For compensating the betatron coupling skew quadrupoles have been introduced at about 120 meters from the IP.

The long H1 solenoid will overlap with one of the combined function machine magnets close to the IP, thus creating a distortion of the closed orbit and of the equilibrium polarisation direction (the periodic solution to the Thomas-BMT equation along the closed orbit). These effects will be locally compensated.

The stronger focusing in the new Interaction Regions and in the FODO cells (where the phase advance has been increased from 60 to 72 degrees in both planes) increases the non-linearities and makes the machine more sensitive to alignment errors.

The additional two spin rotator pairs decrease the maximum polarisation attainable by the Sokolov-Ternov effect from 89% (one rotator pair) to 83.3%.

The results of the simulations have shown that the degree of polarisation is limited by the horizontal betatron motion in the solenoids for the ideal machine including the experiment solenoids and their compensations and, in addition, by the synchrotron motion in the presence of realistic alignment errors. For the latter case, the linear spin motion computations by SITF predict a level of polarisation of 64 ± 2.2 %, whereas the results of the non-linear spin motion simulations by the tracking code SITROS oscillate between 52% and 63%. It should be mentioned that, although the number of points at which radiation takes place in the SITROS simulations has been largely increased, the equilibrium transverse beam size found by the tracking is up to 20% larger than the value computed analytically. This blow up is not confirmed by MAD simulations. It is therefore likely that the SITROS values for the beam polarisation are somewhat pessimistic.

3.1.3 Linear Collider and FEL Experiments at the TESLA Test Facility Linac

P. Castro for the TESLA Collaboration pcastro@mail.desy.de DESY

3.1.3.1 Overview of the TESLA Test Facility

The major challenge for the TESLA collaboration was to prove the feasibility and reliability of achieving accelerating gradients well above 20 MV/m, i.e. high enough for the 500 GeV linear collider. The TESLA Test Facility linac (TTFL) at DESY was constructed to show that the high gradients achieved in the cavities could be maintained during assembly into a linac test string, and then successfully operated with auxiliary systems to accelerate an electron beam to a few hundred MeV. The basic characteristics of the TTFL were designed to be as consistent as possible with the parameters of the TESLA linear collider design.

The original proposal for the TTF [1] was for a linac test string of four cryogenic modules, each containing eight superconducting nine-cell TESLA structures. The initial design goal was 15 MV/m, which was at that time substantially higher than superconducting cavities operated at other accelerator laboratories. Shortly after finishing the first design of the TTFL, it became clear that the test linac would be almost ideal to drive a Free Electron Laser (FEL) based on the principle of Self Amplified Spontaneous Emission (SASE): therefore the overall layout was changed and the FEL became part of the TTF project [2, 3].

The TTF (linac) programme for the accelerator modules was planned to check many of the aspects of operation in the linear collider:

- gradient achievable in a standard linac module;
- input coupler and higher-order mode (HOM) coupler performance;
- radio frequency (RF) control of multi-cavity systems;
- Lorentz force detuning and microphonic noise effects;

- RF conditioning of cavities and couplers;
- vacuum performance / failure recovery potential;
- cryostat design and cryogenic operation / heat load;
- dark current;
- energy and beam position feedback and control;
- alignment.

The TTF Linac was constructed to gain experience with the new components (cavities, klystrons, diagnostics, etc.) during continuous long term operation. As of writing, the total beam time at the TTFL was about 8,000 h. In addition, important experience with the FEL operation was obtained (see section 3.1.3.10).

3.1.3.2 Layout of the TTF linac

The TTF linac at DESY has been designed, built, installed and operated by the TESLA collaboration. The schematic of the linac is shown in figure 3.10.

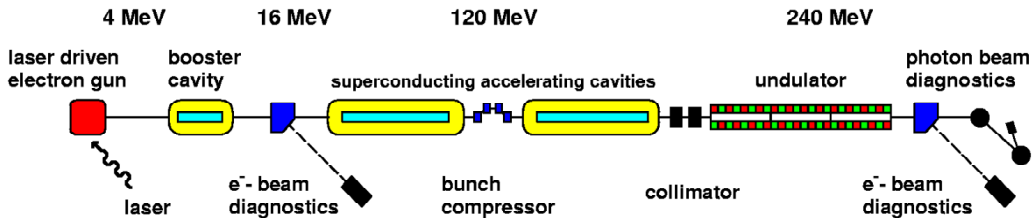

Figure 3.10: Schematic layout of the TESLA Test Facility Linac (TTFL). The total length is about 120 m.

The TTFL in its present set-up consists of the following sections:

- injector area;
- two accelerator modules;
- bunch compressor section;
- collimator section;
- undulator; and
- high energy beam analysis area together with the photon beam diagnostics.

The injector area includes the electron gun, the superconducting booster cavity, focusing lenses, and beam diagnostic equipment for the full characterization of the electron beam properties. The booster cavity is identical to one of the standard nine-cell structures in the main linac. The principal parameters of the injector are listed and discussed in the following sections.

The two installed cryomodules (each 12.2 m in length) comprise the main body of the linac. Each cryomodule contains eight nine-cell cavities, a superconducting quadrupole / steerer package, and a cold cavity type beam position monitor. Each accelerating structure has an input coupler for RF power, a pickup antenna to measure the cavity field amplitude and phase, two HOM damping couplers, and a frequency tuning mechanism. The two cryomodules are connected by a cryogenic line bypassing the bunch compressor.

Injector		TTF Linac design/achieved	
		Inj. I	Inj. II
Injector energy [MeV]		10 / 12	20 / 16
Norm. emittance [π mm mrad]			
at 37 pC (only Inj.I)		5 / 3	
at 8 nC (only Inj.II)			20 / 15
at 1 nC (only Inj.II)			2 / 4
Bunch frequency [MHz]		217 / 217	1-9 / 0.1-2.25
Bunch charge [nC]		0.037 / 0.037	1-8 / 0.1-10
Linac	TESLA	TTF Linac design/achieved	
Linac energy [MeV]	250000	255 / 300	
RF frequency [GHz]	1.3	1.3	
Accel. grad. [MV/m] with beam	23.4	15 / 14, 19, 22	
Unloaded quality factor [10^{10}]	1.0	0.3 / $>$ 1.0	
No. of cryomodules	2628	4 / 3 + 2	
Energy spread, single bunch rms	5×10^{-4}	$\approx 10^{-3}/10^{-3}$	
Energy variation, bunch to bunch	5×10^{-4}	$\approx 2\times10^{-3}$/2×10^{-3}	
Bunch length, rms [μm]	300	1000 / 400	
Beam current [mA]	9.5	8 / 8	
Beam macro pulse length [μs]	950	800 / 800	

Table 3.4: TESLA-500 – TTF Linac parameters comparison.

The bunch compressor section between the two cryomodules is used to reduce the electron bunch length produced in the electron gun by roughly a factor of four. The shortening of the bunch increases the peak bunch current to several hundred Amperes, which is required for a high gain of the FEL.

A collimator section in front of the undulator protects the vacuum system as well as the permanent magnets of the undulator. Because of the small electron beam diameter in the undulator, a beam loss in this approximately 15 m long section would be a high risk for the linac vacuum system. Radiation from beam losses could also cause a reduction of the magnetisation of the permanent magnet material in the undulator.

The undulator consists of three sections, each 4.5 m in length. The sinusoidal magnetic field has a period of 2.73 cm. Focusing of the beam is accomplished using additional permanent quadrupole magnets. Beam position monitors and wire scanners are installed between each section and in front and behind of the complete undulator. Additional beam position monitors within the undulator sections themselves can be used for improving the needed overlap between the magnetic axis of the undulator, the electron beam, and the emitted photon beam.

The high energy beam analysis area allows the full analysis of the electron beam parameters. Transverse profile, divergence, energy, energy spread, and bunch charge can be measured bunch by bunch. Other measurements (e.g. bunch length) require a scan over several bunches. The photon diagnostic section downstream of the undulator allows the full characterization (intensity, time structure, and spatial distribution) of the FEL photon beam.

The design parameters for the TTF Linac are summarized in table 3.4. The achieved parameters listed summarise the results of the year 2000 run. A description of the various experiments, component development, and achievements is presented in the following sections.

3.1.3.3 Electron gun

The test of superconducting cavities with the design bunch charge and beam pulse current and length was planned as part of the TTF program. A radio frequency (RF) gun is the state-of-the-art way to generate this electron beam. Furthermore, the X-ray FEL requires bunches of sub-picosecond length at 1 nC charge. At present only laser-driven RF photocathode guns are capable of producing such ultrashort bunches. The small emittance can be preserved by rapidly accelerating the electrons to relativistic energies where the effects of space charge forces become small. For these reasons an RF gun was chosen as the electron source for the TTF linac, although the specified beam macro pulse length of 800 μs presented a considerable challenge.

Since the development of the RF gun required some time, a thermionic gun was used in the first injector (Inj. I) [4] of the TTF linac. The grid of the thermionic gun was modulated with a subharmonic of the main RF frequency, 1300/6 = 217 MHz, to produce an 800 μs long train of electron bunches with a charge of 37 pC, a length of 660 ps and a spacing of 4.6 ns. After electrostatic acceleration to 250 keV the electrons were injected into a 217 MHz copper cavity where a velocity modulation was imposed on the particles to achieve a longitudinal compression in the following drift space. A superconducting 9-cell cavity, the booster cavity in figure 3.10, raised the energy to 12 MeV. This electron beam has been used to commission the TTF linac and to check many technical components. In particular it has been possible to operate the superconducting cavities with full beam loading [5] and to verify the proper functioning of the klystron, the high power RF distribution system and the digital RF control system. Furthermore, first studies of higher-order modes and multibunch effects were made using this injector (see below).

The development of an RF gun was started at FNAL [6], based on the existing design of operating RF guns at BNL and Los Alamos. Later, an alternative design was pursued at DESY [7] which tried to optimise the gun with respect to the FEL beam emittance requirements: a coaxial RF input coupler is used, which improves the axial symmetry of the accelerating field and gives more freedom to optimize the pattern of the superimposed magnetic field at the cathode (i.e. the position of focusing solenoids).

The main challenges of the RF gun development were:

- the long macro pulse of 800 μs length;
- the high gradient of 35 MV/m at the cathode surface;
- a long life time of Cs_2Te cathodes with high quantum efficiency;
- experience with a cathode preparation system [8, 9].

In addition, the development of a UV laser with sufficiently high power and a pulse structure suitable to produce the required electron beam time structure [10] presented a considerable challenge.

The FNAL RF gun has been in use at DESY since 1998. The laser, RF supply ($\sim$2.2 MW), amplitude and phase controller, water cooling system, and cathode preparation and handling system are all used routinely. At gradients above 30 MV/m we routinely have 800 μs long RF pulses in the gun. The dark current (typically 100 μA) at the gun exit is low enough to scrape off. The laser produces the required pulse structure, although for FEL operation the pulse length should be shortened. Gun conditioning is, however, problematic and generally time consuming, and additional minor design problems are still under investigation. Details of the results of the operation of the FNAL RF gun are given in [11]. A major concern has been the increase of dark current within several weeks of run with beam. The origin of the dark current and its effects on the linac have been understood to a large extent [12]. In the recent months, several technical solutions were applied, which reduced the amount as well as the effects of dark current. Further R&D on the gun

and beam transport to the first accelerating module will be carried out using the DESY RF gun [13].

3.1.3.4 Booster Cavity and Low Energy Beam Analysis Area

The approximately 4 MeV electron beam from the RF gun is injected into the booster cavity which is a standard nine-cell TESLA cavity. This cavity was one of the first prepared for the TTFL. Its field emission onset is about 14 MV/m. A feedback system [14] allows the cavity to operate with an amplitude stability better than 0.1%, and a phase stability of better than 1°. The cavity was operated with full beam loading and with the design beam parameters. The typical beam energy downstream of the booster cavity is 16 MeV.

The beam transport system at 16 MeV consists of a magnetic dipole chicane, a spectrometer section ending at a beam dump, and the straight matching section to the first accelerator module. The chicane was installed to study bunch shortening at low energies. The challenge facing the injector beam transport is to achieve a low emittance as well as a short bunch length under the presence of large space charge forces. At 1 nC the optimized normalized emittance was measured at 4 mm mrad, and at 8 nC approximately 15 mm mrad [15, 16, 17].

The spectrometer arm is used to tune the injector with respect to energy and energy spread. At 16 MeV beam energy the optimized relative energy spread was measured at 0.2 % (rms).

3.1.3.5 Accelerator modules

The layout of the TTF linac accelerator modules is very similar to the layout for the TESLA main linac, which is described in detail in [18]. The main difference is the length, which is about 12 m for the TTF modules and about 17 m for TESLA. The reason is that the TTF modules accommodate eight 9-cell cavities whereas 12 cavities are foreseen for the TESLA linac modules.

Results of measurements of the static heat load at the various temperature points are listed in table 3.5. The somewhat higher value at 2 K with respect to the design heat load is due to the cables for additional diagnostics (e.g. temperature sensors, vibration sensors), which will not be present in the TESLA linac modules.

	static load (design)	static load (meas.)
at 2 K / Watts	2.8	4
at 4.5 K / Watts	13.9	13
at 70 K / Watts	76.8	78

Table 3.5: Summary of TTF heat load for one accelerator module.

As of writing five accelerator modules have been built since the beginning of the TTF programme. Three of them have been installed in the TTFL; the last two are foreseen for the extension of the linac to higher energies. Cavities operated in the TTFL have shown slightly lower gradients compared to the vertical or horizontal cavity tests. This is because of different field emission onsets, and because the operation of several cavities connected to one single klystron is limited by the worst cavity. The maximum gradients achieved (at quality factors higher or equal to the design value of $Q_0 = 10^{10}$) with the three modules are given in table 3.6.

In the linac a total of 16 cavities are driven by one klystron. The cavities have been routinely operated at a gradient of $\approx$15 MV/m providing a 260 MeV beam for different experiments including stable FEL operation. The achieved relative amplitude stability of 2×10^{-3} and absolute

module No.	module name	RF test ($Q_0 > 10^{10}$)	beam operation
1	1 (ACC1 old)	17.5	14
2	2 (ACC2)	21.2	19
3	3 (ACC1 new)	23.6	22
4	4	25.4	to be tested
5	1*	25.3	to be tested

Table 3.6: Gradients achieved in the TTF Linac accelerator modules.

phase stability of 0.5° complies with the requirements. Residual fluctuations are dominated by a repetitive component which can be further reduced be using an adaptive feedforward, significantly surpassing the design goals [19].

One of the major challenges for the RF control of superconducting cavities is the Lorentz force detuning: the electromagnetic field inside the structures deforms the cavity causing it to detune. The frequency change scales with the square of the accelerating gradient and depends on the mechanical stiffness of the cavities. At high gradients the frequency change is comparable with the bandwidth, and the stabilization of the field amplitude requires additional RF power. Recently an active system was successfully tested which compensates the frequency detuning by means of a piezoelectric tuner [20].

The transport of very low emittance beams along the TESLA linac requires transverse higher-order mode (HOM) damping: the HOM Q values should not exceed $\sim 10^5$. HOM couplers mounted on the beam tubes of the TESLA nine-cell superconducting cavities are foreseen for this purpose. So-called 'trapped' modes whose energy is concentrated in the central cells of the cavity can only be detected using the accelerated electron beam [21]. In a dedicated experiment using an intensity-modulated beam from injector-I, a high-order 2585 MHz dipole mode was found with a Q factor up to 9×10^5 [22]. The mode could be identified with the highest mode of the third dipole passband. The high Q factor is outside the specifications for the TESLA linac, but is expected to be avoidable by a better control of the cavity's geometry or a slight re-positioning of the HOM coupler (or both).

One of the measurements performed with long beam pulses is shown in figure 3.11. An almost 800 μs long macro pulse comprising 1800 bunches with more than 3 nC bunch charge each was accelerated in the TTF Linac. With the macro pulse current being about 8 mA, the bunch charge was stable within ~10%, the achieved energy stability was σ_E/E=0.07%. The above mentioned RF control of the superconducting cavities was used together with a beam loading compensation.

3.1.3.6 Bunch Compressor

The free-electron laser operation mode of the TTFL requires short electron bunches with high intensity. Therefore, a bunch compressor is inserted between the two accelerating modules to increase the peak current of the bunch up to 500 A, corresponding to 0.25 mm bunch length (rms) for a 1 nC bunch with Gaussian density profile. The compression is achieved by making use of the path length difference for particles of different energy in a bending magnet system (chicane). By accelerating the bunches slightly off-crest in the RF wave, particles in the bunch head have a lower energy than in the tail and thus travel a longer distance in the chicane.

It is routinely verified that a large fraction of the bunch charge is compressed to a length below 0.4 mm (rms) [23]. In addition there are indications that the core is compressed even further, giving an estimated peak current of 400 ± 200 A. At these short bunch lengths, coherent synchrotron

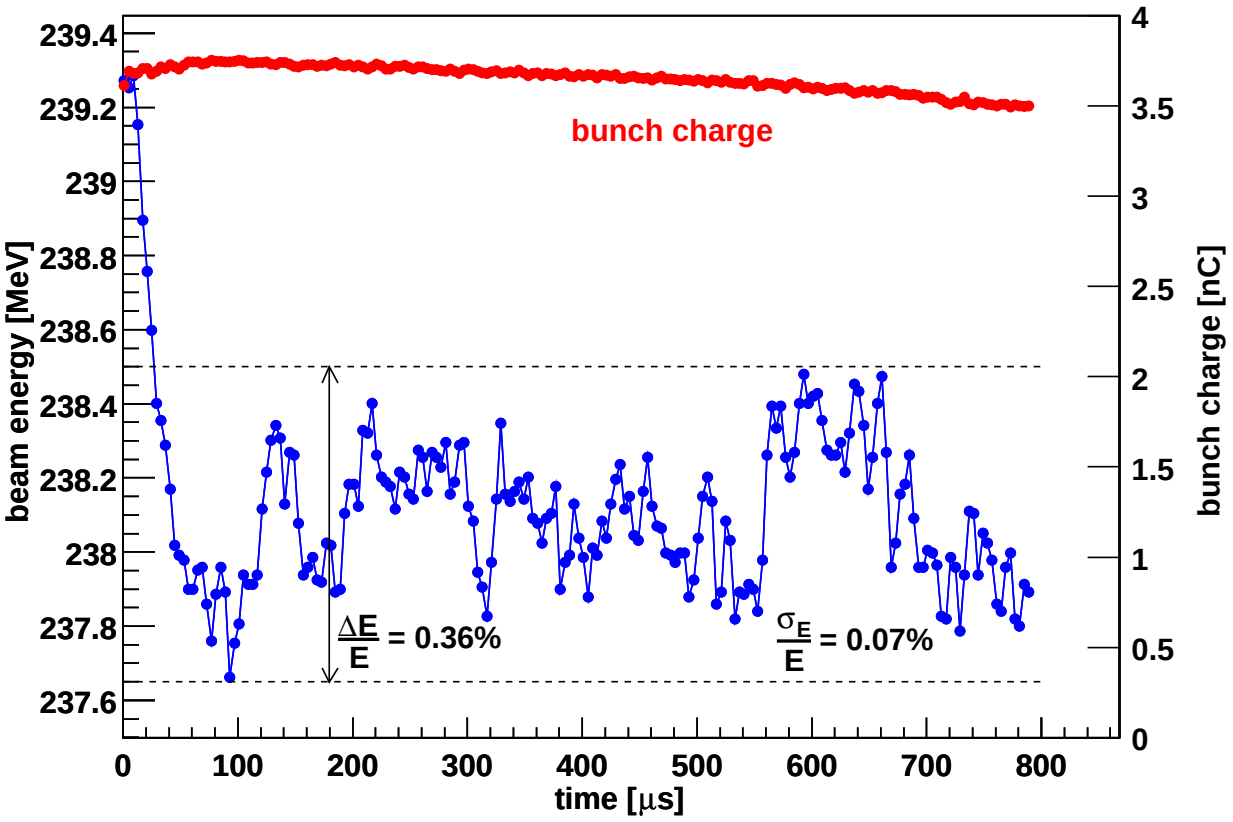

Figure 3.11: Acceleration of long macro pulses. The beam energy and the bunch charge within one single macro pulse are shown. The RF control system was operated with beam loading compensation. The bunch spacing was 444 ns.

radiation produced in the magnetic chicane may affect the emittance and the energy spread of the bunch (see section 3.1.3.9).

3.1.3.7 Collimator

The second installed accelerator module of the TTFL is followed by a collimator section which combines the transverse matching of the electron beam to the undulator with the protection of the undulator vacuum chamber and magnets. As a consequence of the small beta function in the undulator — typically 1 m, corresponding to an rms beam sizes of $\sim$100 μm — it only requires 10 bunches with 1 nC charge to burn a hole into the vacuum chamber. In addition radiation damage of the Sm_2Co_{17} permanent magnets in the undulator from either beam halo (dark current) or direct beam loss could degrade the field quality. The collimator consists of a pair of spoiler / absorber units, and the optics (quadrupole settings) is matched so that the physical apertures of the downstream undulator lie within the collimator shadow.

3.1.3.8 Undulator

An undulator with high magnetic field, and a very good overlap between the photon and the electron bunches are essential for SASE FELs. The undulator is a 12 mm gap permanent magnet device which uses a combined function magnet design [24]. It has a period length of 27.3 mm and a peak magnetic field of 0.46 T, resulting in an undulator parameter of K = 1.17. The undulator field alone was measured to have deviations in the second field integral $\int_0^{L_u} \int_0^s B(s')ds'ds$ from an ideal field between 3 and 6 T·mm^2 rms [25], which would induce an rms orbit deviation of about 5 μm at 300 MeV. The beam pipe diameter in the undulator (9.5 mm) [26] x is much larger than the beam diameter (300 μm). Electron beam focusing is achieved by integrated quadrupoles producing a gradient of 12 T/m superimposed on the periodic undulator field. The alignment of these quadrupoles is better than 50 μm, which reduces their kicks to the electron beam trajectory along the undulator. The vacuum chamber incorporates beam position monitors and orbit correction magnets (one for each quadrupole). The undulator system is subdivided into three segments, each 4.5 m long and containing 10 quadrupole sections, i.e. five full focusing-defocusing (FODO) cells. The FODO lattice periodicity runs smoothly from segment to segment. There is a spacing of 0.3 m between adjacent undulator segments for diagnostics (see section 3.1.3.9). The total length of the undulator section is 14.1 m. The installation and alignment of the three modules with respect to each other and with respect to the linac and the vacuum chamber was accomplished using laser alignment techniques.

The first observation of SASE in a free-electron laser was at the beginning of year 2000 (see section 3.1.3.10). For the radiation intensity measurements different detectors were used [27].

3.1.3.9 Beam Diagnostics

The high energy beam analysis area at the end of the TTFL allows the full analysis of the electron beam parameters. Transverse profile and beam divergence are measured using optical transition radiation (OTR) screens [28] as well as diffraction radiators [29]. Energy and energy spread are measured in the dispersive section again using OTR screens. A system combining the readout of different toroid monitors installed in all sections (from the gun to the beam dump) measures the beam intensity and monitors the transmission along the linac; together with a number of photomultipliers, it forms part of the interlock system and protects the TTFL against excessive beam losses.

The above measurements can be made on a single bunch: measurement of the bunch length requires averaging over several bunches. Several methods to measure the longitudinal charge distribution of the electron bunch have been developed and tested in the TTF linac: coherent transition radiation interferometry [29], longitudinal phase-space tomography and streak camera [30]. The

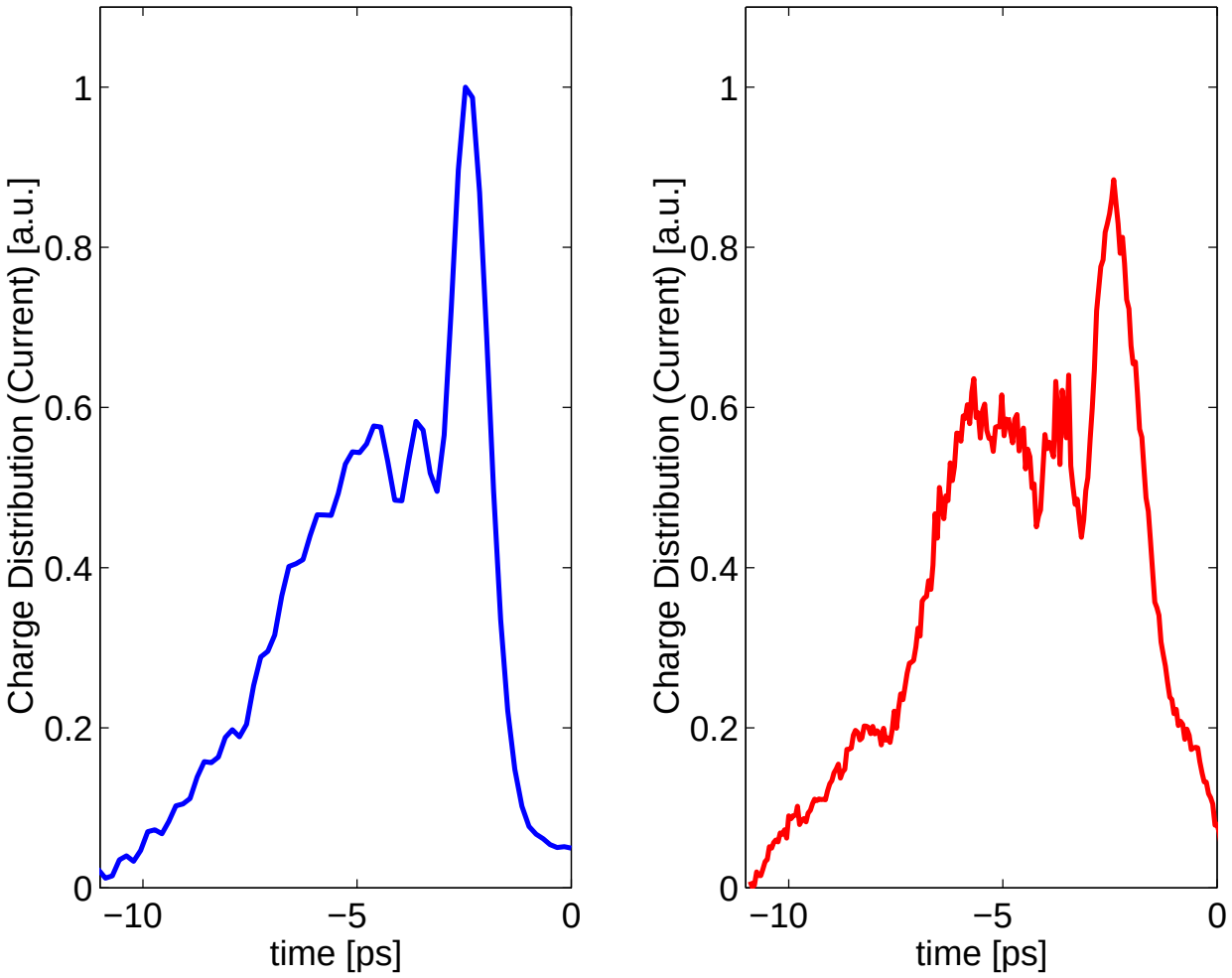

Figure 3.12: Longitudinal profile of the electron bunches as measured with two different methods. Left: A measurement using the coherent transition radiation interferometry method. Right: Projection of the longitudinal phase-space reconstructed by means of the tomography method. Both measurements were taken with a few days separation.

first method employs a Martin-Puplett interferometer to measure the autocorrelation function of the coherent transition radiation emitted when an electron bunch goes through a very thin aluminum foil. The autocorrelation yields by Fourier transformation the absolute magnitude of the bunch form factor. For the reconstruction of an asymmetric bunch, such as shown in figure 3.12, also the phase of the form factor is needed which is computed from a dispersion-relation integral. In the longitudinal tomography method, the phase of the accelerating cavities downstream the bunch compressor is varied in several steps in the range of $\pm 45°$. The energy profile resulting from each phase is measured at a screen downstream the spectrometer dipole. The charge density in the longitudinal phase space can be reconstructed from the measured projections on the energy axis using a tomography method. The longitudinal bunch profile is obtained by projecting the phase space in the longitudinal axis. Measurements of the longitudinal profile of the electron bunches

obtained from the two methods described above are shown in figure 3.12. All measurements reveal a non-Gaussian longitudinal profile with one peak containing about half of the total bunch charge when the bunch is longitudinally compressed. Moreover, the energy distribution measured after a spectrometer dipole, breaks up into several peaks indicating a fragmentation of the longitudinal phase-space when the bunch is fully compressed [31]. Theoretical studies [32] point to coherent synchrotron radiation causing the fragmentation when the radiation emitted by the tail particles in the dipoles interacts with the particles at the head of the bunch. According to these studies, full compression leads to an rms bunch length well below 0.5 mm rms which is consistent with an observed FEL radiation pulse length of only 100 μm [33]. Since such fragmentation would be detrimental to further compression, less aggressive compression in the first compressor chicane and further stages of compression at higher beam energy are foreseen for the second phase of TTF and for TESLA (see section 3.1.3.6). Since detailed understanding of longitudinal dynamics in this new domain of accelerator physics is of paramount importance for FEL performance, further studies and experiments on this subject are planned at TTF. A system of wire scanners is installed at both ends of each undulator module in order to measure the transverse profile of the electron [34]. For a transverse emittance of 4 mm mrad (normalized) the expected beam size at the undulator is about 0.1 mm rms. A horizontal and vertical beam profile measurement taken with the wire scanner is shown in figure 3.13.

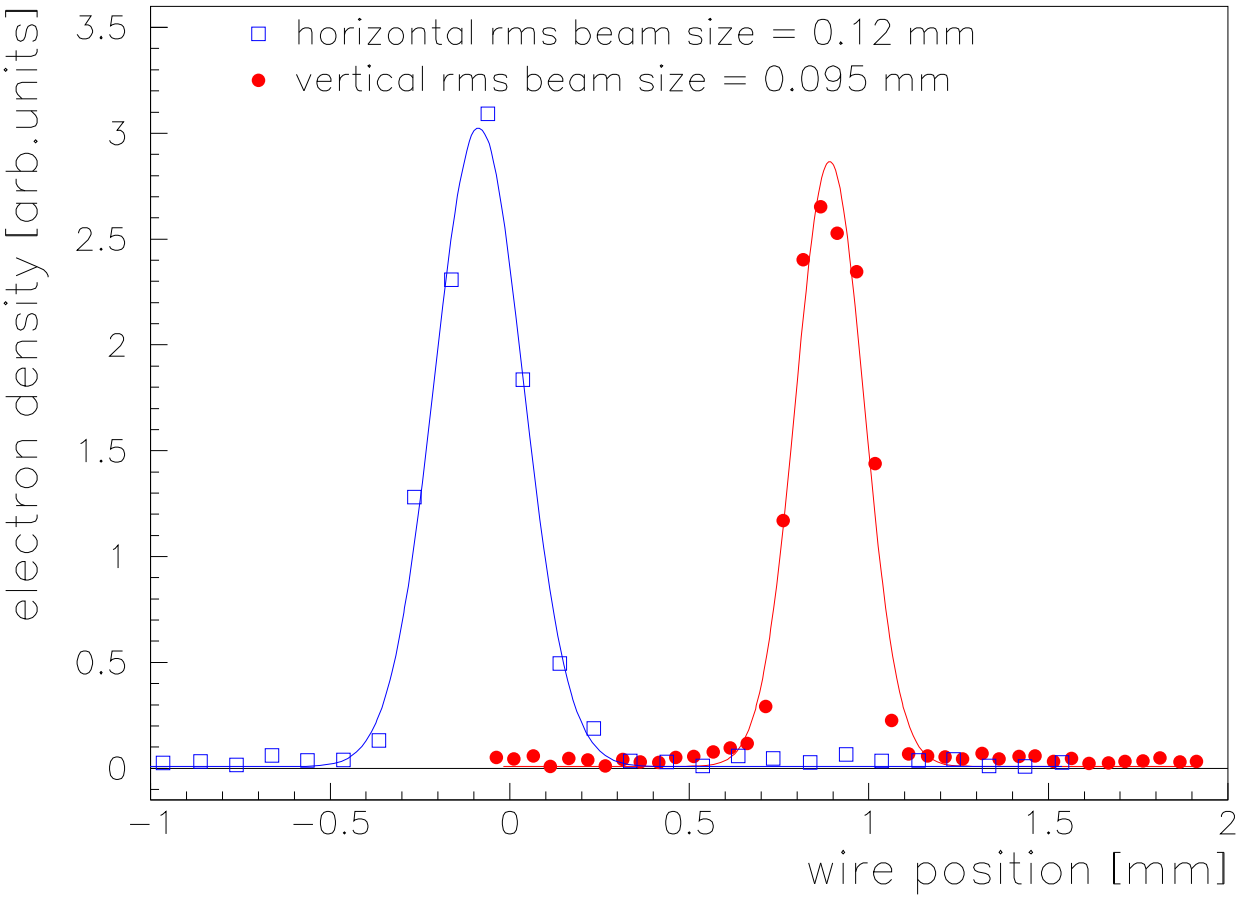

Figure 3.13: Typical transverse beam profiles measured with the wire scanners installed at the undulator section.

The prototype of an orbit correction feedback system installed at TTF consists of a pair of fast vertical kicker magnets controlled by a digital signal processor. This processor takes the signals

from a pair of beam position monitors located downstream and provides two feedback loops: A feed-forward loop corrects beam orbit deviations that appear on every macro pulse and applies a correction to the following macro pulse. The second feedback loop corrects the position deviations from bunch to bunch. A first test [35] demonstrates the possibility to correct fast bunch instabilities appearing at each bunch train as well as slow drifts of the beam position along the bunch train.

The symbiosis between the accelerator module test and FEL operation has proven useful with respect to the development of new diagnostic techniques. The measurement of wakefields excited by bunches of different length [36] and the test of a beam trajectory monitor for the TTF FEL undulator [37] are two good examples.

3.1.3.10 FEL Results

The first lasing of the high gain FEL at the TTF linac was achieved in February 2000 [33], which served as a proof-of-principle for high gain SASE FEL at VUV photon wavelengths. Since then, an FEL photon beam has been delivered over several hundreds of hours at wavelengths between 80 and 180 nm [38], corresponding to electron beam energies between 270 and 180 MeV, demonstrating stable operation and energy tunability of TTF FEL.

The characteristics of the FEL photon beam were studied in great detail at photon wavelengths of around 108 nm, with an FEL gain of a few thousands over the undulator spontaneous emission. The observed wavelength spectrum (see figure 3.14), the angular spread and photon intensity fluctuations agree very well with the expectations [33]. Gain saturation has not yet been observed. A fundamental characteristic of the FEL process is the strongly non-linear dependence of the photon intensity on bunch charge, shown in figure 3.15.

In September 2000, SASE with a gain of 10^5 was observed at 108 nm with bunch charges of 3.5 nC. Additionally, experiments varying the electron beam trajectory inside the undulator have demonstrated the strong dependence of the FEL process on the overlap between the electron and the photon beam along the undulator axis.

3.1.3.11 TTF FEL Performance

The operation of the linac in the 'FEL mode' has been sustained over a period of more than two months, demonstrating the stability and reproducibility of the various linac components (magnets, injector system, RF systems, superconducting cavities, etc.) for delivering small emittance and short electron bunches with good alignment to the undulator axis. The superconducting cavities, the RF control and the cryogenics system showed an excellent performance at moderate gradients of about 15 MeV/m during the entire period of commissioning and operation of TTF FEL. Moreover, the FEL action was recovered within only a week of the linac startup after the shutdown of June-July 2000.

The two most relevant technical factors that have made possible the successful test and operation of the high gain FEL are the field quality of the undulator magnet (described in section 3.1.3.8), which assures a good interaction between the photon and the electron beams, and the capability of the linac components to generate electron bunches with small emittance, compress them to a few tenths of a millimeter and accelerate them while preserving their high charge density.

References

[1] "Proposal for a TESLA Test Facility", Report DESY–TESLA-93-01 (1992)

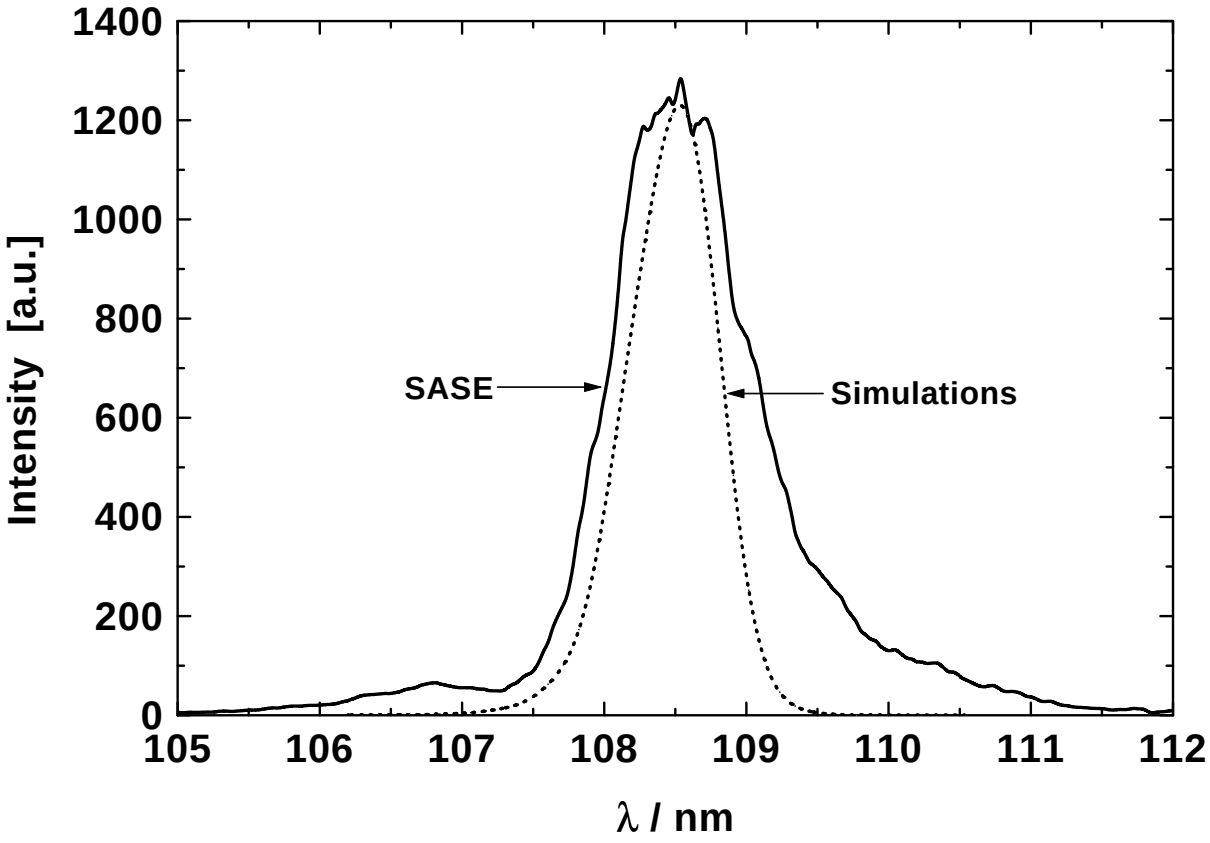

Figure 3.14: Typical wavelength spectrum of the central SASE FEL radiation cone (collimation angle ± 0.2 mrad), taken at the TESLA Test Facility. The dotted line is the result of numerical simulations. The bunch charge is 1 nC. The larger width of the measured spectrum is consistent with the energy spread of the beam.

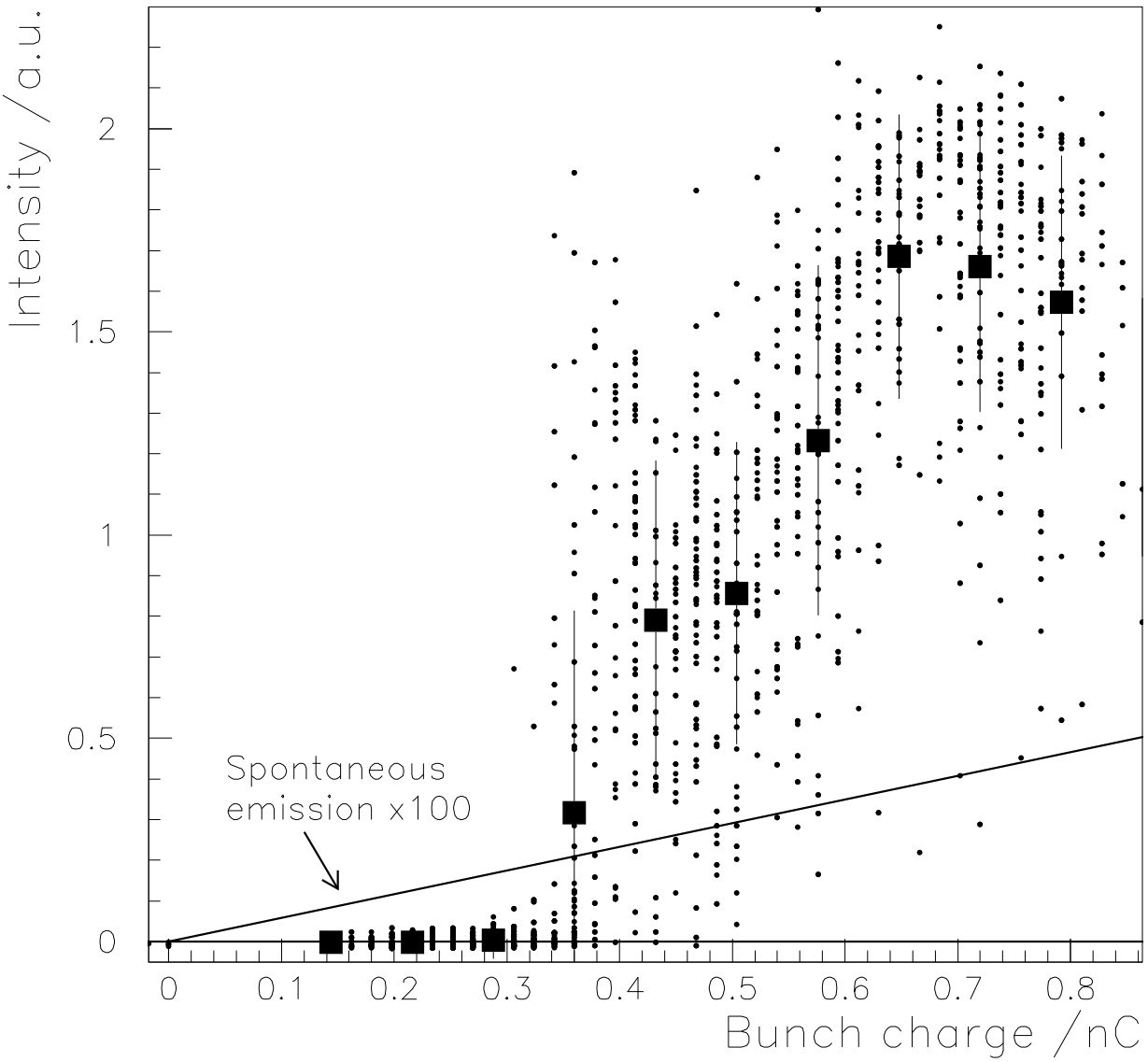

Figure 3.15: SASE FEL intensity versus bunch charge. The straight line is the spontaneous intensity multiplied by a factor of 100. To guide the eye, mean values of the radiation intensity are shown for some bunch charges (full squares). The vertical error bars indicate the standard deviation of intensity fluctuations, which are not an indication of machine instability but are due to the statistical character of the SASE process. For this measurement all accelerator settings were kept constant, except for the bunch charge. Above 0.6 nC there is no further increase of gain without readjustment of accelerator settings which would be necessary to compensate for the changed phase space distribution of the electron bunch.

[2] TESLA Collaboration, D.A. Edwards (ed.), "TESLA Test Facility Linac - Design Report", Report DESY–TESLA-95-01 (1995)

[3] "A VUV Free Electron Laser at the TESLA Test Facility — Conceptual Design Report", Report DESY–TESLA-FEL-95-03 (1995)

[4] B. Aune, M. Jablonka, J. M. Joly and E. Klein, "A Low Charge per Bunch Injection Line for the TESLA Test Facility", Report DESY–TESLA-93-04 (1993)

[5] T. Garvey et al., "First Beam Tests of the TTF Injector", Proceedings of PAC97, Vancouver, p.2823 (1997)

[6] E. Colby, "Experimental Testing of the TTF RF Photoinjector", Proceedings of PAC97, Vancouver, p.2873 (1997)

[7] B. Dwersteg et al., "RF Gun Design for the TESLA VUV Free Electron Laser", Proceedings of FEL96, Rome, p.93 (1996)

[8] P. Michelato et al., "Cs_2Te Photocathode for the TTF Injector II", Proceedings of 5^{th} EPAC, Sitges, p.1510 (1996)

[9] D. Sertore et al., "First Operation of Cesium Telluride Photocathodes in the TTF Injector RF Gun", Nucl. Instr. Meth. **A 445**, 422 (2000)

[10] S. Schreiber et al., "Running Experience with the Laser System for the RF Gun Based Injector at the TESLA Test Facility Linac", Nucl.Instr. and Methods **A445** p.427, (2000)

[11] S. Schreiber for the TESLA Coll., "First Experiments with the RF Gun Based Injector for the TESLA Test Facility Linac", Proceedings of PAC00, New York, p.84 (1999)

[12] S. Schreiber et al., "Performance Status of the RF-gun Based Injector of the TESLA Test Facility Linac", Proceedings of EPAC00, Vienna (2000)

[13] F. Stephan et al., "Photo Injector Test Facility under Construction at DESY Zeuthen", Proceedings of FEL00, to be published in Nucl. Instr. Meth. A (2001)

[14] A. Mosnier et al., "RF Control System for the SC Cavity of the TESLA Test Facility Injector", Proceedings of PAC97, Vancouver, p.2311 (1997)

[15] M. Geitz et al., "Phase Space Tomography at the TESLA Test Facility Linac", Proceedings of PAC99, New York, p.2175 (1999)

[16] H. Edwards et al., "Transverse Emittance Measurements in the TTF Injector", Proceedings of FEL99, II-75 (1999)

[17] A. Cianchi et al., "Transverse Phase Space Studies in TTF Photoinjector During Run 00-01: A Comparison between Simulation and Experiment", Report DESY–TESLA-FEL-00-04, (2000)

[18] R. Brinkmann, G. Materlik, J. Rossbach, A. Wagner, "Conceptual Design of a 500 GeV $e^+ e^-$ Linear Collider with Integrated X-ray Laser Facility", Report DESY–1997-048, ECFA 1997-182 (1997)

[19] S.N. Simrock et al., "Design of the Digital RF Control System for the TESLA Test Facility", Proceedings of EPAC96, Sitges, p.349 (1996)

[20] M. Liepe, W.D. Moeller, S.N. Simrock, "Dynamic Lorentz Force Compensation with a Fast Piezoelectric Tuner", Report DESY–TESLA-01-03 (2001)

[21] S. Fartoukh, "A New Method to Detect the High Impedance Dipole Modes of TESLA Cavities", Report DESY–TESLA-98-13 (1998)

[22] S. Fartoukh et al., “Evidence For a Strongly Coupled Dipole Mode with Insufficient Damping in TTF First Accelerating Module”, Proceedings of PAC, New York, p.922 (1999)

[23] M. Geitz et al., “Sub-Picosecond Bunch Length Measurement at the TESLA Test Facility”, Nucl. Instr. and Methods **A445** p.343 (2000)

[24] Y.M. Nikitina, J. Pflüger, “Two Novel Undulator Schemes With Quadrupolar Focusing for the VUV-FEL at the TESLA Test Facility”, Nucl. Instr. and Methods **A375** p.325 (1996)

[25] J. Pflüger et al., “Magnetic Characterization of the Undulator for the VUV-FEL at the TESLA Test Facility”, Proceedings of FEL99, II-87 (1999)

[26] U. Hahn et al., “Design and Performance of the Vacuum Chambers for the Undulator of the VUV FEL at the TESLA Test Facility at DESY”, Nucl. Instr. and Methods **A445** p.442 (2000)

[27] Ch. Gerth et al., “Photon Diagnostics for the Study of Electron Beam Properties of a VUV SASE FEL at DESY”, Proceedings of FEL00, to be published in Nucl. Instr. Meth. A (2001)

[28] M. Castellano et al., “Time Resolved Energy Measurement of the TESLA Test Facility Beam Through the Analysis of Optical Transition Radiation Angular Distribution”, Proceedings of PAC99, New York, p.2196 (1999)

[29] M. Castellano et al., “Bunch Length Measurements at TTF Using Coherent Diffraction Radiation”, Proceedings of EPAC00, Vienna, p.1699 (2000)

[30] M. Geitz et al., “Determination of the Longitudinal Phase Space Distribution produced with the TTF Photo Injector”, Proceedings of FEL99, Hamburg, II-83 (1999)

[31] M. Huening et al., “Observation of Longitudinal Phase Space Fragmentation at the TESLA Test Facility Free-Electron Laser”, Proceedings of FEL00, to be published in Nucl. Instr. Meth. A (2001)

[32] T. Limberg et al., “An Analysis of Longitudinal Phase Space Fragmentation at the TESLA Test Facility”, Proceedings of FEL00, to be published in Nucl. Instr. Meth. A (2001)

[33] J. Andruszkow et al., “First Observation of Self-Amplified Spontaneous Emission in a Free-Electron Laser at 109 nm Wavelength”, Phys. Rev. Lett. **85** p.3825 (2000)

[34] G. Schmidt et al., “First Results of the High Resolution Wire Scanners for Beam Profile and Absolute Beam Position Measurement at the TTF”, Proceedings of FEL00, to be published in Nucl. Instr. Meth. A (2001)

[35] K. Balewski et al, “Design and Test of a Fast Feedback System for Orbit Correction at TTF and the TESLA Linear Collider”, Preceedings of HEACC01, Tsukuba (2001)

[36] M. Huening et al., “Experimental Setup to Measure the Wake Fields Excited by a Rough Surface”, Nucl.Instr. and Methods **A445** p.362 (2000)

[37] S. Hillert et al., “The Beam trajectory Monitor for the TTF-FEL at DESY”, Proceedings of EPAC00, Vienna, p.1803 (2000)

[38] J. Rossbach, et al., “Observation of Self-Amplified Spontaneous Emission in the Wavelength Range from 80 nm to 180 nm at the TESLA Test Facility at DESY”, Proceedings of FEL00, to be published in Nucl. Instr. Meth. A (2001)

3.1.4 Higher-Order-Modes

R. Wanzenberg DESY
rainer.wanzenberg@desy.de

3.1.4.1 The Passband Structure of the TESLA 9–Cell Cavity

Long range wakefields are important for the beam dynamics of a long train of bunches in the TESLA main linear accelerator since these wakefields can cause multi-bunch instabilities. The long range wakepotential can be represented as a sum over contribution from Higher Order Modes (HOMs). Figure 3.16 shows one 9-cell superconducting cavity of the TESLA Test Facility (TTF). The fundamental mode is a 1.3 GHz π-mode, which is used to accelerate the beam. A detailed review of the TESLA cavity is presented in [1]. At DESY the computer code MAFIA [2, 3] is used to explore the pass band structure of the TESLA cavity for monopole, dipole and quadrupole modes.

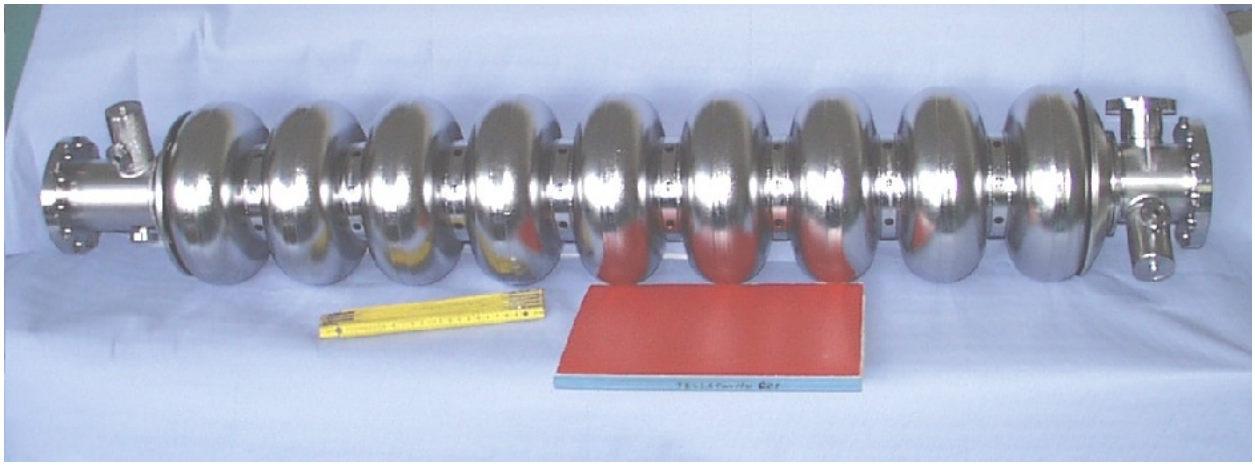

Figure 3.16: Superconducting TESLA 9-cell cavity.

The passband structure of the TESLA cavity can be calculated if periodic boundary conditions are applied to the electric field $\vec{E}$ in a single cavity cell:

$$\vec{E}(r, z + g) = \vec{E}(r, z) \ \exp(i\varphi), \tag{3.2}$$

φ is the phase advance per cell, and g the cell length. The frequencies of the lowest pass-bands are graphically represented in figure 3.17 for monopole, dipole and quadrupole modes. A beam will mainly excite modes which are synchronous to the beam, i.e. modes with a phase velocity equal to the speed of light:

$$c = v_{ph} = 2\,\pi \ g \ \frac{f}{\varphi}, \tag{3.3}$$

where f is the frequency of the mode and $\varphi =$ is the phase advance per cell, which is used as an abscissa in the plots of the dispersions curves. The light cone is the straight line $f(\varphi) = \varphi\, c/(2\,\pi\, g)$, which is folded into the phase range from 0 to $180°$ in figure 3.17 using the periodicity of the structure.

The dipole modes have been studied in detail since these modes can drive a cumulative multi-bunch instability. For each mode in a TESLA 9-cell cavity the frequency, phase advance, R/Q and geometry parameter have been calculated. The lowest 52 dipole modes of the TESLA TTF cavity are represented in the dispersion diagram in figure 3.18 The frequencies of the lowest two passbands are below the cutoff frequency of the cavity beam pipe. All other modes can in principle propagate into the beam pipes. But some passbands (like the 5th one) are very flat and the modes of these bands are potentially trapped.

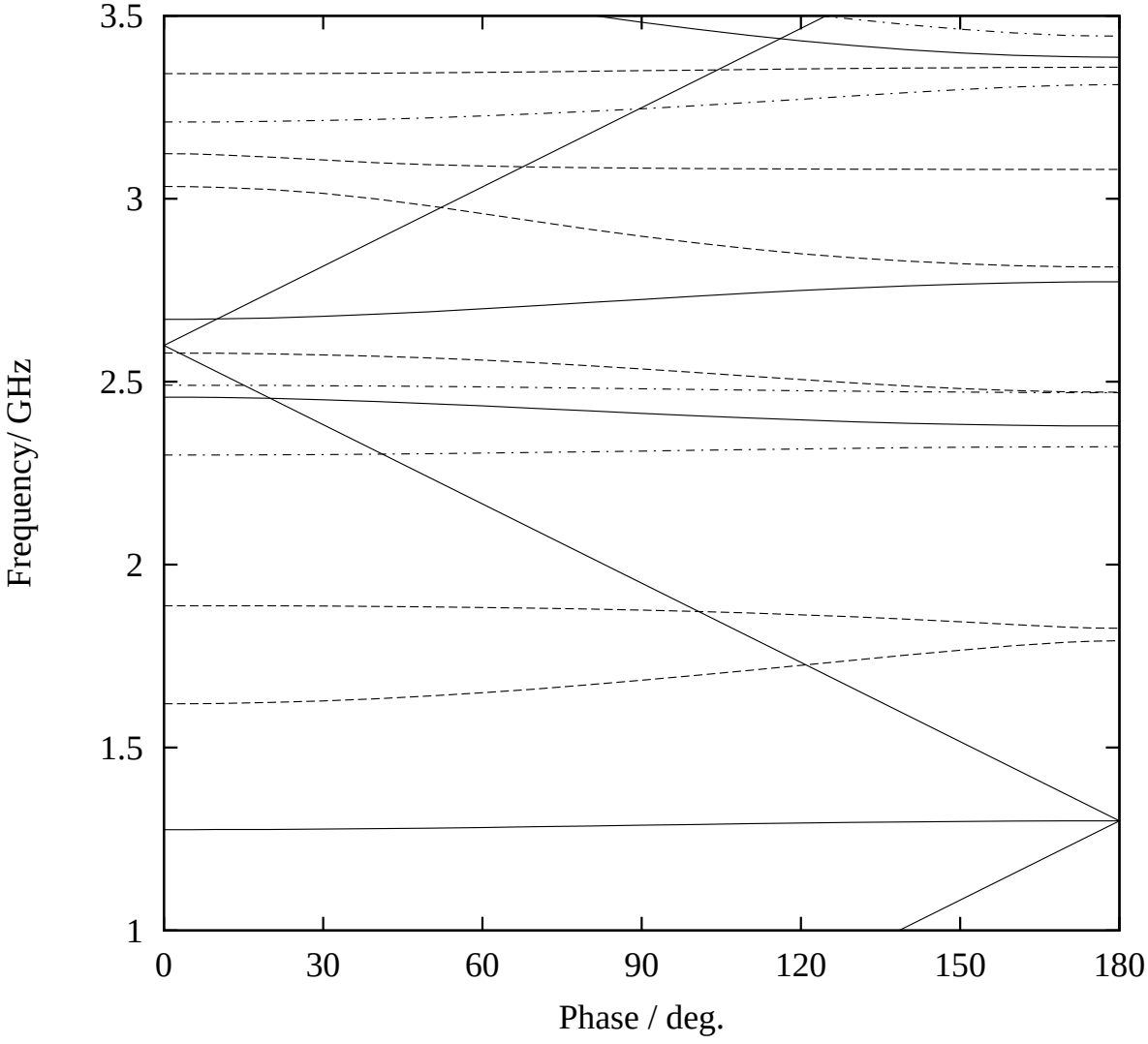

Figure 3.17: Dispersion curves for monopole (solid line), dipole (dashed line) and quadrupole (dash-dotted line) modes.

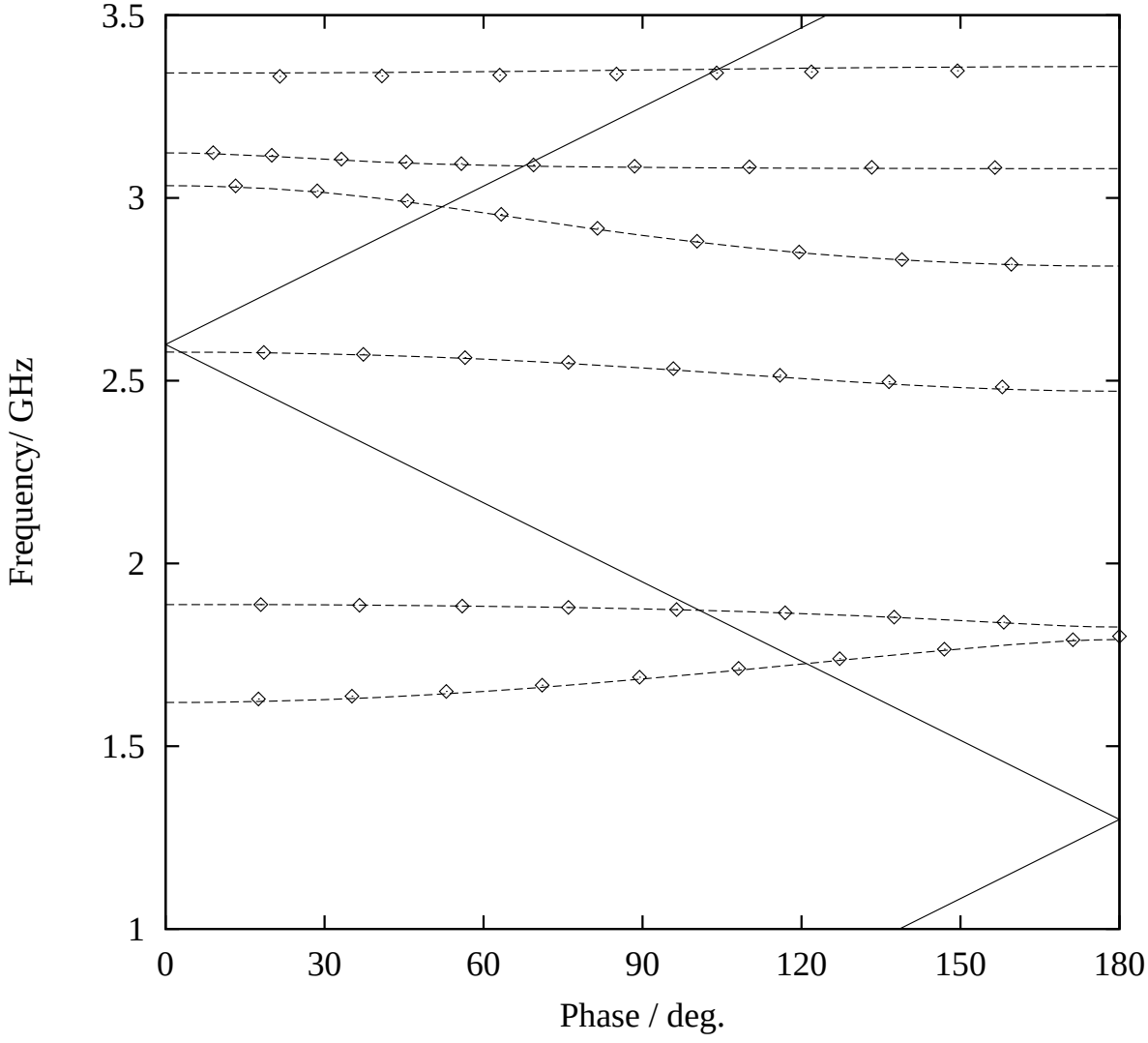

Figure 3.18: Dispersion curves for dipole (dashed line) and the lowest 52 dipole modes in a 9-cell TESLA TTF cavity (diamonds).

At each end of the cavity a HOM-coupler is installed to damp the modes and therefore to avoid multi bunch instabilities in the TESLA linac. Further MAFIA calculations are planned to determine the external Q-values of some modes and compare the results with measurements.

References

[1] B. Aune et al., "The superconducting TESLA cavities", Phys. Rev. ST Accel. Beams**3** 092001 (2000) [physics/0003011].
http://prst-ab.aps.org/abstract/PRSTAB/v3/i9/e092001

[2] T. Weiland, "On the numerical solution of Maxwell's Equations and Applications in the Field of Accelerator Physics", Part. Acc. 15 p.245–292 (1984)

[3] "MAFIA Release 4 (V4.021)" CST GmbH, Büdinger Str. 2a, 64289 Darmstadt, Germany
http://www.cst.de/

3.2 Beam Dynamics Activities in the SL-AP group at CERN

Francesco Ruggiero CERN
Francesco.Ruggiero@cern.ch

The Accelerator Physics group in CERN's SL Division, carries out theoretical and experimental research in the dynamics of particle beams. It contributes to the design and commissioning of new accelerators and takes part in studies aimed at understanding and improving the performance of existing facilities. The group is in charge of

1. LHC beam optics, beam dynamics and performance
2. accelerator physics support and new concepts in beam dynamics
3. studies on future accelerators.

3.2.1 LHC Beam Optics, Beam Dynamics and Performance

3.2.1.1 Lattice Design, Correction Systems, and Collimation

A considerable fraction of the group's effort is devoted to designing and maintaining the coherence of the LHC optics model in all its details. This includes the integration of the detailed description as files for the MAD program with the databases defining the layout, powering, parameters and field quality. The geometry of the machine is itself generated by MAD and passed to the surveyors.

The LHC lattice Version 6.2 incorporates new solutions for most of the insertions. These provide room for auxiliary collimators to protect the dispersion suppressor and arc magnets in case of injection failures. A study of particle losses in the case of mis-injected beams is under way to identify their location and to assess the collimation efficiency. Various beam loss mechanisms for equipment failure modes and the associated time constants have also been investigated. The optics of the collimation insertions have been adapted.

The specification of the closed orbit correctors has been revised and an analysis based on a local correction approach has shown that special long correctors in the insertions can be avoided. Studies of orbit correction with two beams have also started.

At the end of the year, a mini-workshop on the alignment of LHC magnets was organised to compare the tolerances obtained from beam physics considerations with realistic hardware and survey specifications. No significant discrepancy was identified. Simulation and experimental

results on the measurement and correction of linear and non-linear optics were used to help specify the BPM alignment, resolution, and linearity.

3.2.1.2 Dynamic Aperture

The requirements on the field quality of the lattice octupoles have been specified. Studies of the multipolar errors from the warm quadrupoles show that they need to be reduced.

An extensive particle tracking campaign was performed to evaluate the long-term dynamic aperture of the LHC (version 6.1), with the aim of checking the reliability of the latest arc corrector schemes (mainly the new layout of the octupole/dacapole spool pieces) and of studying new options for the installation of the main magnets. The possibility of installing the dipoles in batches of 24 magnets coming from the same production line (the so-called "mini-mixing") has been proposed and looks very promising. This installation strategy is much less constraining than the nominal one (where each of the 8 LHC arcs is assumed to be equipped with 154 dipoles coming from the same production line) without being detrimental to the dynamic aperture and to the possibility of correcting the multipolar field errors.

3.2.1.3 Beam-Beam Effects

Weak-strong simulations with the correct crossing schemes in all IPs, triplet errors from FNAL and KEK (who are building the triplet quadrupoles), and optimised corrector settings, confirm that the dynamic aperture during collision is significantly reduced by parasitic beam-beam encounters. This suggests a larger crossing angle, possibly the largest angle allowed by the hardware. Particle tracking over 10^5 turns indicates a loss of about $2\,\sigma$ in dynamic aperture at injection, compared to the case without beam-beam interaction. Longer-term tracking studies are in progress. An analytical criterion based on resonance overlap has been put forward to estimate the dynamic aperture due to long-range collisions. The effect of image charges on the long-range interactions has been investigated and found to be negligible for the beam offsets considered. A more detailed study is currently under way.

The effects of ground motion on the beam stability and particle diffusion in the presence of head-on beam-beam interaction have also been studied. Diffusion coefficients are determined by particle tracking and analytical calculations, and are used in a numerical integration of the Fokker-Planck equation. The emittance growth over realistic time scales turns out to be negligible.

Coherent beam-beam effects in the strong-strong regime have been further investigated during the year 2000. The proposed countermeasure, to split the tunes of the two beams, gives rise to coherent two-beam resonances resulting in emittance growth when Landau damping is active to damp the coherent modes. The studies have been generalised to multiple IPs and the effects of symmetries and of phase advance adjustments between IPs have been studied in detail. Long-range collisions have been added into the model and have substantially changed the picture, both qualitatively and quantitatively. The appearance of two separate, uncoupled eigenmodes for the head-on and long-range interactions has been explained and demonstrated by perturbation theory and multi-particle tracking. To study coherent beam-beam effects beyond the "soft-Gaussian" approximation, a simulation based on a "Fast Multipole Method" has been developed in collaboration with TRIUMF.

Another simulation program has been developed to study the coherent modes of some 3000 rigid bunches per beam, including the effect of head-on and long-range interactions. The oscillations of the bunches are followed around the self-consistent closed orbits, which are computed in advance. This will allow the investigation of the possible stabilising effects of phase advance errors between

the interaction points, bunch intensity variations, tune variations, etc.

The consequences of the finite-crossing angle on the coherent beam-beam modes have been studied and evaluated for a realistic model. The excitation of synchro-betatron resonances has been demonstrated and shown to have a stabilising effect.

3.2.1.4 Impedance and Collective Effects

During 2000, there were several studies of impedance sources in the LHC. Given the number and variety of elements which have to be considered in collaboration with the various hardware groups, a list of general impedance rules for the design of the LHC beam pipes has been established. In particular, the impedance of specific elements such as cold-warm transitions, "micro-stations" for the ATLAS experiment and RF sliding contacts have been evaluated.

The original design of two LHC elements, namely the septums and the TDI absorber, were found to be incompatible with new constraints imposed by the combination of vacuum, aperture and impedance considerations. Fundamental modifications have been proposed for both elements, and the corresponding solutions are presently under study.

Wakefields in the LHC recombination chambers have been simulated in collaboration with INFN-Frascati and some potential difficulties associated with trapped modes have been identified. The corresponding results have been transferred to the LBNL, where these chambers will be built.

The need for a randomisation of both the position and size of the pumping slots in the LHC beam screen, to avoid a coherent effect from trapped modes, has been confirmed. A Monte-Carlo program simulating the synchrotron radiation flux around the entire LHC has been developed. It includes realistic optics errors, closed orbit perturbations and allows for variations in the reflectivity of the chamber.

The analytical models developed to compute the impedance of SPS and LHC kickers have been completed, and reproduce fairly well the temperature rises observed in the SPS.

Based on the analysis of the experimental results obtained in the small EPA ring at the end of 1999, the study of the RF shielding properties of thin resistive layers has continued. A computational procedure for layered vacuum chamber walls was developed during the year, and was validated by a second set of measurements performed in EPA at the end of 2000. The results obtained for some of the configurations tested will have a direct impact on LHC applications.

An updated review of the LHC programme with ions has been completed and published. A new procedure has been developed to compute Intra-Beam Scattering (IBS) using the Bjorken-Mtingwa model. This procedure is required to compute IBS growth times below transition energy, where the Piwinski formalism is known to be inappropriate.

3.2.2 Accelerator Physics and New Concepts in Beam Dynamics

Our last contribution to the LEP optics consisted of re-matching two of the experimental insertions to reduce the background level. This was successfully put into operation during last year.

3.2.2.1 Electron Cloud studies

A new series of electron cloud simulations were performed for the SPS, LHC, and the PS, following discussions and in response to new observations. In collaboration with the LHC Vacuum Group, low-energy electrons elastically reflected at the beam pipe wall were modelled and shown to play a crucial role both in the electron cloud build-up and for the corresponding heat-load on the LHC beam screen. Simulation results that include these reflected electrons seem to agree better

with observations in the SPS using LHC type beams, especially those with a gap of 12 missing bunches.

The possible degradation of LHC beam-position signals by the electron cloud has also been examined and, in collaboration with the SL/BI Group, the angle and energy spectra of electrons hitting the vacuum chamber in the SPS and LHC was investigated. The energy spectrum strongly depends on the bunch length, and the magnetic field of the beam increases the angular spread of the electrons by about a factor of two in the LHC. In addition, a high correlation between impact angle and energy is observed, which will need to be taken into account in the design of future diagnostics.

A novel, multi-particle simulation code was developed to investigate the single-bunch instability driven by the electron cloud. First results are in agreement with analytic estimates, showing that the instability growth rate depends on the number of electron oscillations during the proton bunch passage, and saturates when this exceeds unity. There are also indications of a possible interplay between conventional and electron-cloud impedance.

3.2.2.2 Beam Optics Programs

Development of the object-oriented accelerator design program MAD-9 continues despite the retirement of its principal author, Chris Iselin. Collaborations with external institutions are under way. A lot of effort has been devoted to testing it in the very demanding context of the development of optics for the LHC. A substantial amount of debugging has been done and the usability of the program has been considerably enhanced. However a lot of work remains to be done. Although the basic description of the LHC is maintained in MAD-9 format, most of the optics studies for the LHC have consequently been de-coupled from MAD-9 developments.

A considerable effort went into upgrading MAD-8 to include the following new features:

- the direction of the particle is now taken into account when going through a magnet
- two rings with common elements can now be matched simultaneously
- acceleration has been incorporated.

A long-standing problem was also solved by modifying MAD-8 so that it can compute the beta functions in the PS to SPS transfer line, which includes a 100% x-y emittance exchange. In addition a new software project, MAD-X, has been launched aimed at a modular and maintainable version of MAD that is based on MAD-8 and still compatible with the MAD-9 syntax. The concept, layout, and main functionality of MAD-X, as well as the conversion procedure have been defined, and a stripped-down closed orbit finding module without ZEBRA banks has been produced and tested.

SixTrack90 is a new code that combines the map definitions of SixTrack with an existing overloaded Fortran90 Normal Form Analysis package. It is aimed at the parametric study of accelerator maps, can handle beam lines and includes some new features not present in SixTrack, such as ‘hard-edge’ fringe fields. Fast, symplectic map tracking has been successfully applied to the LHC lattice version 6, with a simulation speed-up of a factor 10, however multipolar field errors beyond order 7 can not be included in the map.

3.2.2.3 Machine Experiments

The efforts to reduce the SPS impedance in view of its future use as an LHC injector have been followed by a series of detailed measurements. The reproducibility in the determination of the

transverse impedance from the coherent tune shift is now better than 20%. There is a first indication of a small (about 10%) decrease in impedance from the measurements performed in 1999 and 2000. In addition to the measurements at 26 GeV, a dedicated experiment allowed the verification of the proportionally smaller effects at 120 GeV with unprecedented precision. These baseline measurements have been complemented by growth/decay rate measurements as a function of chromaticity, and multi-turn beam position recordings as function of intensity. A broadband impedance is found to be inadequate to model the observations in the horizontal plane.

Several experiments were performed to measure resonance driving terms and to localise sources of non-linearity at 26 GeV and 120 GeV in the SPS. The results are encouraging and are being used to validate the SPS lattice model and the analysis of multi-turn beam position data with kick strength for future application in the commissioning of the LHC. Dynamic aperture and driving-term experiments were also performed at HERA-p and at RHIC, but with limited success because of the insufficient quality of available beam instrumentation and/or hardware failures.

Besides contributing to SPS experiments on electron-cloud effects, a transverse beam echo following two dipole kicks was measured in the SPS for the first time. One long SPS machine study in 2000 was dedicated to measurements of the energy loss of coasting proton beams at 120, 170 and 220 GeV, in an energy region where synchrotron radiation is expected to be partially suppressed by the presence of the conducting beam pipe. A similar experiment was also proposed and participated in at HERA. A combined analysis is in progress to search for the first experimental evidence for synchrotron radiation with screening from protons.

3.2.3 Studies on Future Accelerators

3.2.3.1 CLIC Studies: Beam Delivery System and Damping Rings

At the interaction point, the vertical spot-size increase due to synchrotron radiation in the detector solenoid field and its fringe was shown to be significant. This sets a tight upper bound on the maximum possible total crossing angle. For a 4 Tesla solenoid field this limit is about 20 mrad, i.e., equal to the minimum angle required.

A number of short final-focus systems with non-zero dispersion across the final doublet were studied for CLIC at 3 TeV. Unfortunately, all draft optics created so far fall well short of the desired luminosity. A collaboration set up with the University of Valencia aims at improving the performance. Analytical approaches for even shorter final focus systems have been explored, and specifications have been completed for a system based on RF quadrupoles.

Evaluating the combined effect of ionisation heating and image currents, it has been shown that, at several locations in the final focus, the spoilers can survive the full impact of an undiluted beam, provided they are made from the proper material (carbon or beryllium). Simulations launched for studying failure modes in the linac and quantifying the implied emittance growth, have shown that in some cases there is a blow-up by several orders of magnitude. Ultimately this will determine the minimum beta functions required at the collimators.

Expressions for collimator wake fields were compiled and programs for studying scattering from residual gas or thermal photons installed. A collaboration set up with DESY Zeuthen aims at evaluating muon generation and propagation in the CLIC beam delivery system, using software tools developed for TESLA. Layouts with an overall crossing angle and example parameters have been explored for photon-photon collisions at CLIC, and potential problems were identified.

The 3 TeV CLIC design parameters make very demanding requirements on the damping rings, with full-intensity emittances an order of magnitude below the world record values achieved at low intensity. In collaboration with Daresbury laboratory, first optics designs for the damping

rings have been produced. Established design strategies, based essentially on optical considerations, lead to a TME arc lattice and wigglers in straight sections. It has been shown that this strategy produces designs in which intra-beam scattering growth rates overwhelm the synchrotron radiation damping. The same conclusion will hold for the 1 TeV damping rings. In addition to IBS, some novel instabilities have severe growth rates. In such a ring at 1.98 GeV, estimated growth times for the fast beam-ion instability are about 1.5 turns at 1 nTorr, and 10 turns for the electron-cloud instability. In response to these findings, the design strategies are being extended to include intensity-dependent effects in the optimisation and to explore the options of rings at higher energy with larger circumference, possibly even as large as that of LEP. In such a ring, radiation damping, IBS and quantum excitation would occur mainly in the wiggler sections.

Final-focus stabilisation problems were vigorously addressed in collaboration with other laboratories, and a comprehensive R&D program has now been launched at CERN.

3.2.3.2 Neutrino Factory and Muon Collider Studies

Neutrino factory modules have been developed to the requirements established by the Neutrino Oscillation Working Group at CERN; in particular the proton driver, the recirculating muon linear accelerators and the muon storage ring. Instabilities, space charge and electron-cloud effects have been investigated in the proton driver. The design of the re-circulators has now been automated.

Optics studies for triangular and bow-tie geometries were performed with a view to the design of the muon storage ring. The effect of fringe fields was also investigated, and led to the recommendation of lengthening some quadrupoles to lower their gradient and to reduce the loss of dynamic aperture. Other studies concerned the identification of additional electron losses in the dispersion suppressors due to muon decay in the straight sections. A logical R&D program for muon acceleration has been proposed, including engineering and simulation milestones.

References

[1] S. Petracca, “Beam coupling impedances for perforated beam pipes with general shape from impedance boundary conditions”, CERN-SL-99-003-AP, February 1999, and Phys. Rev. E **60** (1999) 6030.

[2] Y. Papaphilippou and F. Zimmermann, “Weak-strong beam-beam simulations for the Large Hadron Collider,” CERN-SL-99-039-AP, April 1999, and Phys. Rev. ST Accel. Beams **2** (1999) 104001.

[3] C. Biino, M. Clément, N. Doble, K. Elsener, L. Gatignon, P. Grafström, W. Herr, P. Keppler, J. Major, U. Mikkelsen, A. Taratin, M. Velasco, “Deflection of 32.8-TeV/c fully stripped Pb ions by means of a bent Si crystal,” CERN-SL-99-035-EA, May 1999, and Nucl. Instrum. Meth. B **160** (2000) 536.

[4] A. Mostacci, L. Palumbo and F. Ruggiero, “Impedance and loss factor of a coaxial liner with many holes: Effect of the attenuation,” Phys. Rev. ST Accel. Beams **2** (1999) 124401.

[5] R.B. Palmer, C. Johnson and E. Keil, “A cost-effective design for a neutrino factory,” CERN-SL-99-070-AP, BNL-66971, CERN Neutrino Factory Note 09, November 1999, and Nucl. Instrum. Meth. A **451** (2000) 265.

[6] M.P. Zorzano and F. Zimmermann, “Simulations of coherent beam-beam modes at the Large Hadron Collider,” CERN LHC Project Report 314, November 1999, and Phys. Rev. ST Accel. Beams **3** (2000) 044401.

[7] L.H. Leunissen, G. Ripken and F. Schmidt, "6D beam-beam kick including coupled motion," CERN LHC Project Report 369, February 2000, and Phys. Rev. ST Accel. Beams **3** (2000) 124002.

[8] K. Ohmi and F. Zimmermann, "Head-tail instability caused by electron cloud in positron storage rings," CERN-SL-2000-015-AP, May 2000, and Phys. Rev. Lett. **85** (2000) 3821.

[9] E. Keil, "Neutrino factories: Accelerator facilities," CERN-SL-2000-043-AP, CERN Neutrino Factory Note 33, July 2000, and Nucl. Phys. Proc. Suppl. **91** (2000) 239.

[10] A. Mostacci, F. Ruggiero, M. Angelici, M. Migliorati, L. Palumbo, S. Ugoli, "Wakefields due to surface waves in a beam pipe with a periodic rough surface", see CERN LHC Project Report 406, August 2000, submitted to Phys. Rev. ST Accel. Beams (EPAC 2000 Conference Edition).

[11] A. Baurichter, C. Biino, M. Clément, N. Doble, K. Elsener, G. Fidecaro, A. Freund, L. Gatignon, P. Grafström, M. Gyr, M. Hage-Ali, W. Herr, P. Keppler, K. Kirsebom, J. Klem, J. Major, R. Medenwaldt, U. Mikkelsen, S.P. Moller, P. Siffert, E. Uggerhoj, Z.Z. Vilakazi, E. Weisse, "Channeling of high-energy particles in bent crystals: Experiments at the CERN SPS," Nucl. Instrum. Meth. B **164-165** (2000) 27.

[12] D. Brandt, H. Burkhardt, M. Lamont, S. Myers and J. Wenninger, "Accelerator physics at LEP," CERN-SL-2000-037-DI, July 2000, Rept. Prog. Phys. **63** (2000) 939.

[13] G. Franchetti, I. Hofmann and G. Rumolo, "Effect of space charge on bunch compression near the transition," Phys. Rev. ST Accel. Beams **3** (2000) 084201.

[14] T. Okugi, H. Hayano, K. Kubo, T. Naito, N. Terunuma, J. Urakawa, T. Hirose, F. Zimmermann, T. Raubenheimer, "Evaluation of vertical emittance in KEK-ATF by utilizing lifetime measurement," Nucl. Instrum. Meth. A **455** (2000) 207.

[15] F. Ruggiero, G. Rumolo and F. Zimmermann, "Simulation of the electron-cloud build up and its consequences on heat load, beam stability and diagnostics," CERN-SL-2000-073-AP, October 2000, and Phys. Rev. ST Accel. Beams **4** (2001) 012801.

[16] R. L. Gluckstern, "Analytic methods for calculating coupling impedances," CERN Yellow Report 2000-011 (November 2000).

3.3 Beam Dynamics Activities at ELETTRA

E. Karantzoulis for the ELETTRA
Accelerator Physics Group
karantzoulis@elettra.trieste.it

ELETTRA (http://www.elettra.trieste.it/) is a third generation light source operating at 2.0 and 2.4 GeV with an injection energy of 1.0 GeV. Many new projects are in the state of design, commissioning or realization to further improve its performance. Recent activities at ELETTRA include:

1. Controlling the impact on the dynamic acceptance and on operations of the newly installed elliptical insertion devices of the APPLE-II type. Studying the impact on the dynamic acceptance of future devices like a superconducting wiggler, a Figure-8 undulator and short devices in the dispersive arcs,

2. providing support for the commissioning of the Free Electron Laser and

3. for that of the transverse multi-bunch digital feedback system, and

4. the participation in the design of a new full energy injector.

Since ELETTRA is a storage ring dedicated to the production of synchrotron light, dynamic aperture issues in relation to insertion devices have always been a concern. The breaking of its twelve-fold symmetry due to the optics distortion of the devices and the introduction of their non-linear fields has implied many dynamic aperture simulations and measurements. Currently, when three of the six elliptical insertion devices are closed at minimum gap, a reduction of 1.5 mm in the vertical dynamic aperture has been measured with respect to the situation previous to their installation. The results are in good agreement with simulations [1]. Measurements including the remaining elliptical devices will be carried out in the near future. Although at the moment the only compensation which is necessary in order to maintain the requested lifetime is the compensation of the tune shifts induced by the devices, other compensation schemes such as alpha matching and minimization of the beta-beat are available. In relation to the design of the new full energy injector top up studies are in progress [2]. Recently it was possible to inject into the storage with the insertion devices closed to gap values giving the same linear distortion effects at the injection energy as those at minimum gap at 2.0 GeV.

To control the drift of the orbit at the light source points, the present slow feedback program corrects the angle at the bending light source point and the position and angle at the center of the long straight sections, using closed bumps. The future installation of the short devices in the dispersive arcs implies the control of the orbit also at these points. To achieve this, a new version is being written to correct the position and angle also at the short insertions devices points. Both a slow and fast global orbit feedback systems are also under study in relation to the new booster.

A UV/VUV Storage Ring Free-Electron Laser is under commissioning at ELETTRA. The project, supported by the European Community in the framework of a TMR-RTD network, involves researchers from six European laboratories and research institutions [3]. (For more details see http://www.elettra.trieste.it/sites/euprojects/fel/) First lasing at 350 nm was achieved on February 29th 2000 and has been successfully lasing for almost a year in the range of 220-350 nm. On February 6th, 2001, the FEL lased below 190 nm, the shortest wavelength obtained so far with FEL oscillators. For the FEL the machine operates at 1GeV with 4 equidistant very stable bunches of about 15 mA/bunch. The maximum current achieved in this configuration was 25 mA/bunch. A very good longitudinal stability has been obtained by appropriate tuning of the 4 rf- cavities so that mode cancellation occurs [4]. The lifetime was of the order of 1 hour with 60 mA total current. Increasing the emittance coupling from 0.5 to 2 lifetime could be achieved. Head tail instabilities were avoided (when above threshold) by carefully adjusting the sextupole strengths.

The new injector consists of a 100 MeV linac and a booster synchrotron of up to 2.5 GeV nominal energy. The new injector complex will be installed in the empty circular courtyard on the inside of the annular ELETTRA storage ring building. Many magnet lattices made of FODO cells have been studied for the full energy booster. The chosen one is a two-fold symmetry lattice with free-dispersion long straight sections to ease the injection and extraction [5]. Its circumference is 118.8 m to get a good synchronism with the storage ring and to provide enough spaces for the injection, extraction, diagnostics, etc. The working point is 5.39 horizontal and 3.42 vertical for which the emittance at 2.5 GeV is 306 nm.rad The design phase is under way. Simulations of dynamic aperture including multipole errors obtained in the pre-designed bending magnets are being done. Other simulations are underway regarding the impact of the necessary changes of the septa and the kickers used in the injection to the storage ring. The transfer lines linac to booster

and booster to storage ring have been calculated, the latter one making use of the booster magnets [6].

A fully digital multi-bunch feedback system is being successfully commissioned and will soon start operating for the users. The system also provides means for acquiring data which can be analyzed off-line. The possibility of visualizing the details of the time evolution of the single bunches opens a variety of accelerator physics experiments [7] [8] which range from damping and anti-damping time measurements, resistive impedance measurements, phase space painting and the study of the transients of the transverse modes.

References

[1] O. Ferrando, L. Tosi, in preparation.

[2] L. Tosi, C.J. Bocchetta, "Top Up: Injecting with Closed Insertion Devices", in preparation.

[3] R. P. Walker "The European UV/VUV Stotage Ring FEL project at ELETTRA", procs. EPAC 2000, p. 93

[4] E. Karantzoulis et al., "Collective effects at ELETTRA", procs. EPAC 98, p. 960

[5] F. Iazzourene, "Updated Lattice for the ELETTRA Booster Synchrotron", Internal report ST/M-00/2, September 2000.

[6] O. Ferrando, "The Booster to Storage Ring Transfer Line Design with the same Booster Magnets", internal technical note ST/M-TN-01/03, January 2001.

[7] V. Smaluk, E. Karantzoulis, L. Tosi, "Measurements of Non-Linear Dynamics at ELETTRA", to be presented at DIPAC 2001 Conference.

[8] L. Tosi, D. Bulfone, E. Karantzoulis, M. Lonza, V. Smaluk and M. Svandrlik, "Diagnostics and Analysis of Instabilities With the Digital Transverse Multibunch Feedback System at ELETTRA", to be presented at PAC 2001 Conference.

3.4 Beam Dynamics Activities at SLS

M. Böge michael.boege@psi.ch PSI
A. Streun andreas.streun@psi.ch PSI

SLS, the national Swiss Light Source is presently under commissioning at Paul Scherrer Institut, Villigen. It consists of a 2.4 GeV low emittance storage ring, a full energy booster synchrotron and a 100 MeV injector linac.

The linac was commissioned during Feb.–May 2000 and the results have already been published [1]. Booster commissioning was done during June–Sept. 2000. Ring commissioning started Dec. 2000 and should be finished by Aug. 2001. As a snapshot from the ongoing commissioning process we will report on the beam dynamics aspects of booster and ring commissioning as well as on the beam dynamics software concept.

3.4.1 SLS booster synchrotron commissioning

3.4.1.1 The SLS booster synchrotron

The SLS booster synchrotron is mounted onto the inner wall of the storage ring tunnel. With a circumference of 270 m, 93 small gradient bends in 3 achromatic arcs provide a low emittance of 10 nm·rad at 2.4 GeV. 3 families of lumped quadrupoles placed in 3 straight sections allow variation of the tunes. The diameters of the elliptical vacuum chamber are 30 mm horizontal and 20 mm vertical. Bunch trains up to 1 mA or single bunches are ramped from 0.1 to 2.4 GeV in a 3 Hz cycle powered by a digital power supply (no white circuit). The total power consumption of only 200 kW is suitable for continuos topping up.

3.4.1.2 Machine status March 2001

Rich diagnostic equipment of 54 single turn BPMs and 3 synchrotron radiation monitors with 1 μs shutter cameras provides much insight into the beam dynamics on the ramp. On the other hand, the beam can be controlled on the ramp conveniently by editing the waveforms for the digital power supplies. In this way, variations of betatron tunes due to remanence and dynamic effects leading to partial beam losses while ramping could be corrected by modifying the corresponding time slices of the quadrupole waveforms ("ramp equalizer").

High beam losses at low energies due to gas scattering were alleviated by starting the $(1 - \cos)$ shaped ramp at even lower energy and injecting the beam with delay on the fly, when the magnetic fields are passing the values corresponding to 100 MeV. Consequently the beam is passing faster the low energy regime where it is sensitive to gas scattering. In this way we were able to extract more than 90 % of the injected current at the final energy.

Today the booster is operating with excellent reliability and reproducability – almost a "one button machine". Some pending tasks like detailed optimization of the injection efficiency from linac into booster, which is still limited to 50–60 %, have been postponed after ring commissioning.

3.4.2 SLS storage ring commissioning

3.4.2.1 The SLS storage ring

The SLS storage ring is built up by a 12 TBA ($8° - 14° - 8°$) lattice of 288 m circumference with 6 straights of 4 m length, 3 of 7 m and 3 of 11 m. Four 500 MHz cavities of 600 kV peak voltage occupy two short straights, injection is done in one of the long straights. The lattice is designed to provide an emittance of 5 nm·rad at 2.4 GeV with dispersionfree straight sections and $\approx$ 4 nm·rad when allowing some dispersion. 174 quadrupoles with independent power supplies grouped into 22 soft families allow large flexibility, 120 sextupoles in 9 families are carefully balanced to provide large dynamic apertures. A Touschek dominated beam life time of 3.5 hrs is expected for the design current of 400 mA in the presence of undulators with 4 mm full gap size, and will be raised to 8 hrs in a later upgrade by means of a 3^{rd} harmonic cavity. User operation of SLS is scheduled to start at August 1^{st}, 2001.

3.4.2.2 Machine status March 2001

The storage ring was successfully set into operation for the three most important operation modes (low emittance with and without dispersion in straights, and relaxed). Beam currents up to 200 mA have already been accumulated and raised the vacuum pressure from $< 10^{-9}$ to 10^{-7} mbar. High

current requires careful tuning of the parasitic cavity modes by means of cavity temperature and HOM dampers. An adequate procedure is still under investigation.

Injection efficiencies from booster to ring of nearly 100 % have been achieved. However with respect to these peak values for beam current and injection efficiency, still further work has to be done to improve reproducability and reliability.

The best working point up to now was found near 20.4/8.2, which is not in full agreement with theory.

The orbit rms value has been corrected to $<$350 μm in the horizontal and $<$50 μm in the vertical plane applying the Singular Value Decomposition (SVD) algorithm on the model based response matrix. A few iterations of the transverse orbit correction alternating with adjustments of the RF frequency to center the beam in the sextupoles, were required to achieve a consistent, full (6-dimensional) orbit correction, indicating that path length effects are not negligible.

It should be noted that a precise calibration of the BPM readings with respect to adjacent quadrupoles has still to be done. The vertical dispersion has been measured to be around 2 cm which can be explained by a large betatron coupling, measured to be 5%. Betatron coupling correction with dedicated skew quadrupoles is planned. First response matrix measurements have been performed. Differences of $\approx$ 20% in both planes with respect to the model indicate that the model has to be adjusted in more detail to the actual machine settings.

3.4.3 Beam dynamics software concept

Two main lines of application programming for the SLS are pursued by the Beam Dynamics Group. One follows a more conventional monolithic concept and is based on the commercial data processing and visualization tool IDL (Interactive Data Language). The second line of development involves the framework of a distributed client-server model based on CORBA (Common Object Request Broker Architecture)[2]. It has been established to interface beam dynamics applications to essential software packages such as the accelerator physics package TRACY[4] and the Common DEVice (CDEV) control library[3]. Within this model remote clients can invoke computer intensive methods, such as beam orbit correction procedures, on a dedicated server. Access to the SLS accelerator devices is achieved through a dedicated C++ CDEV server. Client side implementation of the Graphical User Interface is done in Java or Tcl/Tk, whereas the server modules are mostly written in C/C++ for performance reasons.

References

[1] M. Pedrozzi et al., “Commissioning of the SLS linac”, Proc. EPAC 2000, Vienna, Austria, p.851

[2] Object Management Group (OMG), “The Common Object Request Broker: Architecture and Specification, Revision 2.2”, February 1998

[3] M. Böge, J. Chrin, M. Muñoz, A. Streun, “Development of Beam Dynamics Applications Within a CORBA Framework at the SLS”, Proc. 7th European Particle Acc. Conf. (EPAC 2000), 26-30 June 2000, Vienna, Austria, p. 1354.

[4] J. Bengtsson, “TRACY-2 User’s Manual”, SLS Internal Document (1997); M. Böge, “Update on TRACY-2 Documentation”, SLS Internal Note, SLS-TME-TA-1999-0002 (1999), http://slsbd.psi.ch/pub/slsnotes/

3.5 Ongoing collaboration activity between ENEA and LURE

G. Dattoli ENEA
dattoli@frascati.enea.it
A. Renieri ENEA
renieri@frascati.enea.it
M.E.Couprie couprie@lure.u-psud.fr CEA

G. De Ninno deninno@lure.u-psud.fr CEA

3.5.1 Introduction

A FEL essentially consists of three elements: a relativistic electron beam, an undulator producing a periodic magnetic field and an optical resonator in which the emitted synchrotron radiation is stored. In order to allow the light-beam interaction at each pass, the length of the optical resonator is a sub multiple of the storage ring circumference. In the resonator coherence develops pass to pass and the laser signal grows until saturation is reached.
The electron beam quality has an important influence on the FEL performances and, vice versa, theoretical studies confirmed by measurements done on the Super-ACO storage ring lead to the conclusion that the FEL onset may have beneficial effects on the beam stabilisation.
The collaboration between the theory group of the Applied Physics Division of ENEA (Frascati, Italy) and the Free Electron Laser (FEL) group at LURE (Orsay, France) takes place in the framework of the *theory versus experiments* task of the TMR European network *Towards a Storage Ring Free Electron Laser Source at 200 nm* (Contract n: ERBFMRXCT980245).

3.5.2 Beam dynamics activity

Since 1994 an additional harmonic cavity has been installed on the Super-ACO storage ring in order to shorten the bunch length increasing in this way the FEL gain. Such a beneficial effect is partly attenuated by the wake-field which, beyond a certain value of the RF voltage of the harmonic cavity, may induce serious beam instabilities. Systematic campaigns of bunch length and energy spread measurements are periodically carried out in order to characterise the evolution in time of the beam sensitivity to the ring environment. The bunch length measurements are performed with a double sweep streak camera (Hamamatsu) [1] while two different methods can be used to determine the energy spread. In the first one, the energy spread σ_ϵ is deduced from the measurements of the beam horizontal dimension in a dispersive section of the ring according to the well-known relation

$$\sigma_x^2 = \epsilon_x \beta_x + (D_x \sigma_\epsilon)^2 \tag{3.4}$$

where σ_x is the horizontal size, ϵ_x is the emittance, β_x the beta function and D_x the dispersion at the measurement point. The second method is based on the analysis of the synchrotron radiation spectrum emitted by the optical klystron [2]. The emission spectrum consists in a set of fringes resulting from the interference between the emission in each undulator. The fringe modulation rate f is defined by [3]

$$f = f_0 exp\left\{-2[2\pi(N + N_d)\sigma_\epsilon]^2\right\} \tag{3.5}$$

where f_0 summarises the contribution of the size, divergence and position of the beam in the optical klistron and in principle does not change with current, N is the number of periods of the undulator and N_d is the equivalent number of periods of the dispersive section. The curve of σ_ϵ is deduced

from the measurements of the spectra for several gaps of the dispersive section as a function of the beam current.
The main parameters of the Super-ACO FEL are listed in table 3.7.

Beam energy (MeV)	800
Revolution period (ns)	240
Energy spread	$5 \cdot 10^4$
RMS bunch length (ps)	90
Momentum compaction	$1.48 \cdot 10^{-2}$
Boussard current threshold (mA)	5.5
FEL spectral range (nm)	vis. - 300
FEL spectral width	10^{-4}
FEL temporal width (ps)	20 (RMS)
FEL laser gain (%)	2.5

Table 3.7: Characteristic parameters of the Super-ACO storage ring FEL.

Measurements done by using the double sweep streak camera have also revealed the presence of high (tens of KHz) and low (about 100 Hz) frequency longitudinal instabilities. When use is made of only the main (100 MHz) RF cavity, the high frequency instabilities manifest themselves as coherent synchrotron oscillations of quadrupolar, sextupolar and octupolar type. Every type is characterised by defined, generally not overlapping, current ranges. If the harmonic cavity is instead active, synchrotron oscillations of different types may be observed in the same current range. Their combination can lead to very complex and exotic behaviours of the particle beam. The presence of a low current anti-threshold (below which instabilities become particularly evident) has been detected when the harmonic cavity is active. The observed low frequency (microwave) instabilities are of saw-tooth type and appears as a fast blow up of the bunch length (or energy spread) followed by damping.

The theoretical understanding of these phenomena requires a correct modelling of the interaction between the beam and the ring environment and, in particular, a reliable estimation of the machine impedance. A first approximated analysis of the beam energy spread and bunch length dependence on the beam current has been carried out by using the Boussard criterion. According to what is stated in [4], if the beam current I exceeds a threshold value I_{th}, which is a function of the machine impedance Z_n/n (where n is the harmonic of the revolution frequency at which the impedance is measured), the microwave instability may manifest and the induced energy spread increases as

$$\sigma_\epsilon = \sigma_{\epsilon,n} \frac{I}{I_{th}} \tag{3.6}$$

(where $\sigma_{\epsilon,n}$ is the natural energy spread). The previous expression, together with that for the bunch length $\sigma_\tau = (\alpha/\Omega)\sigma_\epsilon$ (where α is the machine momentum compaction and Ω is the synchrotron pulsation) can be used to fit the experimental data obtaining in this way an estimate of the impedance (see Table 1). The same procedure has been applied to the case of the ELETTRA storage ring [5]. The quite important difference detected in the two cases (Z_n/n is about 4.5 Ω for the case of Super-ACO and about 0.2 Ω for the case of ELETTRA) depends on the fact that the two machines belong to different generations (second generation Super-ACO and third generation

ELETTRA). A more accurate analysis based on a turn-by-turn tracking code including a broad band impedance model gave essentially the same results.

3.5.3 The FEL action on the beam stability

The behaviour of the saw-tooth instability growth rate and the anomalous bunch lengthening can be modelled by using a set of non-linear Volterra type equations. Theoretical results suggest that the process could be due to a micro-bunching of the electron phase-space induced by the coupling between the electron bunch and the wake field. In practice, the instability grows until when the self-induced energy spread generates the necessary saturation mechanism and the damping restores the conditions for a new start-up of the instability. Such a process is similar to the FEL dynamics whose principal saturation mechanism is associated with the self-induced turn-by-turn energy spread. Anyway, in spite of the analogies, a remarkable difference between the two phenomena is due to the fact that the FEL may reach a steady state behaviour while the instability always keeps oscillating.
The interplay between the FEL onset and the instability dynamics can be investigated by coupling the Volterra-type equations of ref. [6] with a non-linear differential equation accounting for the evolution of the laser intracavity power:

$$\begin{cases} \dfrac{\mathrm{d}}{\mathrm{d}t}\alpha = \left[\dfrac{A}{(1+\sigma^2)^{1/4}} - B(1+\sigma^2)^{1/2}\right]\alpha \\ \dfrac{\mathrm{d}}{\mathrm{d}t}\sigma^2 = \alpha\sigma^2 - \dfrac{2}{\tau_s}(\sigma^2 - \bar{x}) \\ \dfrac{\mathrm{d}}{\mathrm{d}t}x(\tau,t) = E\left[x(\tau+\delta,t)G(\tau,\sigma) - rx(\tau,t)\right] + S(\tau) \end{cases} \tag{3.7}$$

The dynamics of the instability is characterised by α, the parameter accounting for its growth rate; the laser evolution is described by means of the intracavity power x; σ denotes the ratio between the induced and the natural energy spread; τ is the longitudinal coordinate normalised to the electron bunch length and G is the gain function including the spectral and spatial dependence, the longitudinal distribution of the electron bunch and the inhomogeneous degradation due to the induced energy spread; the factor δ specifies the amount of mismatch of the peak of the optical pulse distribution with respect to that of the electron bunch. The coefficients A, B and E are linked to the accelerator and laser parameters; r is the ratio between cavity losses and maximum homogeneous FEL small signal gain, the term S plays the role of spontaneous emission contribution and $\bar{x} = \int_{-\infty}^{+\infty} x(\tau,t)\mathrm{d}t$.

The condition for the switching off of the instability $\dfrac{\mathrm{d}}{\mathrm{d}t}\alpha = 0$ is fixed by the Boussard criterion which allows one to define a threshold value for σ above which the instability, if present, is switched off. According to simulations, when the energy spread is well above this threshold value, the laser reaches the same stationary value it would reach in absence of instability. When the energy spread is very close to the threshold the FEL seems to be able to develop and to counteract the instability. This process lasts until when the gain becomes insufficient and the system reaches a stationary configuration after the FEL decay. As confirmed by experimental results on the Super-ACO FEL [8], [7], even when the FEL is able to reach a steady state regime, the instability is damped but not really switched off: if for some reason the laser intensity decay (for example due to a sudden external perturbation), the instability is ready to grow again.

In conclusion: if the induced energy spread is larger than a given threshold value, the FEL onset may cure the growth of the saw-tooth instability. The same results has been proved for the case of the head-tail transverse instability [9].

References

[1] R. Roux et al., Nucl. Inst. Meth. A 393 (1997) 33.

[2] N.A. Vinokurov et al., Preprint INP77.59 Novossibirsk (1977).

[3] P. Ellaume, PhD thesis, Université Paris Sud, Orsay (1984).

[4] D. Boussard, CERN LABII/75-2 (1975).

[5] G. Dattoli et al., accepted by Nucl. Inst. Meth. A.

[6] G. Dattoli at al., NIM A 393, 70 (1997).

[7] R. Bartolini et al., submitted to Physical Review Letters.

[8] M.E. Couprie et al., Nucl. Inst. Meth. A 429 (1999) 165.

[9] G. Dattoli et al., Phys. Rev. E 58 (1998) 6570.

3.6 Space Charge Studies at the University of Bologna

A. Bazzani, S. Rambaldi,G. Turchetti bazzani@bo.infn.it University of Bologna

Here we report on recent space charge studies at the department of Physics of the Bologna University. This research is connected to the Italian TRASCO project and is performed in collaboration with the INFN laboratory of Legnaro (Andrea Pisent (AP) and Michele Comunian (MC)). The code for the solution of the Vlasov-Poisson problem has been mainly developed by SR and GT whereas the Frequency Map (FM) analysis has been studied by AB, MC and AP. The study of the collision effects by using a stochastic approach will be performed in collaboration with Helmut Mais at DESY.

3.6.1 Statistical description of space charge effects

A statistical description of the dynamics of a high intensity bunch of particles in an accelerator requires the solution of the Liouville equation for the density function in $\mathbf{R}^{6N}$ phase space where N is the number of particles[1]. Since $N \simeq 10^{10} - 10^{12}$, a direct solution of the problem exceeds the capacity of the existing computers and some approximations have to be introduced. Usually one defines the particle distribution function $F(\mathbf{r}, \mathbf{p}; s)$ as the average density of particles in a phase space volume $\Delta\mathbf{r}\Delta\mathbf{p}$ of $\mathbf{R}^6$ centered at the point $(\mathbf{r}, \mathbf{p})$, where s is the arc length of the reference orbit, $\mathbf{r}$ is the particle coordinate with respect to the reference particle and $\mathbf{p} = d\mathbf{r}/d\,s$ is the corresponding momentum. The particle density $n(\mathbf{r}; s)$ is computed by integrating over the momentum space and we define the velocity distribution $f(\mathbf{r}, \mathbf{p}; s)$ according to

$$F(\mathbf{r}, \mathbf{p}; s) = n(\mathbf{r}; s) f(\mathbf{r}, \mathbf{p}; s) \tag{3.8}$$

The density $n(\mathbf{r}; s)$ provides a continuum description of the particle distribution so that we neglect the fluctuations Δn of the average density. By assuming that the fluctuations are due to incoherent

motion of the particles in the bunch reference frame, we can estimate $\Delta n \simeq \sqrt{n}$. As a consequence, the Coulomb potential U due to the n particles in the space volume $\Delta\mathbf{r}$ changes according to $\Delta U = e^2\Delta n/\|\mathbf{r}' - \mathbf{r}\|$; when ΔU becomes comparable to the average kinetic energy T of the particles we cannot neglect the effect of fluctuations. However if n is too small the relative density fluctuations $\Delta n/n$ do not allow to treat the particle distribution as a continuous function. The distance Δr_D defined by the condition

$$\frac{\Delta U}{U} \simeq \frac{\Delta U}{T} \Rightarrow \frac{1}{\sqrt{n\Delta r_D^3}} \simeq \frac{e^2\sqrt{n\Delta r_D^3}}{T\Delta r_D} \Rightarrow \Delta r_D \simeq \sqrt{\frac{T}{ne^2}} \tag{3.9}$$

gives an estimate of the spatial dimension at which the particle distribution $n(\mathbf{r}; s)$ can be treated as a smooth function; according to plasma physics Δr_D is called the Debye radius [2]; an estimate gives $\Delta r_D \simeq 10^{-5} - 10^{-6}\ m$. Then we consider the following two possibilities:
1) the effect of Coulomb collisions between the particles inside each volume element can be neglected;
2) only the head to head collisions can be neglected, but the particles inside each volume element feel the effect of long range Coulomb collisions with many particles.

In the first case we describe the evolution of the particle distribution function $F(\mathbf{r}, \mathbf{p}; s)$ by the Vlasov equation

$$\frac{\partial F}{\partial s} = -\mathbf{p}\frac{\partial F}{\partial \mathbf{r}} - \left(\mathbf{k} - \frac{\partial V}{\partial \mathbf{r}}\right)\frac{\partial F}{\partial \mathbf{p}} \tag{3.10}$$

where $V(\mathbf{r}; s)$ is the Coulomb potential due to the particle density $n(\mathbf{r}; s)$ (space charge potential) and fulfills the Poisson equation $\nabla^2 V = -4\pi n$; $\mathbf{k}(\mathbf{r}; s)$ is defined by the external magnetic field. The Vlasov equation describes the evolution of the particle distribution in the regions where $F(\mathbf{r}, \mathbf{p}; s)$ is slowly varying with respect to the dimension of the phase space volume $\Delta\mathbf{r}\Delta\mathbf{p}$. The solution of equation (3.10) is a self-consistency problem due to the definition of the potential V[3].

In the second case the effect of collisions can be taken into account by introducing a stochastic process $\delta\mathbf{p}(\mathbf{r}, \mathbf{p}; f, \xi)$ that describes the discontinuous change of the momentum of a particle in the phase space volume $\Delta\mathbf{r}\Delta\mathbf{p}$

$$\mathbf{p}' = \mathbf{p} + \delta\mathbf{p} \tag{3.11}$$

The process $\delta\mathbf{p}$ depends on the distribution function in the velocity space and on a ramdon variable ξ that takes into account the distribution of the impact parameters of the collisions. Under the assumption that we can neglect the terms of order $\delta\mathbf{p}^3$ the stochastic map (3.11) transforms the Vlasov equation (3.10) into the Vlasov-Fokker-Planck (VFP) equation[2]

$$\frac{\partial F}{\partial s} = -\mathbf{p}\frac{\partial F}{\partial \mathbf{r}} - \left(\mathbf{k} - \frac{\partial V}{\partial \mathbf{r}}\right)\frac{\partial F}{\partial \mathbf{p}} - \frac{\partial}{\partial \mathbf{p}} < \delta\mathbf{p} > F + \frac{1}{2}\frac{\partial^2}{\partial\mathbf{p}\partial\mathbf{p}} < \delta\mathbf{p}^2 > F \tag{3.12}$$

where $<\ >$ denotes the average with respect to the stochastic variable ξ. The presence of the drift $< \delta\mathbf{p} >$ and the diffusion coefficients $< \delta\mathbf{p}^2 >$ destroy the Hamiltonian character of the dynamics[4]. The solution of the equation (3.12) is a self consistency problem both due to the definition of the potential V and due to the stochastic process $\delta\mathbf{p}$.

3.6.2 Solution of the Poisson-Vlasov problem

The numerical solution of the Poisson-Vlasov equation is divided into two steps: a) tracking of an ensemble of macro-particles for a step size Δs under the influence of the external fields $\mathbf{k}$ and of a given potential $V(\mathbf{r}; s)$ by using a symplectic scheme (micromaps)[5], and the computation of

the particle density $n(\mathbf{r};s)$ on an uniform grid of volume elements; b) the solution of the Poisson equation by using a FFT and a tridiagonal matrix inversion, and the computation of the potential $V(\mathbf{r};s)$ at each particle position by using a bilinear interpolation.

In a)we use a kick code to take into account the nonlinear forces due to the space charge and the multipole magnetic components whereas the linear fields are integrated exactly. Since we consider a great number of particles the tracking code is very cumbersome from a computational point of view, but it can be easily parallelized.

The solution of the Poisson equation (step b)) allows to introduce Dirichlet conditions on a cylinder with a base curve Γ, by replacing Γ with a polygon of vertex $\mathbf{r}_k$ on the grid of points, finding the Green's function $\Delta G_k(\mathbf{r}) = \delta_{\mathbf{r},\mathbf{r}_k}$ and writing the potential $V(\mathbf{r}) = V_0(\mathbf{r}) + \sum_j \alpha_j G_j(\mathbf{r})$ where the coefficients α_j are determined by imposing $V(\mathbf{r_k}) = 0$[6].

The simulation depends on three basic parameters: the number of macroparticles N_p, the number of micromaps n_{map} in a lattice period and the number of Fourier components K on each axis that corresponds to a grid size l/K where l is the dimension of the spatial region D considered in the code (usually we choose l 10 times the beam envelopes). We introduce a relation between N_p and K by requiring that the particle density resolution is of the same order as the spatial resolution so that

$$N_n = K^{d+2}\frac{\mathrm{Vol}(D)}{l^d} \tag{3.13}$$

where d is the number of degrees of freedom. We have checked the program by evolving the Kapcinski-Vladimiski self-consistent distribution (uniform ellipsoidal distribution) in a linear FODO cell in the 2 dimensional case, verifying that the emittances and the rms radii (matched case) are preserved by the simulation.

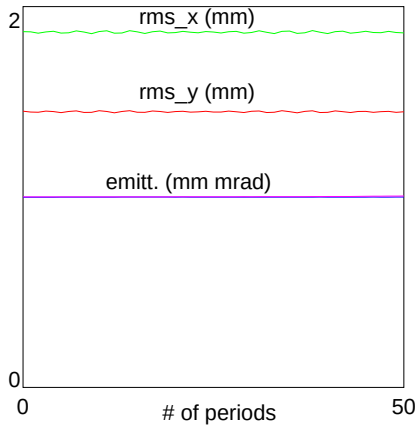

Figure 3.19: Evolution of rms x, y radii and of the emittance for a KV distribution in a linear FODO period versus the number of periods. The tune depression is 70%.

We are using the program to study the equilibrium distributions of a bunch in a FODO line for a high intensity linac and to study the relaxation times as a function of the space charge force. Moreover we are comparing the simulations with the results of the particle in core model in order to validate this approach to the problem of halo formation. The program is running in 2 and 3 dimensions, a parallel code in the 2D case is available and a 3D parallel version will be available soon. The effect of collisions will be included by introducing a random perturbation in the momentum space in the particle tracking.

3.6.3 Halo formation study by using FM analysis

We have studied the problem of halo formation in high intensity linacs by using the particle in core model (PC)[3]. This model considers the dynamics of a test particle spilled out from the beam core under the influence of the space charge force and of the external magnetic fields. The PC model assumes that the equilibrium distribution of the beam core can be approximated by a uniform ellipsoidal distribution and one computes the space charge fields as a function of the second moments whose evolution is given by the envelope equations[7].

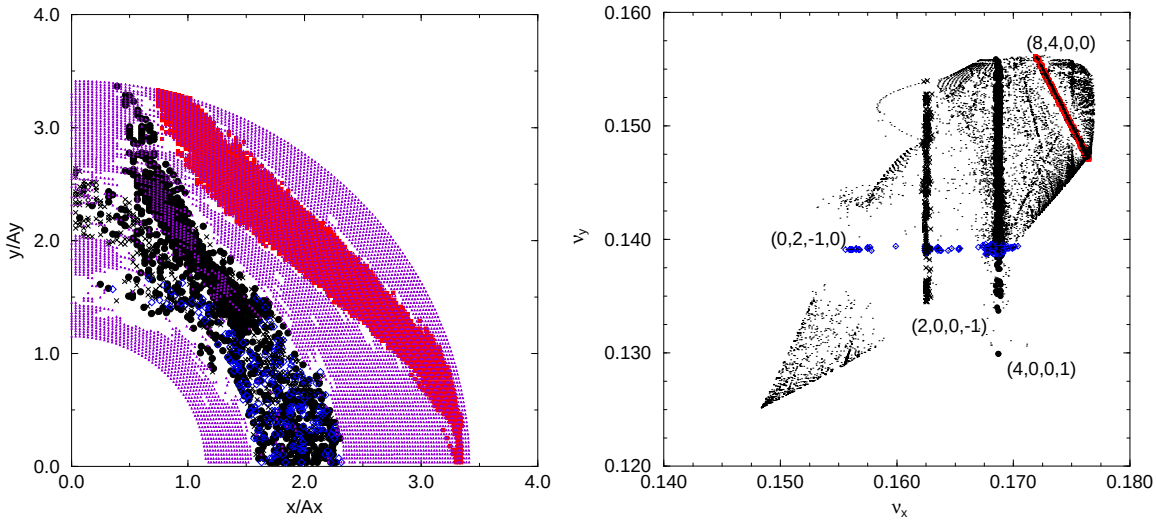

Figure 3.20: FM analysis of the PC model phase space of the same FODO cell as in fig (3.19) in a 20% mismatched case: the frequency space is plotted in the right figure and the low order resonances between the betatron frequencies and the envelope modes are indicated; the uniform grid of points that defines the initial conditions of the stable orbits is plotted in the left part and the resonant orbits are signed by different markers; the empty regions correspond to chaotic orbits due to resonance overlap (the scales are normalized to the beam envelopes **A**).

The test particle dynamics turns out to be Hamiltonian, but in the mismatched case the Hamiltonian is not periodic but only almost-periodic with s due to the presence of beam envelope modes[3]. Therefore it is difficult to get a phase space plot in order to study the effect of nonlinear resonances and chaotic regions. We have considered this problem by using the FM analysis that gives a picture of the phase space by using the map that associates to each orbit the corresponding betatron

frequencies. The computation of the frequencies uses an interpolated FFT with a Hanning filter on the results of a tracking program: this method provides a precision of order $1/N^4$ on the frequency values for a regular orbit, where N is the iteration number[8]. The FM allows to detect the resonant and the chaotic regions in the phase space and to introduce a criterion for the definition of a dynamic aperture for the halo formation[9]. We have computed the FM for a bunch in a FODO cell of a high intensity linac in the 2 and 3 dimensional cases. We checked the reliability of the PC models by comparing the space charge force of a uniform ellipsoidal distribution with the numerical solution of the Vlasov-Poisson problem. The preliminary results show that the PC model gives a good description of the test particle dynamics if one excludes a small region near the beam border[6].

We are planning to introduce the effect of collisions in PC models by computing the second moment equation for the VFP equation and by taking into account the emittance growth due to the diffusion coefficient. If the diffusion can be described as an adiabatic process we can still apply the FM analysis to see the evolution of the phase space structure. A similar approach could be used to describe the effect of the accelerating RF cavities.

References

[1] R.Balescu: Statistical Mechanics of charged particles, Interscience Pub., London, 1963.

[2] G.Schmidt: Physics of high temperature plasmas, Academic Press New York and London, 1966.

[3] M.Reiser: Theory and design of charged partciles beams, J.Wiley, 1994.

[4] J.Struckmeier: Phys. Rev. Special Topics, v.3,p.034202-1,2000.

[5] F.Bergamini, G.Franchetti, G.Turchetti: IL Nuovo Cimento v. A112, p. 429,1999.

[6] G.Turchetti, S.Rambaldi, A.Bazzani, M.Comunian, A.Pisent: to be published in Phys. Review Special Topics, Proc. of ICAP2000 conference, Darmstadt 2000.

[7] A.Bazzani, A.Pisent, M.Comunian: AIP Conference Proceedings, v.468 p.15 (1999).

[8] A.BazzaniM.Comunian, A.Pisent: Part.Accel. v.63, p.79, 1999.

[9] A.Bazzani, M.Comunian, A.Pisent: Proc. of EPAC 2000 conference, Vienna, 2000.

3.7 Beam Dynamics Activities at Rostock University

Ursula van Rienen Rostock University
van.rienen@e-technik1.uni-rostock.de

Since 1998 the University of Rostock, Germany, is part of the International TESLA Collaboration. The main focus of the Linear Collider study group in the Department of Electrical Engineering and Information Technology, Institute for General Electrical Engineering, lies on algorithmic developments for and application of beam dynamics simulations. Recent work is described below.

More information can be obtained from the groups site on the web:
http://www-ae.e-technik.uni-rostock.de/nsf/linac.html

3.7.1 Fast Solvers for Tracking of Low-Energy Beams

Gisela Pplau (gisela.poeplau@etechnik.uni-rostock.de)

The tracking of electron beams in the energy range of 1 to 100 MeV has to take into account the contribution of space charge effects. This is done in the framework of the tracking code Q [1] developed in the TEMF group at TU Darmstadt. In the course of the solution of the equation of motion Poisson's equation has to be solved in the beam's restframe for each tracking step ($\approx 10^3$) and for a number of particles in the order of 10^6. These facts demand for the construction of an efficient and robust Poisson solver.

State-of-the-art is the application of multigrid algorithms. Those algorithms work on a certain number of grids becoming coarser and coarser starting e.g. from the primary discretization. The main idea of multigrid techniques is the combination of a few relaxation steps (Jacobi, Gauss–Seidel) on the approximate solution of the system of equations with a coarse grid correction computed on the coarser grids. This leads to a much faster convergence, compared with classical iteration methods. Furthermore the computational work of multigrid algorithms increases only linearly with the number of unknowns, whereas classical methods have a steeper rise of computational effort.

In case of an adaptive discretization, as in the tracking context, the strategy for the construction of the coarser grids is a crucial point with respect to retaining the efficiency of the multigrid algorithm. There are two possibilities which have been tested up to now [2, 3]: First, the geometrical method, that is the real construction of coarser grids, and second, the algebraic method which only operates on matrix entries. It was proved true that especially on rectangular grids, as they are used in Q, the geometrical strategy implies the advantage of fast performance in case of suitable construction of the coarser grids (coarsening).

Next, several possibilities to accelerate the geometric multigrid and further developments of algebraic multigrid codes will be examined. Furthermore, the solver behaviour in case of a large number of time steps will be investigated. Depending on the variation of the charge distributions between two time steps information of the previous step may be used in order to save computational work in the subsequent step. For that, a trade off between large time steps with fewer tracking iterations versus short time steps with faster space charge calculation has to be found.

3.7.2 Tools for Field Computations in Complex Structures

The numerical investigation of broadband rf-properties of rather complex structures often reaches the limits even of most powerful computer systems. As "complex structure" one could think of a TESLA-9-cell structure, for instance, equipped with an input coupler and two HOM couplers. Whereas the cavity itself could be calculated in 2D considering its rotational symmetry, the couplers have tiny details to be analyzed only in high resolution 3D runs. Situation becomes even worse if a chain of cavities connected by beam pipe sections, that act as multimoded rf-waveguides, is under consideration, e.g. for HOM propagation analysis.

3.7.2.1 Use of S-Parameter Based Method: Coupled S-Parameter Calculation (CSC)

Hans-Walter Glock (hans-walter.glock@etechnik.uni-rostock.de),
Karsten Rothemund

One possibility to deal with complex rf-structures is a kind of domain decomposition based on S-parameter calculation for sub-components: The structure is decomposed in less complex subcomponents which can be calculated separately either analytically or with appropriate field solver codes as e.g. Agilent's HFSS or CST's MAFIA or MicroWaveStudio. A dedicated software

called CSC [4] has been developed. It is realized as a *Mathematica*™ package and thus practically platform-independent. CSC imports tables of frequency dependent S-parameters of all subcomponents and calculates the scattering properties with respect to the remaining open ports. It is applicable to arbitrary system topologies and mode numbers. The neighbourhood relations of the subcomponents are expressed as list of index pairs and entered into the *Mathematica* front end.

Some standard operations are included in the package (import filter, analytical description of homogeneous waveguides and rotation of objects, frequency interpolation, check and enforcement of S-matrix unitarity), others like visualization and further evaluation can be done with standard *Mathematica* commands. The calculation time of CSC itself is very short (in the order of a few seconds on usual PC infrastructure) since only explicit expressions of low dimensional matrices are needed. That makes CSC extremely fast and versatile for the analysis of subcomponent modifications, especially if there exists an analytical description.

A first release of CSC is now installed at DESY. The ongoing development includes both functional and usability improvements. Furthermore, the question of introducing an infinitely stiff beam into the concept of scattering description is studied.

3.7.2.2 Eigenmode Analysis with CSC

Karsten Rothemund (karsten.rothemund@etechnik.uni-rostock.de),
Hans-Walter Glock

To investigate the rf-properties of resonator-like structures the determination of HOMs in general and, especially, of so-called trapped modes is of crucial importance. Dedicated eigenmode solvers reach the limit of computational resources of any available computer system if large structures with small but important details have to be investigated (e.g. the beam pipe of a bunch compressor chicane in the TTF-FEL which has an overall length of about $4.5\mathrm{m}$ and contains bellows and vacuum flanges with structure sizes in the order of few cm).

The CSC-*Mathematica*-package, described above, was extended in a way that the special properties of closed structures are considered: Since no open ports remain, a characteristic equation has to be solved, resulting in the resonance frequencies [6, 7]. These solutions are found by scanning the eigenvalue spectrum of a frequency-dependent low-dimensional matrix, searching for eigenvalue 0. The corresponding eigenvectors carry the wave amplitudes needed for the determination of the resonant field patterns using a field solving code, either in frequency domain (preferred) or in time domain.

A comparison between CSC and MAFIA's eigenmode solver E was performed for a purely academic test resonator first. First it was split into 5 subcomponents. Then the S-parameters of the subsections were calculated using MAFIA's time domain solver T3. Special care has to be taken to the phase of the 2D-port-modes which have to be consistent during the whole calculation process; to guarantee this, a special mtk-module was implemented for the use with MAFIA. The frequencies of both methods match very well (deviation is about 10^{-4}), but the frequencies calculated by CSC seem to be systematically higher. The reason for this is still under investigation. Finally the field distributions of the resonant modes were computed using MAFIA's frequency domain solver W3 exciting waves of the appropriate power and phase at each port. This led to field patterns in all sections that match very well those calculated directly with MAFIA-E.

Problems sometimes occur in frequency ranges where waveguide modes do not propagate in the whole resonator. S-parameter calculation then requires crossing cut-off frequencies of waveguide ports which may lead to extremely long computation times (some programs even do not provide S-parameter below cut-off).

The advantage of the CSC-technique is the possibility to calculate both the S-parameters and

the field patterns of each subcomponent in separate runs and with different machines. It benefits from symmetries or repetitions of particular subsections. Further, it easily allows to specify frequency search ranges for the eigenmodes and it eases the study of structure modifications significantly.

Further work will concentrate on application of the method on real world examples like long cavity chains and special beam pipe insertions.

3.7.2.3 Parallel Eigenmode Solver on a SIMD Machine at DESY-Zeuthen

Ursula van Rienen (van.rienen@e-technik1.uni-rostock.de), work by Frank Neugebauer, formerly DESY-Zeuthen

As second possibility to deal with complex rf-structures an environment was set up to perform the time consuming solution of the eigenvalue problem inside an eigenmode computation on the APE-100 and APE-1000 parallel supercomputers at DESY-Zeuthen. In this procedure the front-end for pre- and postprocessing remains on a usual workstation, the transfer of system matrix and solution between workstation and APE-computer is carried out by an mtk-implementation. At moment the Lanczos method is implemented as eigenvalue solver. One advantage of the chosen method is the possibility to choose small frequency windows in higher frequency bands. Simulations e.g. for the 2.585 GHz dipole mode in a geometrically disturbed TESLA 9-cell cavity [5] have proved the efficiency of the method. At moment the work on this tool ceases but an improved implementation on the APE-1000 is foreseen for the next future.

3.7.3 Higher-Order-Modes in TESLA Accelerating Structures

Dirk Hecht (dirk.hecht@etechnik.uni-rostock.de)

For the new design of the TESLA accelerating structures, the so-called superstructure, the eigenmodes of the accelerating cavities have been studied using MAFIA computations. The superstructure consists of four 7-cell superconducting resonators, with a beam pipe between adjacent cavities with length of half an rf-wavelength. The influence of small geometrical variations in the cavities on frequency and field flatness of the accelerating mode was investigated. It was found, that field flatness of the accelerating mode is very sensitive to geometrical variations.

Furthermore several geometrical variations of the TESLA Test-Facility (TTF) 9-cell structure, like cavity distance, length of end cells, total structure length, have been studied regarding their influence on the resonant frequencies and field distributions of the higher oder modes (HOMs) in the cavity chain. By appropriate choice of cavity lengths, shortening of a 9-cell cavity by about 6 mm which is inside production tolerance, it was possible to create a field distribution which is localized in an inner cavity.

Next, the eigenmodes of the recently proposed new type of accelerating structure, composed out of two nine-cell resonators, will be studied.

References

[1] G. Pöplau, U. van Rienen, Multigrid algorithms for the tracking of electron beams, In: Multigrid Methods VI, (E. Dick, K. Riemslagh, J. Vierendeels, eds.), LNSCE, Vol. 14, Springer–Verlag, Berlin, 2000, 214–220.

[2] G. Pöplau, U. van Rienen, J. Staats, T. Weiland, Fast algorithms for the tracking of electron beams, In: Proceedings of the 7^{th} European Particle Accelerator Conference (EPAC 2000), Vienna, 2000, 1387–1389.

[3] G. Pöplau, U. van Rienen, Fast multigrid algorithms for the tracking of electron beams, Proceedings of the 6th International Computational Accelerator Physics Conference (ICAP 2000), Darmstadt, 2000, http://www.icap2000.de.

[4] H.-W. Glock, K. Rothemund, U. van Rienen, CSC - A System for Coupled S-Parameter Calculations, TESLA-Report 2001-25, DESY, Hamburg, March 2001

[5] F. Neugebauer, U. van Rienen, Solution of Very Large Eigenproblems on an APE-100 Supercomputer, Proceedings of the 6th International Computational Accelerator Physics Conference (ICAP 2000), Darmstadt, 2000, http://www.icap2000.de.

[6] K. Rothemund, H.-W. Glock, M. Borecky, U. van Rienen, Eigenmode Calculation in Long and Complex RF-Structures Using the Coupled S-Parameter Calculation Technique, TESLA-Report 2000-33, DESY, Hamburg, November, 2000

[7] K. Rothemund, H.-W. Glock, M. Borecky, U. van Rienen, Calculation of Electromagnetic Eigenmodes in Complex Structure Using Coupled S-Parameter Calculation, to appear in: Lecture Notes in Computational Science and Engineering, Springer, Berlin

3.8 Beam Dynamics Activities at UNM

J.A. Ellison (JE) ellison@math.unm.edu University of New Mexico

M. Vogt (MV) (vogtm@math.unm.edu)
I. Vlaicu (IV) (irina@math.unm.edu)
N. Fitzgerald (NF) (nura@unm.edu)

Here we report on beam dynamics research in the Mathematics and Statistics Department of the University of New Mexico.

There are many significant problems in beam dynamics that are at the forefront of what is understood in dynamical systems, stochastic processes and statistics, and in scientific and high performance computing. This makes it an ideal area for interaction between universities and accelerator laboratories.

The following are people with whom we are currently working: Alejandro Aceves (AA) (Mathematics at UNM), Desmond Barber (DB) (DESY), Pat Colestock (PC) (LANL), Scott Dumas (SD) (Mathematics at U. of Cincinnati), Klaus Heineman (KH) (DESY), Georg Hoffstaetter (GH) (DESY), Bill Sáenz (BS) (Catholic U., NRL), Tanaji Sen (TS) (FNAL), Linda Klamp Spentzouris (LS) (FNAL, IIT), and Bob Warnock (BW) (SLAC).

Much of our work is supported by DOE grant DE-FG03-99ER41104 from the Advanced Technology R & D Program at DOE. This grant was based on a proposal submitted to DOE by Ellison and Tanaji Sen (currently at FNAL).

Our activities have several foci: Vlasov and Vlasov–Fokker–Planck equations and properties of their solutions for the beam–beam interaction, and for longitudinal collective effects due to wake fields; spin dynamics; stochastic processes and perturbation techniques.

3.8.1 Vlasov and Vlasov–Fokker–Planck Equation

3.8.1.1 (1) Numerical

BW and JE have developed the Perron–Frobenius (PF) method for integrating the Vlasov–Fokker–Planck equation [1, 2] and have applied it to two problems. MV, TS and JE are developing the

Weighted Macro–Particle Tracking (WMPT) method in the context of the strong–strong beam–beam [3]. We are extending these algorithms from one to two degrees of freedom (d.o.f.) and pursuing parallel implementation.

3.8.1.2 (2) Analytical

This includes the existence of equilibria (periodic solutions), linearized behavior about these solutions (a generalized Floquet theory) and the associated linear stability and Landau damping, development of a weakly nonlinear theory and three wave coupling, and a study of fully nonlinear effects such as solitary waves, nonlinear Landau damping and turbulence. The weakly nonlinear theory requires a complete solution of the linearized equation. The work of Landau and Case–Van Kampen solves this for the basic plasma problem and we hope to extend these approaches using the the work of Bart and Warnock on integral equations of the third kind [4]. Some progress on the existence of equilibria and solitary waves will be discussed below. In certain situations the Vlasov equation can be approximated by "hydrodynamic" or moment equations and analyzed as above.

3.8.2 Longitudinal Collective Effects Due to Wakefields

3.8.2.1 (1) Bunched beam with radiation

BW and JE made a major advance in simulating the saw–tooth instability in the SLAC damping rings with a realistic wakefield [1]. The Vlasov–Fokker–Planck (VFP) theory was used and good agreement was found with several aspects of observations, including the presence of the bursting (sawtooth) mode with period comparable to the damping time. A special method was needed to treat the Vlasov part of the operator, as the straightforward finite difference approach was unstable. We were successful with the PF approach which is based on the method of characteristics and which allowed us to go to realistic damping times with smooth (low noise) densities. Almost the same method was applied to the beam–beam as discussed in the next section. Analytically, we are trying to understand the details of our numerical results and studying the linearization about the Haïssinski solution using the third kind integral equation. We are extending this work to include a multiturn cavity wake and a nonlinear applied R.F.

3.8.2.2 (2) Coasting beam without radiation

We are extending the pioneering work of Colestock, Spentzouris and Tzenov for proton beams [5]. The work on bunched beams should be directly applicable and we will proceed as discussed in the section on the Vlasov and VFP equation. On the one hand this problem is simpler than the bunched beam case but on the other hand we may encounter numerical stability problems because of no radiation. This is joint work with AA, PC, LS, MV, BW, IV and JE and will form the basis of a Ph.D. thesis by IV. The hydrodynamic approximation has been investigated for soliton behavior by both Tzenov and AA, and AA has derived a KdV equation by multiple time scales.

3.8.2.3 (3) Calculation of longitudinal wake field in a special case

BW and NF have determined analytically the longitudinal wake fields in a tube with smoothly varying radius and finitely conductive wall [6].

3.8.2.4 (4) A simple plasma problem

MV and JE have designed a small project as a senior thesis for NF. Her project is to summarize what is known related to the equations of ion acoustic waves in plasmas [7]. She is proceeding along the lines outlined in the Vlasov and VFP section and is using ideas from Sattinger's article including his discussion of the pseudospectral codes for integrating the KdV equation. What we learn may be useful for the more complicated beam dynamics problems. Bisognano discusses a similar problem in the context of beam dynamics.

3.8.3 Beam–Beam Interaction

3.8.3.1 (1) Beam–beam with radiation using PF

The equilibrium (periodic) phase space distribution of stored colliding electron beams has been studied from the viewpoint of VFP theory using the PF method [2]. Numerical integration of the VFP system in one degree of freedom revealed a nearly Gaussian equilibrium with non–diagonal covariance matrix. This result is reproduced approximately in an analytic theory based on linearization of the beam–beam force (the VFP equation remains nonlinear). Analysis of an integral equation for the equilibrium distribution, without linearization, establishes the existence of a unique equilibrium at sufficiently small current. The role of damping and quantum noise is clarified through a new representation of the propagator of the linear Fokker–Planck equation with harmonic force. Details are discussed in [2]. The proof of the existence of the equilibrium uses an implicit function theorem in an appropriate Banach space and will be published separately by BW and JE.

With MV, we are investigating the behavior of the code without the radiation and with smaller beam–beam parameter for use in the proton case. The code is being extended to 2–d.o.f. and to parallel algorithms. The existence of an equilibrium for the linear beam–beam force has been demonstrated [2] and can also be viewed in terms of a self–consistently determined dynamic beta (as pointed out by MV and others). Our implicit function theorem works for arbitrarily small radiation but in the limit of no radiation there are surely resonance issues and the existence of an equilibrium is an open question. Perturbation theory looks promising for proving the existence of a quasi–equilibrium.

3.8.3.2 (2) Beam–beam for hadrons using WMPT

MV, TS and JE have developed a second code [3] for the simulation of beam–beam effects in the strong–strong regime for protons (i.e. without radiation). The code is based on symplectic tracking of macro–particles which are assigned a weight representing the phase space density at their initial conditions. We refer to this as weighted macro–particle tracking (WMPT). We found that this idea, while developed independently, has been used by Wollman [8] on the basic plasma problem. We have treated three different 1–d.o.f. limits of the beam–beam force. Particular emphasis was put on development of efficient algorithms for the computation of the beam–beam kick. With this simulation code we have so far studied the time evolution of the moments of the density and in particular the frequency spectrum of the centroid motion. We are investigating the possible coupling of the π and σ modes and also the existence of analogous modes when the tunes are separated. The code will be extended to 2–d.o.f..

3.8.3.3 (3) Weak–Strong Beam–Beam with fluctuations

We are investigating the impact of fluctuating fields on emittance growth in the presence of the weak–strong beam–beam in a hadron collider. We model fluctuations by an Ornstein–Uhlenbeck process and then analytically derive diffusion coefficients in action in the presence of three different sources of fluctuations: fluctuations in offsets between the beams, tune fluctuations and fluctuations in beam size. Integration of the diffusion Fokker–Planck equation with these diffusion coefficients leads to predictions on emittance growth. We apply our results to the LHC. This is work by TS, with help from Maria–Paz Zorzano, IV and JE and is an extension of the 1–d.o.f. case [9].

3.8.4 Spin Dynamics

3.8.4.1 (1) Spin tune

The paper "A quasiperiodic treatment of spin motion in storage rings — a new perspective on spin tune" with DB, KH and JE is nearly complete. In this paper we show how spin motion on the periodic closed orbit of a storage ring can be analyzed in terms of the Floquet theorem for equations of motion with periodic parameters. The spin tune on the closed orbit emerges as an extra frequency of the system which is contained in the Floquet exponent in analogy with the wave vector in the Bloch wave functions for electrons in periodic atomic structures. We then proceed to show how to analyze spin motion on quasi–periodic synchro–betatron orbits in terms of a generalization of the Floquet theorem and we find that, provided small divisors are controlled by applying a Diophantine condition, a spin tune can again be defined and that it again emerges as an extra frequency in a Floquet–like exponent. We thereby obtain a deeper insight into the concept of "spin tune" and the conditions for its existence.

3.8.4.2 (2) Existence of a stationary polarization

KH and JE are applying ergodic theorems to stroboscopic averaging of Liouville densities and spin fields. A class of orbital systems with volume preserving flows is defined. Performing stroboscopic averaging and applying the Birkhoff ergodic theorem, Liouville densities, periodic in the azimuthal variable, are obtained. More importantly, particles with both spin and integrable orbital motion are considered. By performing stroboscopic averaging on the polarization densities one gets, via the Birkhoff and Von Neumann Ergodic Theorems, polarization densities which are periodic in the azimuthal variable. This demonstrates that the tracking algorithm, encoded in the program SPRINT and used in the simulation of spin polarized storage rings, is mathematically well founded.

3.8.4.3 (3) Adiabatic invariance of the invariant spin field

GH has written a *Habilitation* thesis [10] on modern concepts of spin dynamics in accelerators. SD and JE are collaborating with GH on a theoretical aspect of this work; techniques from rigorous averaging theory are being used to directly show that the invariant spin field is an adiabatic invariant under slow changes in parameters such as beam energy. This requires special care because many resonances are crossed during the acceleration process. We have an elementary proof in a special case related to the closed orbit and are optimistic with regard to its extension to phase space trajectories.

3.8.4.4 (4) Polarized protons for the VLHC

MV has analyzed spin motion in the combined function lattice of the 2×20 TeV so called stage 1 low field collider. The results suggest the possibility that polarized protons at about 80 times the RHIC energy can be achieved with reasonable effort.

3.8.5 Stochastic Averaging and Single Realization Noise

In [11], JE introduced the single realization problem and argued in a relevant example that single realization noise plus nonlinearity can lead to diffusion. This was done by developing a new stochastic averaging formalism and applying it in a heuristic way. However, we now have a proof in the very special case of [12, Example 8.1, pages 257–259] which gives us added confidence in the approach.

3.8.6 Perturbation theory

It is the view of JE that the KAM and Nekhoroshev theorems are great foundational works in dynamical systems but they are mostly irrelevant to beam dynamics because the perturbation parameter, call it ϵ, must be much, much smaller than typical beam dynamics parameters. The KAM theorem is valid for infinite times on Cantor–like sets whereas Nekhoroshev theorems are valid for exponentially long times on open sets or even on all of phase space. For rigorous results, we believe first and second order averaging theorems (where there are only modest restrictions on ϵ and which give error bounds) are much more applicable. First order averaging theorems give $O(\epsilon)$ error bounds at $O(1/\epsilon)$ times whereas second order theorems can give $O(\epsilon^2)$ errors at $O(1/\epsilon)$ times or in special cases $O(\epsilon)$ errors at $O(1/\epsilon^2)$ times. Jeng Shih and JE discussed such theorems with beam dynamics in mind in [13] and we are pursuing several extensions and complements.

Theorem 2 on p. 595 of [13] requires the convergence of two series which suffers from the small divisor problem (i.e. the series will only converge on a Cantor set in ω space). We have modified this condition using the work of SD on "cut–off Diophantine conditions" (See [14]) which gives a much more satisfying condition on an open set of ω values.

The above theorems are basically about trajectories. However in beam dynamics we are primarily interested in quasi–invariants. BS, SD and JE are extending the averaging results to the case where invariants of an associated unperturbed problem are quasi–invariants for the full problem, at $O(1/\epsilon^2)$ times.

In many problems the perturbation is a delta function and standard averaging theorems do not apply. We have developed a set of averaging theorems for maps, to include this kick case.

Because the averaging theorems require ϵ to be small, it is important to know how small in a given context. BW and JE plan to investigate this numerically using the recent work [15].

We are extending our averaging approaches to the Vlasov equation both in terms of the collective force and in terms of the weakly nonlinear theory.

References

[1] R. L. Warnock and J. A. Ellison, A general method for propagation of the phase space distribution, with application to the saw–tooth instability, *Proc. 2-nd ICFA Workshop on High Brightness Beams*, UCLA, 1999 and preprint SLAC-PUB-8404 (2000).

[2] J. A. Ellison and R. L. Warnock, Existence and properties of an equilibrium state with beam–beam collisions, *Proc. 2-nd ICFA Workshop on Quantum Aspects of Beam Physics*, Capri, October 2000, and preprint SLAC-PUB-8778 (2001).

[3] M. Vogt, T. Sen and J. A. Ellison, Simulations of Three 1-D Limits of the Strong–Strong Beam–Beam Interaction in Hadron Colliders Using Weighted Macro–Particle Tracking, to be published as a FNAL Report.

[4] G. R. Bart and R. L. Warnock, Linear Integral Equations of the Third Kind, *SIAM J. Math. Anal.* **4** (4), p. 609–622, (1973); G. R. Bart, Three Theorems on Third–Kind Linear Integral Equations, *J. Math. Anal and App.* **79** (1), p. 48–57, (1981).

[5] L. K. Spentzouris, Coherent Nonlinear Longitudinal Phenomena in Unbunched Synchrotron Beams, Ph.D. Thesis, Northwestern University (1996); S. I. Tzenov, P. L. Colestock and L. K. Spentzouris, Coherent Nonlinear Phenomena in High Energy Synchrotrons: Observations and Theoretical Models, *Proc. International Symposium on Near Beam Physics*, FNAL, (September 1997).

[6] N. Fitzgerald, An Analytic Method of Finding Longitudinal Wake Fields in a Tube with Smoothly Varying Radius and Finitely Conductive Wall, *DOE ERULF/SISE Program*, http://www.slac.stanford.edu/grp/th/erulf-sise/2000/ (2000).

[7] D. H. Sattinger, Scaling, Mathematical Modeling, & Integrable Systems, in *Scaling Limits and Models in Physical Processes*, DMV Seminar, Band 28, Birkhäuser Verlag (1998); R. C. Davidson, Methods in Nonlinear Plasma Theory, Academic Press (1972); J. J. Bisognano, Solitary Waves in Particle Beams, *European Particle Accelerator Conference* (1996).

[8] S. Wollman and E. Ozizmir, Numerical Approximations of the One–Dimensional Vlasov–Poisson System with Periodic Boundary Conditions, *SIAM J. Num. Anal.* **33** (4), p. 1377–1409, (1996).

[9] T. Sen and J. A. Ellison, Emittance Growth Due to Fluctuations and the Head–on Beam–Beam Interaction and Fluctuating Fields in Hadron Colliders, *Phys. Rev. Letters* **77** (6), (1996).

[10] G.H. Hoffstaetter, Aspects of the Invariant Spin Field for High Energy Polarized Proton Beams, Habilitation thesis, Darmstadt University of Technology, (2000).

[11] J. A. Ellison, Accelerators and Probability: The Special Effect of Noise in Beam Dynamics, *Proc. of the Workshop on Nonlinear and Stochastic Beam Dynamics in Accelerators — A Challenge to Theoretical and Computational Physics*, Lüneburg, September 1997. Edited by A. Bazzani, J. A. Ellison, H. Mais, G. Turchetti. DESY-Proceedings-1998-03.

[12] M. I. Freidlin and A. D. Wentzell, Random Perturbations of Dynamical Systems, Second Edition, Springer (1998).

[13] J. A. Ellison and H.–J. Shih, The Method of Averaging in Beam Dynamics, in: Y. T. Yan, J. P. Naples, M. J. Syphers (Eds.), Accelerator Physics at the Superconducting Super Collider, AIP Conference Proceedings, p. 326, (1995).

[14] H. S. Dumas, J. A. Ellison and F. Glose, A Mathematical Theory of Planar Particle Channeling in Crystals, *Physica D* **146** p. 341–366, (2000).

[15] R. L. Warnock, Improved *a priori* Error Bounds for Approximate Solutions of Ordinary Differential Equations, SLAC-PUB-8638, (2001).

4: Review of Beam Dynamics Problems

4.1 The Stern-Gerlach Force in Beam Dynamics

M. Conte Mario.Conte@ge.infn.it University of Genova

M. Ferro Marconi Communications
Maximiliano.Ferro@marconi.com

G. Gemme INFN Genova
Gianluca.Gemme@ge.infn.it

W.W. MacKay mackay@bnl.gov RHIC

R. Parodi INFN Genova
Renzo.Parodi@ge.infn.it

M. Pusterla University of Padova
Modesto.Pusterla@pd.infn.it

4.1.1 Introduction

As it is well known, either at atomic level or at nuclear and subnuclear level, the intensity of the Stern-Gerlach force is much lower than the corresponding Lorentz force, whenever the latter is present. Therefore, this force is widely used in electrically neutral systems, such as neutron traps and atomic beams [1][2][3].

As far as the charged particles are concerned, the Stern-Gerlach force has been considered for the spin states separation (the so-called spin-splitter) with the purpose of converting unpolarized beams into polarized ones, making use of either transverse impulses[4][5][6][7] acting on betatron oscillations, or longitudinal kicks[8][9] acting on synchrotron oscillations. The most important issue for both methods is that the momentum and/or energy kicks sum up coherently.

The Stern-Gerlach interaction has been also proposed as a polarimeter[10][11] based upon the energy exchanged between polarized particles and the e.m. field within a RF cavity.

4.1.2 General Considerations

The Stern-Gerlach force acts on particles, carrying a magnetic moment, which cross inhomogeneous magnetic fields. In a reference frame where particles are at rest, the expression of this force is

$$\vec{f}_{SG} = -\nabla U \tag{4.1}$$

where

$$U = -\vec{\mu} \cdot \vec{B} \tag{4.2}$$

is the magnetic potential energy and

$$\vec{\mu} = g\frac{e}{2m}\vec{S}. \tag{4.3}$$

is the magnetic moment, where $e = \pm 1.602 \times 10^{-19}$ C is the elementary charge with $+$ for p, e^+ and $-$ for $\bar{p}, e^-$, making $\vec{\mu}$ and $\vec{S}$ either parallel or antiparallel, respectively; m is the rest mass, i.e. 9.11×10^{-31} kg for $e^\pm$ and 1.67×10^{-27} kg for $p, \bar{p}$, the gyromagnetic ratio g is 2.002 for $e^\pm$ and 5.586 for $p, \bar{p}$. Then we have:

$$\mu = |\vec{\mu}| = g\frac{|e|\hbar}{4m} = \begin{cases} 9.28 \times 10^{-24}\ \mathrm{JT}^{-1} & (e^{\pm}) \\ 1.41 \times 10^{-26}\ \mathrm{JT}^{-1} & (p, \bar{p}) \end{cases} \tag{4.4}$$

To derive the general expression of the Stern-Gerlach force in the laboratory frame, we have first to carry out the Lorentz transformation of the electric and magnetic field from the laboratory frame to the center-of-mass frame, where particles are at rest and we can correctly evaluate such a force. Then this force must be boosted back to the laboratory frame.

In order to accomplish the sequence of Lorentz boosts, we introduce the 4-dimension [12] vectors $X \equiv (x, y, z, ict)$, where $i = \sqrt{-1}$, in laboratory frame and $X' \equiv (x', y', z', ict')$ in the particle's rest frame. Considering the variables z and t only, the Lorentz boosts $X' = MX$ and $X = M^{-1}X$, with M and M^{-1}, yield

$$\begin{pmatrix} z' \\ ict' \end{pmatrix} = \begin{cases} z' = \gamma(z - \beta ct) \\ t' = \gamma\left(t - \frac{\beta}{c}z\right) \end{cases} \quad \text{and} \quad \begin{pmatrix} z \\ ict \end{pmatrix} = \begin{cases} z = \gamma(z' + \beta ct') \\ t = \gamma\left(t' + \frac{\beta}{c}z'\right) \end{cases} \tag{4.5}$$

with

$$\left\{\beta = |\vec{\beta}| = \frac{|\vec{v}|}{c}, \quad \gamma = \frac{1}{\sqrt{1-\beta^2}}\right\}$$

and then we have:

$$\frac{\partial}{\partial z'} = \gamma\left(\frac{\partial}{\partial z} + \frac{\beta}{c}\frac{\partial}{\partial t}\right) \tag{4.6}$$

The 4-vector formalism is still applied for undergoing the Lorentz transformation of a force; let us introduce

$$u_\mu = \frac{dx_\mu}{d\tau} \quad \text{and} \quad d\tau = \frac{ds}{c} = \frac{dt}{\gamma} \tag{4.7}$$

as the 4-velocity and the differential of the proper time respectively, we may define the 4-momentum as the product of the rest mass m times this 4-velocity, i.e.

$$P_\mu = m\, u_\mu = (\vec{p}, i\gamma mc) \tag{4.8}$$

Then the 4-force is just the derivative of the 4-momentum (4.8) with respect to the proper time, that is

$$F_\mu = \frac{dP_\mu}{d\tau} = \left(\gamma\frac{d\vec{p}}{dt}, i\frac{\gamma}{c}\frac{d(\gamma mc^2)}{dt}\right) = \left(\gamma\vec{f}, i\frac{\gamma}{c}\frac{dE_{\mathrm{tot}}}{dt}\right) \tag{4.9}$$

where $\vec{f}$ is the ordinary force. In the c.m. system eq. (4.9) reduces to

$$F'_\mu = (\vec{f}', 0) \tag{4.10}$$

since $\gamma' = 1$ and $E_{\mathrm{tot}} = mc^2$ is a constant. Bearing in mind the last step of the whole procedure, i.e. the boost of any force from rest to laboratory frame, we use the relation $F_\mu = M^{-1}F'_\mu$ and obtain

$$\vec{f}_\perp = \frac{1}{\gamma}\vec{f}'_\perp \quad \text{and} \quad \vec{f}_{||} = \vec{f}'_{||} \quad (f_z = f'_z) \tag{4.11}$$

4.1.3 Stern-Gerlach Force

The Stern-Gerlach force, as described by eq. (4.1), must be evaluated in the particle rest frame where it takes the form

$$\vec{f}'_{SG} = \nabla'(\vec{\mu}^* \cdot \vec{B}') = \frac{\partial}{\partial x'}(\vec{\mu}^* \cdot \vec{B}')\hat{x} + \frac{\partial}{\partial y'}(\vec{\mu}^* \cdot \vec{B}')\hat{y} + \frac{\partial}{\partial z'}(\vec{\mu}^* \cdot \vec{B}')\hat{z} \tag{4.12}$$

having defined the magnetic moment as μ^*, rather than μ', for opportune reasons. By applying the transformations (4.6) and (4.11), the force (4.12) is boosted to the laboratory system becoming

$$\vec{f}_{SG} = \frac{1}{\gamma}\frac{\partial}{\partial x}(\vec{\mu}^* \cdot \vec{B}')\hat{x} + \frac{1}{\gamma}\frac{\partial}{\partial y}(\vec{\mu}^* \cdot \vec{B}')\hat{y} + \frac{\partial}{\partial z'}(\vec{\mu}^* \cdot \vec{B}')\hat{z} \tag{4.13}$$

Bearing in mind the Lorentz transformation[13] of the fields $\vec{E}, \vec{B}$ and $\vec{E}', \vec{B}'$

$$\vec{E}' = \gamma(\vec{E} + c\vec{\beta} \times \vec{B}) - \frac{\gamma^2}{\gamma + 1}\vec{\beta}(\vec{\beta} \cdot \vec{E}) \tag{4.14}$$

$$\vec{B}' = \gamma\left(\vec{B} - \frac{\vec{\beta}}{c} \times \vec{E}\right) - \frac{\gamma^2}{\gamma + 1}\vec{\beta}(\vec{\beta} \cdot \vec{B}) \tag{4.15}$$

the energy $(\vec{\mu}^* \cdot \vec{B}') = \mu_x B'_x + \mu_y B'_y + \mu_z B'_z$ becomes

$$(\vec{\mu}^* \cdot \vec{B}') = \gamma\mu^*_x\left(B_x + \frac{\beta}{c}E_y\right) + \gamma\mu^*_y\left(B_y - \frac{\beta}{c}E_x\right) + \mu^*_z B_z \tag{4.16}$$

If we introduce eq. (4.16) into eq. (4.13) and take into account eq. (4.6), we can finally obtain the Stern-Gerlach force components in the laboratory frame:

$$f_x = \mu^*_x\left(\frac{\partial B_x}{\partial x} + \frac{\beta}{c}\frac{\partial E_y}{\partial x}\right) + \mu^*_y\left(\frac{\partial B_y}{\partial x} - \frac{\beta}{c}\frac{\partial E_x}{\partial x}\right) + \frac{1}{\gamma}\mu^*_z\frac{\partial B_z}{\partial x} \tag{4.17}$$

$$f_y = \mu^*_x\left(\frac{\partial B_x}{\partial y} + \frac{\beta}{c}\frac{\partial E_y}{\partial y}\right) + \mu^*_y\left(\frac{\partial B_y}{\partial y} - \frac{\beta}{c}\frac{\partial E_x}{\partial y}\right) + \frac{1}{\gamma}\mu^*_z\frac{\partial B_z}{\partial y} \tag{4.18}$$

$$f_z = \mu^*_x C_{zx} + \mu^*_y C_{zy} + \mu^*_z C_{zz} \tag{4.19}$$

with

$$C_{zx} = \gamma^2\left[\left(\frac{\partial B_x}{\partial z} + \frac{\beta}{c}\frac{\partial B_x}{\partial t}\right) + \frac{\beta}{c}\left(\frac{\partial E_y}{\partial z} + \frac{\beta}{c}\frac{\partial E_y}{\partial t}\right)\right] \tag{4.20}$$

$$C_{zy} = \gamma^2\left[\left(\frac{\partial B_y}{\partial z} + \frac{\beta}{c}\frac{\partial B_y}{\partial t}\right) - \frac{\beta}{c}\left(\frac{\partial E_x}{\partial z} + \frac{\beta}{c}\frac{\partial E_x}{\partial t}\right)\right] \tag{4.21}$$

$$C_{zz} = \gamma\left(\frac{\partial B_z}{\partial z} + \frac{\beta}{c}\frac{\partial B_z}{\partial t}\right) \tag{4.22}$$

4.1.4 The Rectangular Cavity

We shall consider a rectangular resonator of width a (parallel to the x axis), height b (parallel to the y axis) and length d (parallel to the z axis), excited in the TE_{011} mode, whose main characteristics (see Ref. [14] for details) are:

$$K_c = \frac{\pi}{b} \tag{4.23}$$

$$\omega = c\sqrt{\left(\frac{\pi}{b}\right)^2 + \left(\frac{\pi}{d}\right)^2} \tag{4.24}$$

$$\beta_{\rm ph} = \frac{d}{\pi}\sqrt{\left(\frac{\pi}{b}\right)^2 + \left(\frac{\pi}{d}\right)^2} \tag{4.25}$$

where $v_{\rm ph} = \beta_{\rm ph} c$ is the wave's phase velocity. A glance at the SG-force components (4.17)-(4.22) suggests that f_z will dominate at high energy, since terms proportional to γ^2 appear, whereas the transverse components have terms independent of γ, not to mention the γ^{-1} terms. The most appropriate choice of the spin orientation seems to be the one parallel to $\hat{y}$ i.e. to $\vec{B}_{\rm ring}$, i.e. the force component is given by the insertion of eq. (4.21) into eq. (4.19), since no spin rotation will be required, beyond the advantage of the factor γ^2. Therefore, if we consider that the beam crosses the centre of the cavity wall, the field components are

$$B_x = B_z = 0 \tag{4.26}$$

$$B_y = -B_0 \frac{b}{d} \cos\left(\frac{\pi z}{d}\right) \cos\,\omega t \tag{4.27}$$

$$E_x = -\omega\, B_0 \frac{b}{\pi} \sin\left(\frac{\pi z}{d}\right) \sin\,\omega t \tag{4.28}$$

$$E_y = E_z = 0 \tag{4.29}$$

Finally, we can write

$$f_z = \mu^* \gamma^2 B_0 b \left\{ \frac{1}{\pi} \left[\left(\frac{\pi}{d}\right)^2 + \left(\frac{\beta\omega}{c}\right)^2 \right] \sin\left(\frac{\pi z}{d}\right) \cos\,\omega t + \frac{2}{d}\left(\frac{\beta\omega}{c}\right) \cos\left(\frac{\pi z}{d}\right) \sin\,\omega t \right\} \tag{4.30}$$

4.1.5 Involved Energy

The energy gained, or lost, by a particle with a magnetic moment after having crossed a RF cavity can be evaluated by integrating the Stern-Gerlach force (4.13) over the cavity length, namely:

$$\Delta U = \int_0^d dU = \int_0^d \vec{f} \cdot d\vec{r} = \int_0^d f_z dz = \int_0^d \mu^* C_{zy} dz \tag{4.31}$$

Bearing in mind eq. (4.30) and carrying out the trivial substitution $\omega t = \frac{\omega z}{\beta c}$, the integral (4.31) becomes

$$\Delta U = \mu^* \gamma^2 B_0 b \left\{ \frac{1}{\pi} \left[\left(\frac{\pi}{d}\right)^2 + \left(\frac{\beta\omega}{c}\right)^2 \right] I_1 + \frac{2}{d}\left(\frac{\beta\omega}{c}\right) I_2 \right\}$$

where I_1 and I_2 are simple integrals[1] of trigonometric functions; then

$$\Delta U = \mu^* \gamma^2 B_0 \frac{b}{d} \frac{\left(\frac{\pi}{d}\right)^2 + \left(\frac{\beta\omega}{c}\right)^2 - \left(\frac{\omega}{c}\right)^2}{\left(\frac{\pi}{d}\right)^2 - \left(\frac{\omega}{\beta c}\right)^2} \left[1 + \cos\left(\frac{\omega d}{\beta c}\right)\right] \tag{4.32}$$

Taking into account the stationary wave conditions (eqs. 4.24 and 4.25) and that the length of the cavity can be expressed as

$$d = \frac{1}{2}\beta_{\rm ph}\lambda \tag{4.33}$$

we can write eq. (4.32) as

$$\Delta U = \mu^* B_0 \frac{b}{d} \left[\beta^2\gamma^2 \frac{\beta_{\rm ph}^2 - 1}{\beta_{\rm ph}^2 - \beta^2} + \frac{\beta_{\rm ph}^2\beta^2}{\beta_{\rm ph}^2 - \beta^2}\right] \left(1 + \cos\frac{\beta_{\rm ph}}{\beta}\pi\right)$$

In the ultrarelativistic limit ($\gamma \gg 1$ and $\beta \simeq 1$),

$$\Delta U \simeq \mu^* B_0 \frac{b}{d}\gamma^2(1 + \cos\beta_{\rm ph}\pi) = 2\,\mu^* B_0 \frac{b}{d}\gamma^2 \quad (\beta_{\rm ph} = \text{even integer}) \tag{4.34}$$

Before proceeding, we need to compare the energy gain/loss due to the Stern-Gerlach interaction with the same quantity caused by the electric field. To this aim, we emphasize that

$$dU_E = \vec{f}_E \cdot d\vec{r} = eE_x dx \tag{4.35}$$

as can be easily understood looking at eqs. (4.28) and (4.29). Since the carrier particle travels from 0 to d along the z-axis, the only integral which makes sense is the following:

$$\Delta U_E = \int_0^d eE_x\,dx = \int_0^d eE_x \frac{dx}{dz}dz = \int_0^d eE_x\,x'dz \tag{4.36}$$

or

$$\Delta U_E = -x'e\omega B_0 \frac{b}{\pi}\int_0^d \sin\left(\frac{\pi z}{d}\right)\sin\left(\frac{\omega z}{\beta c}\right)dz = -x'e\omega B_0 \frac{b}{d}\frac{\sin\left(\frac{\omega d}{\beta c}\right)}{\left(\frac{\pi}{d}\right)^2 - \left(\frac{\omega}{\beta c}\right)^2}$$

or

$$\Delta U_E = \left[e\omega B_0 \frac{bd}{\pi^2}\frac{\beta^2}{\beta_{\rm ph}^2 - \beta^2}\sin\frac{\beta_{\rm ph}}{\beta}\pi\right] x' = \kappa x' \tag{4.37}$$

having proceeded as before.

The Stern-Gerlach interaction has been proposed[8] for separating in energy particles with opposite spin states via the following mechanism: spin up particles receive (or loose) the amount of energy given (4.34) at each rf cavity crossing, and this will take place all over the time required; simultaneously, spin down particles behave in the opposite way, i.e. they loose (or gain) the same amount of energy turn after turn. The final energy separation after N revolutions is:

---

[1]

$$I_1 = \int_0^d \sin\left(\frac{\pi z}{d}\right)\cos\left(\frac{\omega z}{\beta c}\right)dz = \frac{\frac{\pi}{d}}{\left(\frac{\pi}{d}\right)^2 - \left(\frac{\omega}{\beta c}\right)^2}\left[1 + \cos\left(\frac{\omega d}{\beta c}\right)\right]$$

$$I_2 = \int_0^d \cos\left(\frac{\pi z}{d}\right)\sin\left(\frac{\omega z}{\beta c}\right)dz = -\frac{\frac{\omega}{\beta c}}{\left(\frac{\pi}{d}\right)^2 - \left(\frac{\omega}{\beta c}\right)^2}\left[1 + \cos\left(\frac{\omega d}{\beta c}\right)\right]$$

$$\Delta U_{\uparrow\downarrow} = \sum \{\Delta U_{\uparrow} - (-\Delta U_{\downarrow})\} = 4\frac{b}{d} N\,\mu^* B_0\,\gamma^2 \simeq 4\,N\,\mu^* B_0\,\gamma^2 \tag{4.38}$$

Instead, the adding up of the energy contribution (4.37) due to the electric field is

$$(\Delta U_E)_{tot} = \sum \Delta U_E = \kappa \sum x' = 0 \tag{4.39}$$

since x' changes continuosly its sign with a periodicity related to the betatron oscillations.

The absolute polarimeter[10] could be another aplication of the Stern-Gerlach interaction. In this example we are interested in the instantaneous interaction between magnetic moment and the rf fields: therefore the zero-averaging due to the betatron oscillations incoherence would not help us. Notwithstanding, setting $\beta_{\rm ph}$ equal to an **integer** in eq. (4.37), we have for U.R. particles:

$$\Delta U_E = -\frac{x' e\omega B_0\, bd}{\pi^2(\beta_{\rm ph}^2 - 1)} \sin\left(\beta_{\rm ph}\pi + \frac{\beta_{\rm ph}\pi}{2\gamma^2}\right) \simeq \pm\frac{x' bd}{2\pi}\frac{\beta_{\rm ph}}{\beta_{\rm ph}^2 - 1}\frac{e\omega B_0}{\gamma^2} \tag{4.40}$$

This $1/\gamma^2$ dependence of the spurious signal, compared to the γ^2 dependence of the signal (4.34) to be measured, sounds quite interesting for the feasibility of this kind of polarimeter; however, one must realize that if $\beta_{\rm ph}$ is not exactly an integer, eq. (4.40) would become

$$\Delta U_E \simeq \pm\frac{x' bd}{2\pi}\frac{e\omega B_0}{\beta_{\rm ph}^2 - 1}\left(\epsilon + \frac{\beta_{\rm ph}}{\gamma^2}\right) \tag{4.41}$$

where ϵ is the error in $\beta_{\rm ph}$.

4.1.6 A Few Numerical Examples

4.1.6.1 Spin-splitter

The spin-splitter principle requires a repetitive crossing of $N_{\rm cav}$ cavities distributed along the ring, each of them resonating in the TE mode. After each revolution, the particle experiences a variation, or **kick**, of its energy or of its momentum spread

$$\zeta = \frac{\delta p}{p} = \frac{1}{\beta^2}\frac{\delta E}{E} \simeq \frac{N_{\rm cav}\Delta U}{E} \simeq \frac{2\sqrt{3}}{3}\,N_{\rm cav}\frac{B_0}{B_\infty}\gamma \tag{4.42}$$

having made use of eq. (4.34), further simplified by reasonably setting $\beta_{\rm ph} = 2$, and with

$$B_\infty = \frac{mc^2}{\mu^*} = \frac{1.503 \times 10^{-10}\ J}{1.41 \times 10^{-26}\ JT^{-1}} \simeq 10^{16}\ T \tag{4.43}$$

for (anti)protons. From eq. (4.42) we may find as the number of turns needed for attaining a momentum separation equal to $2\left(\frac{\Delta p}{p}\right)$

$$N = \frac{\left(\frac{\Delta p}{p}\right)}{\zeta} = \frac{1}{2\,N_{\rm cav}\gamma}\frac{B_\infty}{B_0}\left(\frac{\Delta p}{p}\right) \tag{4.44}$$

Multiplying N by the revolution period $\tau_{\rm rev}$ we obtain

$$\Delta t = N\,\tau_{\rm rev} \tag{4.45}$$

as the actual time spent in this operation. For the sake of having some data, we consider RHIC[15] and HERA[16]. Table 4.1 gathers some parameters, pertaining to these rings, and what can be found by making use of eqs. (4.44) and (4.45) where $B_0 \simeq 0.1\ T$ and $N_{\rm cav} = 200$ have been chosen as realistic values.

Table 4.1: RHIC and HERA parameters

	RHIC	HERA
E(GeV)	250	820
γ	266.5	874.2
$\tau_{\rm rev}(\mu s)$	12.8	21.1
$\frac{\Delta p}{p}$	4.1×10^{-3}	5×10^{-5}
N	6.67×10^{9}	2.48×10^{7}
Δt	$8.52 \times 10^{4}\ s\ \simeq\ 23.7\ h$	523 s

4.1.6.2 Polarimeter

The beam polarization can be measured through the energy transferred to a RF cavity placed on the beam axis. For a single rectangular cavity, with a peak magnetic field B_0, and for a bunch train made up of N particles, eq. (4.34) gives as total energy transfer

$$\Delta U \simeq 2NP\mu^* B_0 \frac{b}{d}\gamma^2 \tag{4.46}$$

where P is the polarization of a beam, revolving in a ring whose guide field is $\vec{B}_{\rm ring}$, defined as

$$P = \frac{\tilde{N}_\uparrow - \tilde{N}_\downarrow}{\tilde{N}_\uparrow + \tilde{N}_\downarrow} = \frac{\tilde{N}_\uparrow - \tilde{N}_\downarrow}{N} \tag{4.47}$$

where $\tilde{N}_\uparrow$ and $\tilde{N}_\downarrow$ indicate the macroscopic averages over the particle distribution in the beam, after computing the quantum expectation values (by the statistical matrix) of the observables $N_\uparrow$ and $N_\downarrow$ that represent respectively the number of particles with spin parallel or antiparallel to $\vec{B}_{\rm ring}$. An unpolarized beam has $P = 0$ or $\tilde{N}_\uparrow = \tilde{N}_\downarrow$.

We propose to build a polarimeter based upon a two coupled cavity scheme, which acts as a parametric amplifier as the one considered [17] for a completely different application. Such a scheme has two oscillation states, for each single cavity scheme, which correspond to the symmetric and antisymetric modes of the coupled system.

If the frequency separation of the two modes is equal to the revolution frequency $\omega_{\rm rev}/2\pi$ of the bunch(es) in the machine, it is easy to show[18] that our system will act as a parametric converter[19][20]. Since the average power transferred is

$$W = \frac{\Delta U}{\tau_{\rm rev}} \tag{4.48}$$

the power related to the second cavity is

$$W_2 = \frac{\omega_{\rm RF}}{\omega_{\rm rev}} W = \frac{\tau_{\rm rev}}{\tau_{\rm RF}} W = \frac{\Delta U}{\tau_{\rm RF}} \tag{4.49}$$

where $\omega_{\rm RF}/2\pi$ is the working frequency of the resonant cavity (tipically in the GHz range); finally we get

$$W_2 \simeq \frac{2}{\pi} N\, P\, \omega_{\rm RF}\, \mu^* B_0 \frac{b}{d}\gamma^2 \tag{4.50}$$

Table 4.2: MIT-Bates parameters

$\tau_{\rm rev}$	634 nsec
$\omega_{\rm rev}/2\pi$	1.576 MHz
$N_{electrons}$	$3.6 \times 10^8 \cdot 225 = 8.1 \times 10^{10}$
γ	$\simeq 10^3$
b/d	$\simeq 1$
B_0	$\simeq 0.1$ T
$\omega_{\rm rf}/\omega_{\rm rev}$	1820
μ^*	$9.27 \times 10^{-24}\ JT^{-1}$

A feasibility test of the polarimeter principle has been proposed[10] and studied[18] to be carried out in the 500 MeV electron ring[11] of MIT-Bates, whose main charactristics are gathered in Table 4.2. From these data we obtain:

$$\frac{W_2}{P} \simeq 431 \text{ watt} \tag{4.51}$$

As a last check, we may compare the energy exchanges ($\vec{\mu} \Leftrightarrow \vec{B}$) and ($e \Leftrightarrow \vec{E}$). Taking into account eqs. (4.33), (4.34) and (4.40), and setting $x' \simeq 1$ mrad, $\beta_{\rm ph} = 2$ and $\lambda = 10$ cm, we have for the MIT-Bates ring:

$$r = \frac{\Delta U_E}{\Delta U} = \frac{x'}{8}\,\frac{\beta_{\rm ph}^3}{\beta_{\rm ph}^2 - 1}\,\frac{\lambda e c}{\mu^*}\,\frac{1}{\gamma^4} = 1.72 \times 10^{-4} \tag{4.52}$$

i.e. the spurious signal, depending upon the electric interaction between e and $\vec{E}$, is absolutely negligible with respect to the measurable signal generated by the magnetic interaction.

4.1.7 Conclusions

The Stern-Gerlach interaction, between a time varying e.m. field and a moving charged particle carrying a magnetic moment, seems very promising either for attaining the self polarization of a $p(\bar{p})$ beam or for realizing an absolute polarimeter.

In the first example the problem raised[9] by the rf filamentation still holds on, although some tricks can be conceived: the extreme one could be the implementation of a triangular waveform in the TM cavity which bunches the beam. The second example requires nothing but carrying out that experimental test at the MIT-Bates electron ring. Moreover, the γ^2 factor makes sure that the whole procedure does not undergo the constraints of the uncertainty principle

$$\Delta E\ \Delta t \geq h = 6.625 \times 10^{-34}\ Js \tag{4.53}$$

In fact, in the example of the test to be performed at the MIT-Bates ring, we have:

$$\Delta E = |\Delta U| \simeq \gamma^2 2\mu^* B_0 \tag{4.54}$$

which, for $B_0 = 0.1\ T$, yields

$$\Delta E\ \Delta t \simeq \begin{cases} \gamma^2 1.85 \times 10^{-34}\ Js \\ \gamma^2 2.82 \times 10^{-37}\ Js \end{cases} \tag{4.55}$$

having chosen as Δt a quantity of the order of $\frac{1}{2}\tau_{RF} \simeq 10^{-10}\ s$. This means that the uncertainty principle constraints (4.53) can be overwhelmed, provided that γ is greater than 1.84 for $e^{\pm}$ and 48.47 for $p, \bar{p}$ respectively.

However, an ultimate check should be made by considering either a rectangular or a cylindrical cavity inserted in a real machine. This would imply numerical simulations with spin-tracking[21] and cavity-designing[22] codes and would require further studies and some longer time to spend.

References

[1] H.M. Brash, D.M. Campbell, P.S. Farago, A.G.A. Rae, H.Chr. Siegmann and J.S. Wykes, Proc. Royal Society of Edinburgh, Sect. A (1968) 158.

[2] K.J. Kügler, K. Moritz, W. Paul and Trinks, Nucl. Instr. and Meth., 228 (1985) 240.

[3] K. Hirata, private communication.

[4] T. Niinikoski and R. Rossmanith, Nucl. Instrum. Methods, A255 (1987) 460.

[5] Y. Onel, A. Penzo and R. Rossmanith, A Spin-Splitter for Antiprotons in Low Energy Storage Rings, AIP Conf. Proc., Vol. 150, edited by R.G. Lernerand and D.F. Geesaman (American Institute of Physics, New York, N.Y., 1986), p. 1229.

[6] M. Conte, A. Penzo, A. Pisent and M. Pusterla, "Analytical Treatment of the Spin-Splitter", Internal Report INFN/TC-88/25.

[7] M. Conte and M. Pusterla, Quantum-Mechanical Implications for Polarized Antiprotons in the Spin-Splitter Device, Il Nuovo Cimento, **103A** (1990) 1087.

[8] M. Conte, A. Penzo and M. Pusterla, Il Nuovo Cimento, **A108** (1995) 127.

[9] M. Conte, W.W. MacKay and R. Parodi, "An Overview of the Longitudinal Stern-Gerlach Effect", BNL-52541, UC-414, November 17 1997.

[10] P. Cameron et al., "An RF Resonant Polarimeter Phase 1 Proof-of-Principle Experiment", RHIC/AP/126, January 6 1998.

[11] K.D. Jacobs et al., "Commissioning the MIT-Bates South Hall Ring", Proceedings PAC1, 1995.

[12] J.L. Synge, *Relativity: The Special Theory*, North Holland Publ. Co., Amsterdam, 1956.

[13] J.D. Jackson, *Classical Electrodynamics*, John Wiley and & Sons, New York, 1975.

[14] S. Ramo, J.R. Whinnery and T. Van Duzer, *Fields and Waves in Communication Electronics*, John Wiley and & Sons, New York, 1965.

[15] M.A. Harrison, "The RHIC Project", Proceedings of EPAC96, p. 13, Sitges (Barcelona), 1996.

[16] E. Gianfelice-Wendt, "HERA Upgrade Plans", Proceedings of EPAC98, p. 118, Stockholm, 1998.

[17] Ph. Bernard, G. Gemme, R. Parodi and E. Picasso, Particle Accelerators, **61** (1998) [343]/79.

[18] M. Ferro, Thesis of Degree, Genoa University, April 22 1999.

[19] J.M. Manley, H.E. Rowe, “Some General Properties of Nonlinear Elements - Part I. General Energy Relations”, Proceedings of the IRE, 44 (1956) 904.

[20] W.H. Louisell, *Coupled Modes and Parametric Electronics*, John Wiley & Sons, New York, 1965.

[21] A. Luccio, “Numerical Spin Tracking in a Synchrotron. Computer Code SPINK - Examples (RHIC)”, BNL-52481, September 18 1995.

[22] P. Fernandes and R. Parodi, “Oscar2D User’s Guide”, INFN/TC-90/04.

5: Recent Doctoral Theses in Beam Dynamics

5.1 Bounds on the Maximum Attainable Equilibrium Spin Polarization of Protons at High Energy in HERA

Mathias Vogt vogtm@math.unm.edu University of New Mexico

Institution: DESY/University of Hamburg
Title: Bounds on the Maximum Attainable Equilibrium Spin Polarization of Protons at High Energy in HERA.
Date: June 2000.
Supervisor: Dr. D. P. Barber (mpybar@mail.desy.de), DESY.
Reference: http://www-mpy.desy.de/proton_pol/hoffpapers/00vogt.ps.gz
Keywords: Polarised proton beams, storage rings, HERA, T–BMT equation, invariant spin field, amplitude dependent spin tune, static polarisation limit, dynamic polarisation, factorisation spin–orbit resonances, mid–plane symmetry, Siberian Snakes, snake resonances, acceleration, adiabatic invariance, Froissart–Stora formula, numerical methods, dynamical systems, maps.
Abstract: For some years HERA has been supplying longitudinally spin polarised electron and positron ($e^{\pm}$) beams to the HERMES experiment and in the future longitudinal polarisation will be supplied to the H1 and ZEUS experiments. As a result there has been a development of interest in complementing the polarised $e^{\pm}$ beams with polarised protons. In contrast to the case of $e^{\pm}$ where spin flip due to synchrotron radiation in the main bending dipoles leads to self polarisation owing to an up–down asymmetry in the spin flip rates (Sokolov–Ternov effect), there is no convincing self polarisation mechanism for protons at high energy. Therefore protons must be polarised almost at rest in a source and then accelerated to the working energy.

At HERA, if no special measures are adopted, this means that the spins must cross several thousand "spin–orbit resonances". Resonance crossing can lead to loss of polarisation and at high energy such effects are potentially strong since spin precession is very pronounced in the very large magnetic fields needed to contain the proton beam in HERA–p. Moreover simple models which have been successfully used to describe spin motion at low and medium energies are no longer adequate. Instead, careful numerical spin–orbit tracking simulations are needed and a new, mathematically rigorous look at the theoretical concepts is required.

This thesis describes the underlying theoretical concepts, the computational tools (SPRINT) and the results of such a study. In particular strong emphasis is put on the concept of the invariant spin field and its non–perturbative construction. The invariant spin field is then used to define the amplitude dependent spin tune and to obtain numerical non–perturbative estimates of the latter. By means of these two key concepts the nature of higher order resonances in the presence of snakes is clarified and their impact on the beam polarisation is analysed. We then go on to discuss the special aspects of the HERA–p ring and measures for minimising the perturbations to the spin motion ($\rightarrow$ depolarisation) and thereby obtain first upper bounds on the permissible beam emittances needed to maintain polarisation up to high energy in HERA–p.

In the near future, first experimental results on acceleration and storage of polarized protons in RHIC will be available. RHIC will be operated at less than a third of the top energy of HERA–p, is flat and has a higher superperiodicity (P=6). It will be interesting to see in how far the effects on polarisation, e.g. partial depolarisation due to crossing of higher order resonances in the presence of snakes, as predicted by the theory described in this thesis and found numerically for the HERA–p ring can already be clearly resolved experimentally in RHIC.

6: Announcements of the Beam Dynamics Panel

6.1 ICFA Workshops on Advanced Beam Dynamics

6.1.1 23rd Advanced ICFA Beam Dynamics Workshop High Luminosity e^+e^- Circular Colliders

David Rice dhr1@cornell.edu Cornell University

The 23rd Advanced ICFA Beam Dynamics Workshop will be hosted by the Laboratory of Nuclear Studies at Cornell University in Ithaca, NY, USA on October 15-19, 2001. The topic of this workshop will be High Luminosity e^+e^- Circular Colliders.

The Workshop will examine in detail the features and performance of high luminosity electron-positron circular colliders by:

1. reviewing experience from operation of the present generation machines
2. discussing issues of performance improvements over the next few years
3. exploring avenues toward the next generation of circular e^+e^- colliders.

Approximately one half of the time of the workshop is scheduled for working groups to focus on the details of specific issues. The working groups will endeavor to suggest solutions both to the problems of existing machines, and to the design challenges of future machines.

We expect 40-60 participants in the workshop, with representatives from all of the e+e- colliders in operation or design phases.

The workshop will be held in the conference facilities of the Ramada Inn in Ithaca, NY. The Ramada is adjacent to several shopping centers and is less than 2 miles from the Ithaca airport.

The weather in Ithaca during October is usually quite pleasant and the foliage colors are often brilliant.

A web page with the latest details of the workshop is available at:

www.lns.cornell.edu/icfa/

6.1.2 Shanghai Symposium on Intermediate Energy Light Sources

The Shanghai Symposium on Intermediate Energy Light Sources to be held September 24 - 26, 2001 will cover various topics ranging from insertion devices/beamlines to lattices and technology. The contact person in Shanghai is Xu Tongzhou (xutz@ssrc.ac.cn), in Europe Dieter Einfeld (einfeld@anka.fzk.de) and in the US J. Corbett (corbett@slac.stanford.edu).

For further information please see the home page of the ICFA Beam Dynamics Panel given below.

6.2 ICFA Beam Dynamics Newsletter

Editors in chief

Kohji Hirata (hirata@kekvax.kek.jp) and John M. Jowett (John.Jowett@cern.ch)

Editors
Swapan Chattopadhyay (swapan@jlab.org),
Weiren Chou (chou@adcon.fnal.gov),
Sergei Ivanov (ivanov_s@mx.ihep.su),
Helmut Mais (mais@mail.desy.de),
Jie Wei (wei1@bnl.gov),
Chuang Zhang (zhangc@bepc3.ihep.ac.cn)

6.2.1 Aim of the Newsletter

The ICFA Beam Dynamics Newsletter is intended as a channel for describing unsolved problems and highlighting important ongoing works, and not as substitute for journal articles and conference proceedings which usually describe completed work. It is published by the ICFA Beam Dynamics Panel, one of whose missions is to encourage international collaboration in beam dynamics.

It is published every April, August and December. The deadlines are 15 March, 15 July and 15 November, respectively.

6.2.2 Categories of Articles

The categories of articles in the newsletter are the following:

1. Anouncements from the panel
2. Reports of Beam Dynamics Activity of a group
3. Reports of Beam Dynamics related workshops and meetings
4. Anouncements of future Beam Dynamics related international workshops and meetings.

   Those who want to use newsletter to anounce their workshops etc can do so. Articles should typically fit within half a page and include descriptions of the subject, date, place and details of the contact person.
5. Review of Beam Dynamics Problems

   This is a place to put forward unsolved problems and not to be used as the achievement report. Clear and short highlights on the problem is encouraged.
6. Letters to the editor

   It is a forum open to everyone. Anybody can show his/her opinion on the beam dynamics and related activities, by sending it to one of the editors. The editors keep the right to reject a contribution.
7. Editorial

All articles except for 6) are by invitation only. The editors request an article following a recommendation by panel members. Those who wish to submit an article are encouraged to contact a nearby panel member.

The manuscript should be sent to one of the editors as a LaTeX file or plain text. The former is encouraged and authors are asked to follow the example below.

Each article should have the title, author's name(s) and his/her/their e-mail address(es).

6.2.3 How to prepare the manuscript

Instructions can be found in WWW at

http://www-acc-theory.kek.jp/ICFA/instruction.html

6.2.4 World-Wide Web

Recent issues of this newsletter are available through the World-Wide-Web via the address given below. This is now intended as the *primary method of communication.*

The home page of the ICFA Beam Dynamics Panel is at the address

`http://wwwslap.cern.ch/icfa/`

This Web page provides access to the Newsletters, information about Future and Past Workshops, and other information useful to accelerator physicists. There are links to pages of information of local interest for each area.

6.2.5 Distribution

The ICFA Beam Dynamics Newsletters are distributed through the following distributors:

W. Chou	chou@adcon.fnal.gov	North and South Americas
Helmut Mais	mais@mail.desy.de	Europe* and Africa
Susumu Kamada	Susumu.Kamada@kek.jp	Asia** and Pacific

(*) including former Soviet Union.
(**) For mainland China, Chuang Zhang (`zhangc@bepc5.ihep.ac.cn`) takes care of the distribution with Ms. Su Ping, Secretariat of PASC, P.O.Box 918, Beijing 100039, China.

It can be distributed on a personal basis. Those who wish to receive it regularly can request this from one of the distributors. In order to reduce the distribution cost, however, please use the Web as much as possible. In particular, if you no longer need a paper copy, please inform the appropriate distributor.

6.2.6 Regular Correspondents

Since it is impossible for the editors and panel members to watch always what is going on all around the world, we have started to have *Regular Correspondents*. They are expected to find interesting activities and appropriate persons to report them and/or report them by themselves. We hope that we will have a ”compact and complete” list covering all over the world eventually. The present *Regular Correspondents* are as follows

Liu Lin (liu@ns.lnls.br)	LNLS	Brazil
S. Krishnagopal (skrishna@cat.ernet.in)	CAT	India
Ian C. Hsu (ichsu@ins.nthu.edu.tw)	SRRC	Taiwan

We are calling for more volunteers as *Regular Correspondents*.

6.3 ICFA Beam Dynamics Panel Members

Swapan Chattopadhyay (swapan@jlab.org)	TJNL
Pisin Chen (chen@slac.stanford.edu)	SLAC
Weiren Chou (chou@adcon.fnal.gov)	Fermilab
Yoshihiro Funakoshi (yoshihiro.funakoshi@kek.jp)	KEK
Kohji Hirata (hirata@soken.ac.jp)	Sokendai/KEK
Ingo Hofmann (I.Hofmann@gsi.DE)	GSI
Sergei Ivanov (IHEP (Protvino))	ivanov_s@mx.ihep.su
John M. Jowett (John.Jowett@cern.ch)	CERN
Kwang-Je Kim (Kwang_Je_Kim@macmail.lbl.gov)	LBNL
Jean-Louis Laclare (jllaclare@cea.fr)	DSM-DAPNIA-SEA
Kwang-Je Kim (kwangje@aps.anl.gov)	ANL
Helmut Mais (mais@mail.desy.de)	DESY
Luigi Palumbo (lpalumbo@uniroma1.it)	Univ.Rome/LNF-INFN
Claudio Pellegrini (pellegrini@physics.ucla.edu)	UCLA
Elcuno A. Perelstein (perel@nu.jinr.ru)	JINR
Dmitri Pestrikov (pestrikov@inp.nsk.su)	BINP
Chuang Zhang (zhangc@bepc3.ihep.ac.cn)	IHEP(Beijing)
Jie Wei (wei1@bnl.gov)	BNL

The views expressed in this newsletter do notnecessarily coincide with those of the editors. The individual authors are responsible for their text.